

**Leveraging Technologies for Condition Assessment of Multi-Girder Highway
bridges**

A Thesis

Submitted to the Faculty

Of

Drexel University

By

Shi Ye

In partial fulfillment of the

Requirements for the degree

Of

Doctor of Philosophy

February 2020



© Copyright 2020

Shi Ye, All Rights Reserved

Dedications

I dedicate this thesis to my mother and father, Yuehua Zhu and Minghui Ye, and my sisters, Xin Ye, Pan Ye and Mi Ye, who have been supportive throughout my life and encouraged me to achieve this Doctorate Degree. I also would like to thank my fiancé, Weijin Zhao, for his support and love.

Shi

Acknowledgments

I am very thankful to everyone who has supported me throughout my career at Drexel University. Most importantly, I would like to thank Dr. Ivan Bartoli, Dr. Anu Pradhan and Dr. Emin Aktan for guiding me to pursue my education and supporting me for the past seven years through my Ph.D. program. They have been my teachers, my mentors, my bosses when needed, but most importantly my friends and there are not enough words to express how grateful I am for everything they have done to help me succeed. They stood by me through good times and bad and I would not have been able to do this without them.

I am deeply grateful to the work and contributions of all the researchers and participations of the International Bridge Study. I would like to acknowledge the support and assistance from the Federal Highway Administration and the Long-Term Bridge Performance Program, New Jersey Department of Transportation, the Rutgers Center for Advanced Infrastructure and Transportation. Dr. Emin Aktan, Dr. Franklin Moon and Dr. Jeff Weidner made valuable contributions to the study, and I would like to thank them for leading and organizing the study, documenting and providing all the data and information. Additionally, I would like to thank all the International Bridge Study participants from US, UK, Japan, South Korea, and Europe who demonstrated technologies and techniques as part of this research effort, in particular Dr. Nenad Gucunski, Dr. Branko Glisic, Dr. Yun Zhou, Dr. John Prader, and Dr. Hyun Moo Koh.

I would like to thank all the members of my dissertation committee, Dr. Alan Lau, Dr. L. James Lo, Dr. Marcello Balduccini for dedicating their time in serving on my committee.

I also would like to thank all the friends who have supported me: Xiangang Lai, Dr. Qiang Mao, Michelle Burnworth, Mustafa Omer Furkan and Dr. Matteo Mazzotti.

Table of Contents

Table of Contents.....	i
List of Figures.....	iii
List of Tables	vi
Abstract.....	vii
Chapter 1: Introduction.....	1
1.1 Motivation.....	1
1.2 Objectives and Scope.....	3
1.3 Vision and Challenges	5
1.4 Thesis Outline	6
Chapter 2: Literature Review.....	7
2.1 Overview of Highway Bridge Assessment Systems.....	7
2.1.1 History of the Development of Highway Bridge Assessment Systems.....	7
2.1.2 Highway Bridge Inspection Technologies.....	12
2.2 Bridge Assessment Methods.....	15
2.2.1. Non-Destructive Evaluation.....	16
2.2.2. Structural Health Monitoring.....	17
2.3 Structural Identification Method.....	19
2.3.1 Overview of Structural Identification	19
2.3.2 The Development of Structural Identification for Bridge Assessment.....	22
2.4 Technology Integration Strategy.....	25
Chapter 3: Observation and Conceptualization	28
3.1 Bridge Selection.....	28
3.2 Bridge Description.....	30
3.3 Performance Concerns	32
3.4 Bridge Information Modeling	36
Chapter 4: A-Priori Modeling.....	40
4.1 Purpose of A-prior modeling	40
4.2 The development of an a-prior mode.....	41

	Benchmark Study for Element Type and Mesh Size Selection	42
	Parameter Selection and Model Information	47
4.3	Preliminary analysis and results.....	50
Chapter 5:	Controlled Experimentation and Data Processing	51
4.2.1 5.1	Vibration Testing	52
4.2.2 5.2	Controlled Load Testing	57
5.3	Non-destructive Testing.....	61
5.4	Long-Term Monitoring by Fiber-Optic Sensors.....	65
Chapter 6:	Model Calibration and Parameter Identification.....	68
6.1	Parameters Assumption and Selection.....	68
6.2	Parameter Identification based on Vibration Testing	72
6.3	Parameter Identification based on Load Testing	75
Chapter 7:	Utilization of Model for Pier-Cap Stress Analysis	81
7.1	Benchmark Study of Dynamic Amplification Factor under Moving Loads.....	82
7.2	Pier-Cap Stress Analysis.....	88
7.2.1	Static Analysis for Pier-cap Stress.....	91
7.2.2	Dynamic Analysis for Pier-cap Stress	93
7.3	Summary and Correlation of Test Results	98
Chapter 8:	Conclusions, Recommendations, and Future Work.....	100
8.1	Summary of Conclusions and Recommendations	100
8.2	Further Work.....	103
	List of References	105
	Appendices.....	112
	Vita.....	120

List of Figures

Figure 1. Map of United States with percentage of Deficient bridges in 2019 (ARTRB 2019)	1
Figure 2. Timeline of important milestones influencing the U.S. highway bridge inspection system	11
Figure 3. SHM Cycle with the fundamental components	18
Figure 4. Structural Identification	19
Figure 5. Current technologies for bridge evaluation	26
Figure 6. Technology Integration Framework for Bridge Management	26
Figure 7. US202/NJ23 four-span highway bridge. (a)Field view of the bridge; (b) Bridge location in google maps (marked with red star).	29
Figure 8. The selected bridge: a) view from Google Maps; b) site layout with Span 2 Southbound Highlighted	30
Figure 9. Pier 1 W (View from South to North)	31
Figure 10. Examples of performance concerns: (a) fatigue cracking at girder web, (b) pier 1 cap cracking, (c) cracks on the abutment, (d) damaged bearing, (e) insufficient drainage damage, (f) water main crossing the bridge, (g) gas pipe.	33
Figure 11. BrIM model of IBS bridge in Cl3ver Software	37
Figure 12. Screenshot of bridge model in VR view on Modelo mobile app	39
Figure 13. Simply supported composite beam a) side view of the beam; b) beam cross section	42
Figure 14. Mesh density analysis of solid element model	43
Figure 15. Stress analysis of the composite beam	45
Figure 16. Deflection shapes of the finite element models	46
Figure 17. Two views of the a-prior model in ABAQUS	48
Figure 18. Finite Element Modeling of Girders and Bracing/Cross Frame	49
Figure 19. Frequencies and Mode shapes from the a-prior model	50
Figure 20. Devices used in Forced Vibration Tests	54
Figure 21. Instrumentation Layout and Accelerometers	55
Figure 22. Mode Shapes from Forced Vibration Testing by Drexel Researchers	56
Figure 23. Results of Ambient Vibration Monitoring of Span 2 SB: a) Vertical acceleration time records of Girder #3; b) Averaged Power Spectral Densities at midspan	57
Figure 24. Instrumentation Layout and Sensor Installation Info of Controlled Load Test	58
Figure 25. Truck Locations for the Controlled Load Test	59
Figure 26. Controlled Static Load Testing results: a) Girder Displacement Profiles under 6 Full trucks; b) Midspan Load-Displacement Relations under Three Loading Scenarios at Center (Weidner, 2012)	60
Figure 27. Mid-span Strains from the strain gages at bottom flange for the Three Load Scenarios (Weidner, 2012)	60
Figure 28. Field View of NDE Survey conducted on Span 2 Southbound	63

Figure 29. Field view of NDE survey grid	63
Figure 30. NDE results of span 2 southbound	64
Figure 31. Application of RC Radar: a) field test on pier cap; b) corresponding radar results in P1 pier cap	65
Figure 32. Sensor Instrumentation Layout for Long-term Monitoring with Fiber-Optic sensors.....	66
Figure 33. Neutral Axis Analysis based on Dynamic Strain Data from Large Events.....	66
Figure 34. Neural Axis analysis results of Girder 2 obtained by Princeton University in probabilistic approach with one-year data.	67
Figure 35. Finite Element Model (with Piers) in Abaqus software: a) modeling information; b) view of the model with defined meshes	69
Figure 36. Details of bridge bearings: a) fixed bearing; b) expansion bearing; L and R stand for Left (South) and Right (North).....	69
Figure 37. Comparison of Experimental and Analytical Frequencies and Modes	75
Figure 38. Vertical displacements comparison: a) results obtained from manually calibrated model with initial parameters; b) results obtained from automatically calibrated model with new start point.....	78
Figure 39. Model Information of Finite Element Models of the Two Plates	82
Figure 40. First Two Modes (Frequency and Mode shape) of FE Models of Plate 1 (left) and Plate 2 (right).....	83
Figure 41. Displacements at Center Point under Static and Dynamic Load of Plates 1 and 2.....	84
Figure 42. Stresses at Center Point under Static and Dynamic Loads of Plates 1 and 2 ..	84
Figure 43. Max Reaction Forces at Supports under Static and Dynamic Load.....	86
Figure 44. Pier-Cap Cracking Location of Span 2 SB Pier 1W.....	89
Figure 45. Field View of Cracked Pier-cap (left) and Shear Stress of the Pier-cap (right)	90
Figure 46. Cross Section (left) of Cracked Pier-cap and Shear Stress Distribution (right)	90
Figure 47. Example of loading scenario generating large bearing reaction: two Moving Trucks on Lane 1 and one Moving Truck on Lane 2.....	92
Figure 48. Reaction Force Distribution of Span 1 SB (left) and Span 2SB (right) under Dead Load.....	92
Figure 49. Truck Weights and Dimensions of HS 20 Truck	93
Figure 50. Mid-span Displacements under Truck Load moving along Lane 1 and Lane 2	94
Figure 51. Vertical acceleration at Mid-span due to Moving Truck Load Obtained from Field Test (left) and Abaqus Model (right).....	95
Figure 52. Simulation Results of Three Moving Trucks	97

List of Tables

Table 1. Summary of categorized factors affecting Visual Inspection	13
Table 2. Performance Concerns Under Performance Limit States	35
Table 3. Finite Element Models of Composite Beam.....	43
Table 4. Results comparison for hand calculation and finite element models.....	47
Table 5. Material Properties used in the A-Priori model	49
Table 6. Summary of Tests Conducted by Different Groups	51
Table 7. Comparison of Frequencies Obtained from Ambient Vibration Tests	53
Table 8. Natural Frequencies Comparison Obtained from Forced Vibration Testing.....	54
Table 9. Initial Values of Parameters to be Calibrated in the FE Model	70
Table 10. Comparison of Integrated Experimental Result with Finite Element Model Results.....	71
Table 11. Values of Critical Parameters Updating using Vibration Testing Datasets.....	74
Table 12 Values of Manual Parameters Updating using controlled load testing datasets	77
Table 13 Values of Automated Parameters Updating using controlled load testing datasets	78
Table 14 Summary of model updating leveraging Static Testing.....	79
Table 15. Dynamic Amplification Factor for Maximum Displacement and Stress of Plates 1 and 2.....	85
Table 16. Dynamic Amplification Factor of Total Reaction Force of Plates 1 and 2	86
Table 17. Dynamic Amplification Factor of Total Reaction Force (Model with Springs).....	87
Table 18. Dynamic Amplification of Total Reaction Force	88
Table 19. Shear Stresses of Pier-cap under Dead Load	92
Table 20. DAF for Maximum Displacement under Moving Truck Loads	94
Table 21. DAF for Maximum Total Reaction Force under Moving Truck Loads	94
Table 22. DAF of Maximum Shear Force for Bearings 1S and 1N	95
Table 23 Maximum shear stresses obtained from simulation of three moving trucks	97

Abstract

Leveraging Technologies for Condition Assessment of Multi-Girder Highway bridges

Shi Ye

A majority of US highway bridges were constructed in the mid-20th century. Today, bridge owners have to consider increases in traffic demands and also face concerns related to sustainability, resilience and livability which were virtually unknown in the 1950s. In this context, transportation stakeholders face increasingly complex decisions for repair, retrofit or renewal of their assets. Legislature demands data-driven decisions based on quantitative and reliable bridge condition and performance evaluation. Different technology tools that can provide objective condition evaluations have become available but given the inertia in the practice of bridge engineering and a lack of understanding the challenges to their reliable applications, their use remain limited. Consequently, management decisions are still primarily made without leveraging objective measurement data and without a mechanistic understanding of bridge behavior and performance.

To explore the current state-of-the-art in performance and condition evaluation of constructed systems by leveraging technology, a 30-year old highway bridge in New Jersey, exhibiting multiple complex performance deficiencies, was transformed into a field laboratory. To identify the root causes of performance concerns, Visual Inspection, Operational Monitoring, Forced Excitation Testing, Controlled Load Testing, Non-destructive Probes, Long-term Monitoring and Finite Element Modeling and Parameter Identification were conducted within a Structural Identification framework. The results showed that root causes of some performance deficiencies of the test bridge could be

identified only through the application of field measurements and analyses integrated by following a scientific approach - such as Structural Identification, especially for deficiencies related to unexpected dynamic amplifications and the long-term effects of vibrations. Controlled Load Testing was especially useful in demonstrating the location and impacts of damage although such an approach can only be considered for the most critical cases due to its high cost and disruption to operations. Operational monitoring was shown as a sufficient and cheaper alternative for structural identification permitting the development of a lesser resolution digital twin of the bridge, which was critical in identifying the root causes of its deficiencies and formulating meaningful interventions.

This page is intentionally left blank

Chapter 1: Introduction

1.1 Motivation

There are about 47,000 “structurally deficient” bridges in the United States with 178 million daily crossings, and the average age of those bridges is 62 years compared to 40 years for non-deficient crossings (ARTRB 2019). The map showing the percentage of deficient bridges to the total bridges of each state is shown in Figure 1. Nearly 40% of United States (US) bridges were built over 50 years ago while the expected design-life for bridges is 50 years, and about 18,842 (near 33%) interstate highway bridges have identified repair needs.

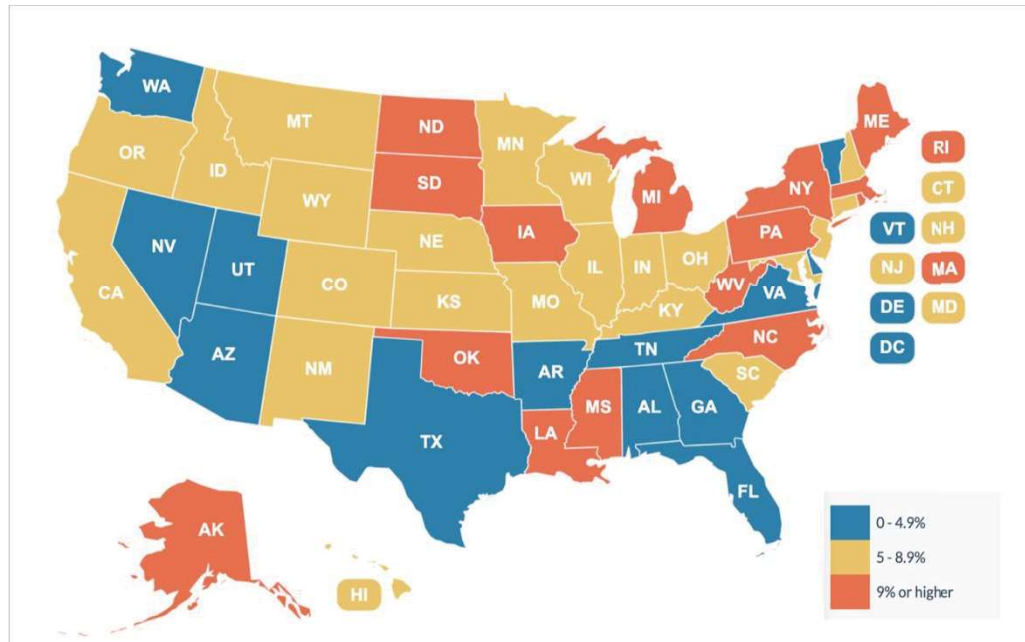


Figure 1. Map of United States with percentage of Deficient bridges in 2019 (ARTRB 2019)

Managing such a significant aging bridge population requires tools to reliably assess the performance, condition and remaining life of these structures based on objective data and in the context of asset management. To this aim, bridge engineering practice needs to adopt condition evaluation tools that will provide objective and quantitative information that will enable sound decisions regarding bridge-foundation-soil safety and stability, as well likely failure modes which may be significantly affected by deterioration and damage. To propose reliable recommendations on managing highway infrastructures, there is an increasing need for leveraging objective measurement data and mechanistic understanding of bridge behavior and performance obtained from different technology tools.

Leveraging technology for condition assessment of existing highway bridges is critical for several reasons:

- 1) The majority of US highway bridges were constructed in the mid-20th century. Due to the growth in traffic volumes, and concerns in sustainability and resilience, the maintenance of highway bridges has faced increasing need for decision making strategies regarding maintenance, repair, retrofit or renewal. It is very important to make appropriate retrofitting decisions based on comprehensive bridge condition evaluation given the potential costs and impacts involved.
- 2) Historical and general information of highway bridges included in the National Bridge Inventory (NBI) database in addition to biannual inspections should facilitate bridge asset management and enable defect detection at an early stage with minimum cost; however, this information relies on visual observations by inspectors (which experience and qualification largely vary across the US). It is obvious that subjective condition assessment

by personnel with varying qualifications may not guarantee an accurate evaluation of bridge condition.

3) Quantitative information should also be collected and integrated with inspection results for reliable assessment by experienced engineers. It has been advocated for many years that in conjunction with visual inspection, objective in-depth assessment technologies such as monitoring operational responses and Non-Destructive Evaluation (NDE) should be deployed.

4) Although different technology advancements for bridge field testing, such as Structural Health Monitoring (SHM) approaches and NDE tools, and advancement of well-known model simulation tools (such as Finite Element (FE) software) have been available to researchers to obtain objective and quantitative data in the past several decades, an integration of the collected data is essential to explain root causes of bridge performance deficiencies, deterioration and other performance concerns. Consequently, maintenance, repair, retrofit or renewal decisions and design methods remain questionable unless data and information from these different methodologies are properly integrated.

1.2 Objectives and Scope

Following the above Introduction, the broader objective of this study is to better illustrate and quantify the concerns regarding existing bridge asset management and to provide guidelines towards an objective data driven framework. The study will take advantage of a comprehensive case that was performed by leveraging a 30-Year old highway bridge as a field laboratory. This bridge was characterized by the State Bridge Engineer as “*a nightmare bridge*,” due to its exhibiting a multitude of performance deficiencies. To

exemplify the state of practice in design and preservation of a bridge on a very critical network in the North East United States, the following questions guided the study:

1. Which design, construction and maintenance defects have led to performance concerns and what are the challenges in identifying the root causes of a multitude of performance deficiencies of the 30-year old bridge on a very critical highway? Is it possible to pinpoint the root cause(s) of each and every performance concern only by heuristics? When is it necessary to complement heuristics with field measurements and experiments? Is it necessary to execute a comprehensive structural identification of the bridge in terms of a finite-element model to identify the root causes and proper interventions?
2. What is the analytical model form and resolution that may be justified given the data we may obtain from various types of experiments conducted on the bridge, in conjunction with the uncertainty prevailing in analytical modeling and in experimental data? Is it meaningful to consider a “digital-twin” such as for aerospace, space or other manufactured systems in the case of an aged and deteriorated constructed system such as the test bridge?
3. What is the cost and information value of measurements from different types of field experiments on full-scale systems? What are the challenges in assuring data quality from each type of experiment, i.e. operational monitoring; modal analysis by multireference impact testing; load testing based on various levels of load and different sensors; and, multi-mode nondestructive scanning of the entire deck?

1.3 Vision and Challenges

With the high speed of development in different domains, especially in the computer science field, researchers and bridge owners can collect and analyze data in a more efficient and effective way. More and more application tools have been developed and introduced, and each application tool and its implemented technologies has certain values for specific purposes. There also is a significant technological growth in sensing, imaging, computing and simulation, and these technologies have been widely used in bridge condition assessment projects but rarely in the bridge inspection routine. Collecting information from multiple approaches lead to more quantitative data and possibly to more reliable condition assessment, which could largely benefit infrastructure management system. However, it may often not prove economical to deploy several methodologies.

Consequently, two research questions are posed: 1) what technologies are useful to understand the performance of a bridge under specific scenarios? 2) how can we leverage these technologies with minimum cost for reliable assessment of bridge condition?

To address the first question, several currently available tools and technologies will be explored and evaluated, and the errors and uncertainties associated with each approach will also be demonstrated in this thesis. For this research, a multi-girder highway bridge will be used as test specimen since this type of bridge is the most common type in the highway bridge systems. It should be noted that the performance of application tools varies for different types of bridges. To address the second question, common performance concerns of highway bridge and the possible root causes will first be analyzed, and then the cost (including equipment, labor, and traffic control) of each approach mentioned will be estimated. It is hard to predict accurate cost of each method due to several factors (such as

price change, unexpected risk, and environmental impact), thus only approximate predictions of the cost will be given based on previous studies and searchable sources. When multiple application tools are selected, an integration of the collected data becomes necessary for proper interpretation and decision making. Many challenges remain in integrating, visualizing and interpreting test and simulation results for diagnosis. To obtain more reliable interpretations of bridge condition and performance, strategies will be proposed to integrate measurement data with other proxy information (such as past inspection and maintenance records, traffic information, NBI data, climate and weather data and others) in optimal and practical ways.

1.4 Thesis Outline

In this thesis, the Structural Identification (St-Id) concept will be leveraged for bridge condition assessment, and technologies involving sensing, simulation and information technology that have been applied or can be used in the fundamental steps of St-Id will be discussed and evaluated. One of the goals of this study is to comprehend what technologies or combination of technologies are necessary to comprehend the root causes of performance concerns.

After discussing the needs and challenges of bridge asset management discussed in Chapter 1, a background on U.S. highway bridge management history, bridge assessment methods, structural identification (St-Id) concepts, and information integration strategies are discussed in Chapter 2. Chapter 3 presents the objectives of this work, hypotheses of the study, and approach used to accomplish these goals.

Chapters 4-7, demonstrate a case study of technology implementation for the assessment of a highway bridge following the five steps of the Structural Identification method. This represents a step towards a broad objective that is to show how to integrate, visualize and interpret information, test and simulation results in optimal and practical ways for reliable assessment of bridge condition and performance. The deliverables of this case study summarized in Chapter 8 include the analysis of the root causes of some performance concerns that cannot be appreciated by simple visual inspection. Chapter 8 also explains some of the future work and extensions of the research presented and the concluding remarks.

Chapter 2: Literature Review

2.1 Overview of Highway Bridge Assessment Systems

The current approaches to assess and characterize highway bridges primarily rely on visual inspection which remains a critical part of bridge management system even after the wider adoption of sensing, simulation and information technologies. To understand the current and potential role of each technology application, bridge condition estimation standards and queries which drive managers to adopt technology tools need to be discussed. By first overviewing the current highway bridge assessment practice, technologies that have been incorporated to the current practice and their roles are described in the following.

2.1.1 History of the Development of Highway Bridge Assessment Systems

In 1956, President Dwight D. Eisenhower signed the Federal Aid Highway Act of 1956 into law, which authorized the construction of 41,000 miles of the Interstate Highway System (e.g., a national network of highways). The construction of the original system was

completed in 1992 with \$114 billion cost (Minnesota Department of Transportation 2006). According to the 2016 highway statistics data from Federal Highway Administration (FHWA) website, the length of the interstate highway system has extended to 48,489 miles. During the highway system construction boom of 1950's and 1960's, most emphasis was on new and economical construction, and safety inspection and maintenance of bridges did not gain much attention from most highway departments.

In 1967, the Silver Bridge, a towering suspension bridge over the Ohio River between West Virginia and Ohio, collapsed during rush-hour, causing 46 fatalities and 9 injuries. At that time, there was no systematic bridge inspection program to assess the condition of existing bridges, the exact number of which was unknown. After this event, two major bridge safety programs were established to ensure periodic inspection and provide mechanisms for bridge replacement and rehabilitation funding (U.S. Department of Transportation 2014). One program is the National Bridge Inspection Program (NBIP) established to ensure the safety of public transportation by the Federal-Aid Highway Act of 1968. Congress directed the Secretary of Transportation in cooperation with State Highway officials to establish National Bridge Inspection Standards (NBIS) and a bridge inspection training program. NBIS, the first national-level standards for bridge inspection and safety evaluation, was then developed by FHWA and American Association of State Highway and Transportation Officials (AASHTO, formerly known as AASHO) and enacted as part of the Federal-Aid Highway Act of 1970. NBIS established national policy regarding inspection procedures, inspection frequency, qualifications of personnel, inspection reports, and maintenance of state bridge inventory (Ryan et al. 2012). For bridges subject to NBIS, inspection results are required to be collected and maintained in the National Bridge Inventory (NBI). The

Bridge Inspector's Training Manual was subsequently developed, and training courses based on the manual were prepared to provide specialized training. The other program is now known as Highway Bridge Replacement and Rehabilitation Program (HBRRP) expanded on the Special Bridge Replacement Program (SBRP) in 1978, and it uses a rating system to numerically rate bridges between 0 to 100 on 84 items relating to safety, serviceability, essentiality, and reductions for special deficiencies. The bridges classified as structural deficient or functionally obsolete were eligible for rehabilitation with a sufficiency rating of 80 or less, and eligible for replacement with a sufficiency rating of less than 50 (FHWA 1992).

Other two failures, the structural failure of Mianus River Bridge in 1983 and the scour caused failure of the Schoharie Creek Bridge in 1987, have also drawn national attention on fracture-critical inspections and underwater bridge inspections. Inspection of Fracture Critical Bridge Members was then published in September 1986, and a technical advisory was published by FHWA in September 1988 to provide guidance on underwater bridge inspections. As a result, NBIS was modified to require states to identify bridges with additional fracture-critical and underwater details and establish in-depth fracture-critical and underwater inspection procedures (Ryan et al. 2012).

In 1991, a bridge management system called Pontis (now known as BrM, short for AASHTOWare Bridge Management) was developed to assist the management of bridges and other structures under a National Cooperative Highway Research Program (NCHRP) project first sponsored by the FHWA and then transferred to AASHTO. BrM contains three primary components: a database storing bridge inspection and inventory data, a user

interface supporting 2D or 3D description of a bridge, and computational engines providing recommendations for bridge projects.

To improve the assessment of highway infrastructure assets, the Nondestructive Evaluation (NDE) Center was established by FHWA in 1998 to conduct state-of-the-art research, development, and implementation of nondestructive testing systems and technologies. The NDE laboratory, the main part of the center, equipped with advanced instruments was designed to act as an open resource for transportation agencies, industries, and academic researchers to develop and test innovative NDE technologies. The laboratory has recently developed the NDE Web Manual which is a web tool providing a fundamental understanding of properly selected NDE technologies for the condition assessment of bridge decks and superstructures (FHWA 2015).

To provide funding for the construction and maintenance projects of the newly expanded National Highway System which includes the interstate system and principal transportation arteries, the National Highway Performance Program (NHPP) was established under the Moving Ahead for Progress in the 21st Century Act (i.e., MAP-21) signed into law by President Obama on July 6, 2012. NHPP funded surface transportation programs at over \$105 billion for fiscal years 2013 and 2014, and fiscal years 2015 and 2016 under extension of MAP-21 (FHWA 2016). Following that, the Fixing America's Surface Transportation (FAST) Act signed on Dec. 4, 2015 has authorized \$305 billion over fiscal years 2016 to 2020 for surface transportation and infrastructure planning and investment.

In addition to these programs and manuals, other major standards and manuals related to bridge inspection were developed and published by FHWA or AASHTO, such as the Manual for Maintenance Inspection of Bridges, the Guide Manual for Bridge Element

Inspection, the Manual for Condition Evaluation of Bridges, the Manual for Maintenance Inspection of Bridges, the Bridge Inspector's Reference Manual, and the Bridge Inspector's Training Manual 90 (Freeby 2013). The timeline of important milestones of U.S. highway bridge inspection system is summarized in Figure 2.

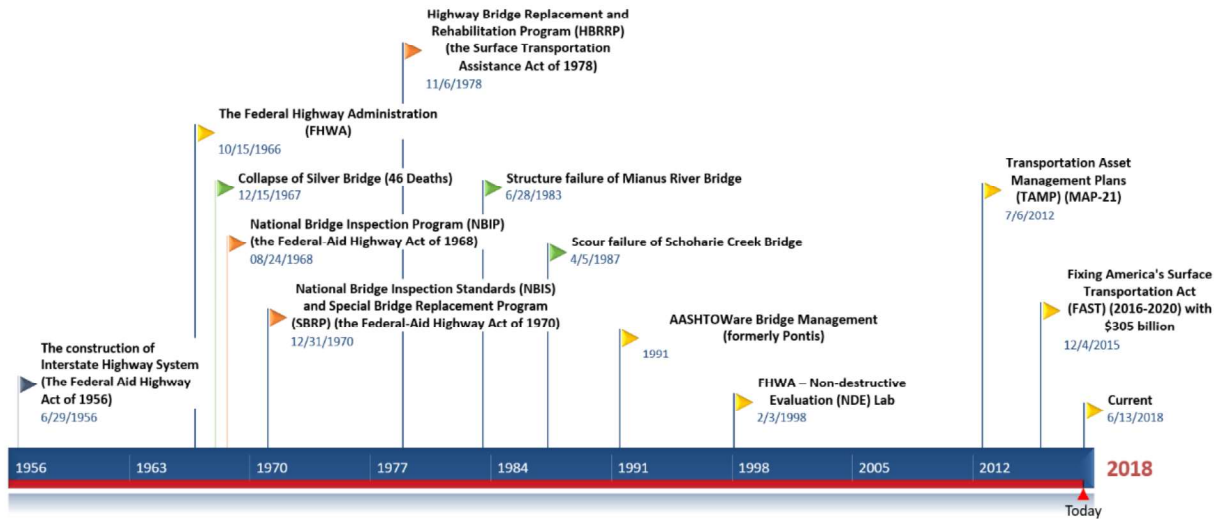


Figure 2. Timeline of important milestones influencing the U.S. highway bridge inspection system

The current bridge assessment practice in U.S. requires four main pieces of information: condition rating, information of national bridge inventory (NBI) items, load rating/capacity, and indices and designations for decision-making (Aktan, Moon, and Weidner 2016). During regular inspection procedures, bridge inspectors evaluate bridges and assign condition ratings using the National Bridge Inspection Rating Scale, ranging from 0 to 9 with 0 being a failed condition and 9 being excellent condition, based on NBIS. According to the Pavement and Bridge Condition Performance Measures final rule published in 2017, the bridge condition is classified as Good if the lowest rating of ratings for 4 NBI items (i.e., Deck, Superstructure, Substructure, Culvert) is greater than or equal to 7, Fair if the

lowest rating is 5 or 6, or Poor if the lowest rating is less than or equal to 4. If a bridge is classified as Poor, then the bridge is also Structurally Deficient, eligible for rehabilitation if the sufficiency rating is equal to or less than 80 and eligible for replacement if the sufficiency rating is less than 50. The term, Functionally Obsolete, is no longer used to classify the bridge condition since 2016 (FHWA 2018). The load rating is a measure of bridge live load capacity, and it includes inventory rating and operating rating as defined in the current AASHTO Manual for Bridge Evaluation (FHWA 2006). The ratings are computed and reported into the NBI as either a Rating Factor (RF) or in metric tons, and the RF is based on Load Factor Rating (LFR) methods using MS28 loading or Load and Resistance Factor Rating (LRFR) Methods using HL-93 loading (FHWA 2006). However, only 12% of bridges are posted for load rating based on the NBI 2012 report, and 77% of load posted bridges and culverts have unknown design live load or were designed for live load equal to or less than H15. Most of the load ratings are determined by computational methods (93%), and only 1% of load ratings result from load tests (National Academies of Sciences, Engineering 2014).

2.1.2 Highway Bridge Inspection Technologies

There are five basic types of bridge inspections: initial, routine, in-depth, damage, and special (FHWA 2015). Among the five types, routine and in-depth inspection are the two prevalent inspection forms implemented by state departments of transportation. The routine inspection is the most common type which identifies the condition changes and determines the physical and functional conditions of bridges on a regularly basis, and it is generally required at least every 24 months by NBIS for highway bridges located on public roads that exceed 20 feet in total length. The in-depth inspection is a close-up and hands-

on inspection usually performed as a follow-up inspection to better identify specific deficiencies that are hardly detectable by other inspection types.

Visual inspection is usually the first and often the only step to periodically obtain information on bridge conditions (such as visible corrosion, cracks and vibration) and possibly observe the causes leading to deterioration of highway structures (such as trapped water, road salt, temperature, live loads, wind and others). However, there are many factors that will affect the visual inspection accuracy and reliability. Megaw (Megaw 1979) classified the factors believed to influence visual inspection accuracy into four categories: Subject, Physical and Environmental, Task, and Organizational factors. A summary of some categorized factors is listed in Table 1.

Table 1. Summary of categorized factors affecting Visual Inspection

Categories	Subject Factors	Physical and Environmental Factors	Task Factors	Organizational Factors
Factors	-Visual acuity (Static, Dynamic, Peripheral) -Color Vision -Eye Movement -Inspector-related (Experience, Personality, Intelligence)	-Work-place Lighting -Aids (Magnification, Overlays, Viewing screen, Automatic scanner) -Background noise -Workplace design	-Inspection time -Viewing area -Items complexity -Fault probability, mix, and conspicuity	-Number of inspectors -Feedback -Training -Briefing/instructions -Standards -Cost -Job rotation

A comprehensive study of the accuracy and reliability of routine and in-depth visual inspection for highway bridges has been conducted by FHWA, and a final report of the findings was published on June 2001 (FHWA 2001). Based on Megaw's finding, the factors investigated in the study were summarized into physical, environmental and managerial categories. In this study, 49 inspectors from 25 State agencies performed 10 inspection tasks at 7 test bridges. The final report indicated that: 1) for routine inspections, the condition ratings assigned can vary significantly, and factors that may affect routine inspection accuracy include fear of traffic, visual acuity, color vision, light intensity, inspector rushed level, and perceptions of maintenance, complexity and accessibility; 2) for in-depth inspections, using visual inspection alone can hardly identify specific types of prescribed defects nor reveal deficiencies beyond those that could be recorded during routine inspections, the related factors are inspector overall thoroughness, inspection time, structure complexity and accessibility, viewing of area, flashlight use, and inspection frequency.

One well-known, recent bridge failure is the collapse of I-35 bridge in Minnesota that caused 13 deaths and 145 injuries and happened in August 2007. After a comprehensive investigation, the National Transportation Safety Board (NTSB) announced that this collapse was preliminarily caused by a design flaw related to gusset plates and additional load (i.e., dead load of 2 inches concrete added to deck over the years, weight of construction equipment and material resting on the bridge, and traffic load at rush hour) on the bridge at the time of collapse. The NTSB also determined that bridge engineers and inspectors did not have a system to double check the safety of the bridge (NTSB 2008). To prevent this type of failure, it was concluded that systematic quality control and quality

assurance procedures and/or a closer monitoring of structures should be implemented into the entire bridge management operation and bridge management systems.

In summary, visual inspections operated by bridge inspectors, while remaining essential, have some known limitations. Inspections using visual inspection alone are not likely to recognize unknown reserve capacities nor discover deficiencies that are not visible (e.g. delaminated deck) leaving much uncertainty in the actual condition and performance of existing bridges. It has been advocated for many years that objective in-depth assessment technologies (such as monitoring operational responses and nondestructive tests) should be deployed in conjunction with visual inspection.

Two major areas of research that have been pursued to supplement the qualitative results of visual inspection for the highway bridge assessment system are NDE and SHM. When multiple approaches are used, an integration of the collected data becomes necessary for proper interpretation and decision making. However, effective integration of information collected from different SHM and NDE sources can be very challenging. This research focuses on optimal and practical ways to obtain and integrate measurement data with other proxy information (such as past inspection and maintenance records, traffic information, NBI data, climate and weather data and others) for highway bridge assessment.

2.2 Bridge Assessment Methods

Novel sensing technologies and analytical methods have been developed and applied to identify structural damage in highway bridges. Commonly used strategies fall within the broad paradigms of NDE and SHM.

2.2.1. Non-Destructive Evaluation

While NDE is well established in aerospace and mechanical engineering, its widespread use in bridge assessment is somehow lagging. Approaches used in aerospace are applicable on steel elements of bridges. One of the challenges of NDE for concrete bridge components, is the complexity of the material when compared to metals. It is so primarily due to the composite nature of concrete and the quality that is not easily reproduced during concrete production and placement.

Some NDE technologies currently used in bridge deck evaluation are impact-echo (IE), ground penetrating radar (GPR), electrical resistivity (ER), ultrasonic surface waves (USW) testing, half-cell potential (HCP), imaging, etc. (Gucunski et al. 2010). HCP can detect and characterize active corrosion, and ER and GPR can be used to evaluate potential for corrosive environment. USW detects concrete degradation by quantitative measurement of elastic modulus, and GPR can quantitatively identify concrete degradation by estimating the depth of concrete cover. Delamination detection can be located using IE and GPR, the latter one showing effectiveness in the zones of progressed delamination. A new microwave-based technology, MoistScan, can provide the information about the variability of the moisture content.

For a comprehensive and in-depth assessment, the fusion of information obtained from multiple NDE techniques is required to identify and locate deck deterioration, such as rebar corrosion, concrete degradation, and delamination. Five NDE technologies were applied in (Huston et al. 2011) and studied on the reinforced concrete deck of the Van Buren Road Bridge, and the development of automated multi-sensor systems for data fusion to meet the

increasing demands for highly-efficient, cost-effective and safety-guaranteed inspection and evaluation was discussed.

A robotic platform, the Robotic Assisted Bridge Inspection Tool (RABIT), has been designed and developed by FHWA to characterize common deterioration types mentioned above. The platform implements five NDE technologies: ER, IE, GPR, USW, and high-resolution imaging, and it collects NDE data faster and at higher spatial resolution than traditional contact NDE equipment. The validation and field implementation of IE and USW was conducted by Gucunski et al. on a 9m long and 3.6m wide fabricated bridge structure with various types of artificial defects (Gucunski et al. 2015). In addition, the same research team has conducted a series of NDE tests on several bridges, and the performance of common NDE technologies was assessed (Gucunski et al. 2012; N. Gucunski et al. 2011).

2.2.2. Structural Health Monitoring

SHM is the process of monitoring structures over time based on a combination of real-time or periodic sensor measurements often combined with modeling, analysis, and damage detection algorithms. The stated goal of SHM system is to detect and locate structural damage. NDE can be incorporated into the SHM system to detect hidden defects at the material level and often NDE and SHM intersect. The use of NDE is typically confined to local damage assessment. A more global approach can be achieved with global SHM methods. Although SHM has not been widely adopted to routine bridge monitoring in U.S., many bridges have been instrumented with SHM systems with different purposes to monitor specific damage that affect bridge performance. The damage refers to local or global defects or deficiencies.

The common components of SHM systems shown in Figure 3 are data collection, data processing and interpretation, and condition assessment. The functionality of an SHM system highly depends on the sensor types and the design of the sensor layout, so the design of the sensing system is a critical part of SHM.

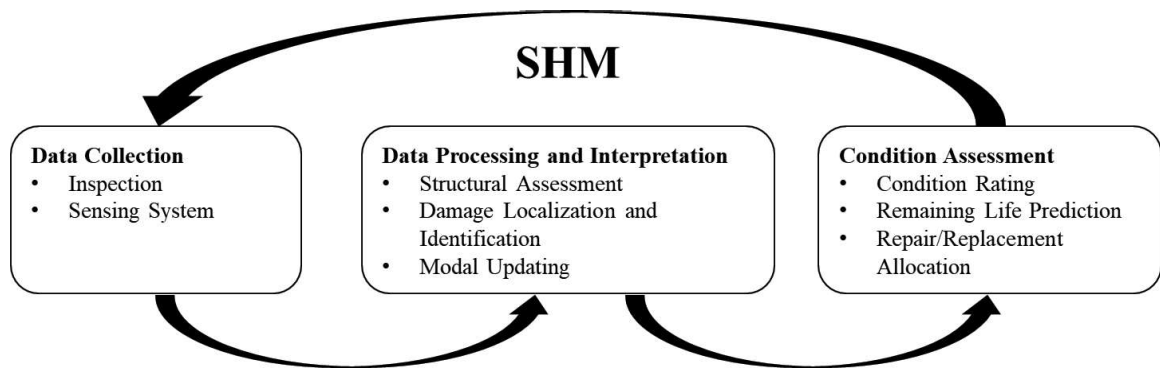


Figure 3. SHM Cycle with the fundamental components

Strain gauges, accelerometers, optical-fiber sensors and other sensing devices have been used in SHM sensing system to measure structural responses (Ko and Ni 2005; Webb, Vardanega, and Middleton 2015). Compared to strain gauges and accelerometers, fiber-optic sensors can provide distributed measurements with strong immunity from electrical noise (Li, Li, and Song 2004). Some other technologies used in the sensing system include global positioning system (GPS) (Cosser et al. 2003), radar-based systems (Guan et al. 2015), video (Chan et al. 2009), and laser-based measurements (Fuchs et al. 2004; Rossi et al. 2002). In most cases, environmental factors that may lead to damage should also be monitored, such as temperature, wind velocity, and humidity. Three key advanced technologies being currently considered in SHM are imaging and computer vision, microelectromechanical systems sensors (Ferri et al. 2011), and bio-inspired sensors (Tata et al. 2009). The imaging and computer vision technologies contain infrared imaging (Washer, Fenwick, and Bolleni 2010), digital image correlation (DIC) (Te, Take, and Olton

2003), and crack width detection and concrete spalling (German, Brilakis, and DesRoches 2012; Kabir 2010).

The other two components are described in the following section, as these components are incorporated into the structural identification process.

2.3 Structural Identification Method

2.3.1 Overview of Structural Identification

Structural Identification (St-Id) leverages civil engineering heuristics and field experiments in conjunction with analytical modeling for reliable estimation of the performance and vulnerability of structural systems (Çatbaş et al. 1998).

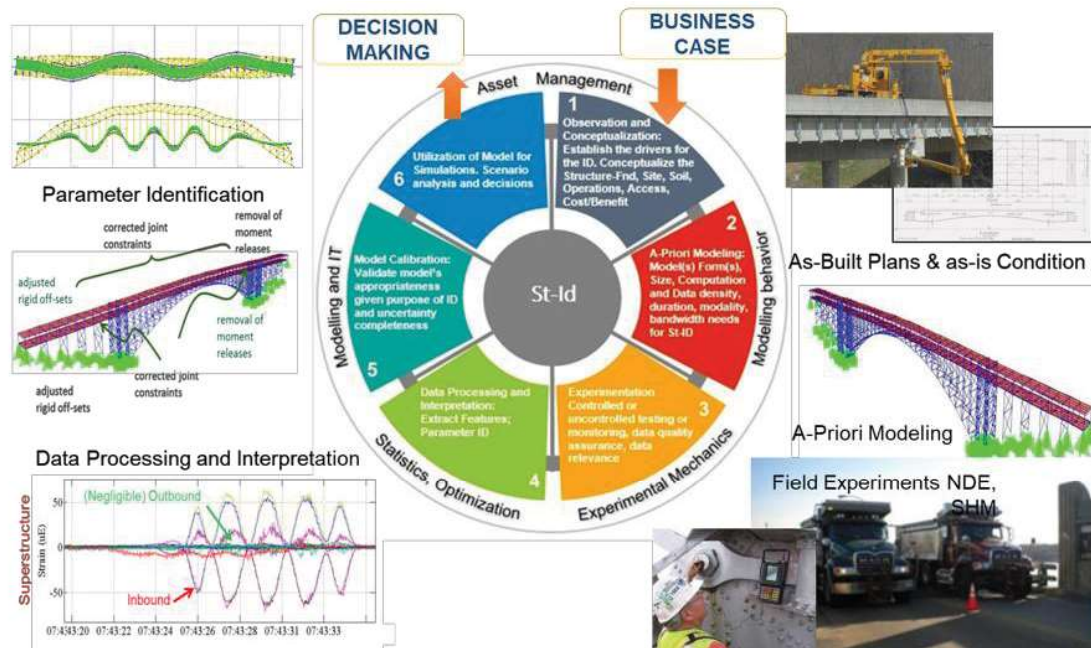


Figure 4. Structural Identification

St-Id, if properly deployed, is a powerful tool bridging the gaps between real structures and models. St-Id has been incorporated to investigate the structural behavior and performance

affected by material deterioration, cracks/defects, rigid body rotation, ect. and for bridge condition evaluation and bridge management.

The six primary steps of St-Id are shown in Figure 4, which have been adopted by the ASCE's Structural Identification of Constructed Systems Committee (American Society of Civil Engineers 2013).

As shown in the figure, the steps are: 1) Observation and Conceptualization: the drivers for Identifications, such as performance concerns, load-capacity rating, maintenance and management are defined here; 2) A-Priori Modeling: develop a-priori model to aid in the selection of experimental approaches, sensors, instrumentation plans for next step; 3) Controlled Experimentation: conduct NDE and structural assessment tests, and ensure the accuracy and reliability of acquired data; 4) Processing and Interpretation of Data: extract features, such as dynamic properties and structural responses, and interpret objective and quantitative data with data reduction, visualization and analysis; 5) Model Calibration and Parameter Identification: evaluate model errors and uncertainties, and identify structural parameters; and 6) Utilization of Model: utilize the calibrated model for simulations, scenarios analysis, and decision making (Catbas and Kijewski-Correa 2013).

The first step of St-Id involves observing all concerns and issues that are driving the application as well as conceptualizing the structure, and advanced tools and technologies such as data mining and computer vision technologies can be employed in this step to improve the efficiency of information collection. To properly guide the application of St-Id, it is critical to identify potential uncertainties associated with loading mechanisms, kinematics, and intrinsic force distribution in this step. In the second step, a priori model (usually an FE model) is created based on the information collected in the first step, and

this model is utilized to provide structural responses to aid in the selection of appropriate experimental approaches, sensors, instrumentation plans which are executed in the following step. For Step 3, although sensing and information technologies have been significantly improved in the last decade, this step still involves making a series of trade-offs to ensure the accuracy and reliability of acquired data without significant cost. The fourth step involves the processing and interpretation of the experimental data. This invariably aims to remove data errors and noise (averaging, windowing, filtering), extract key response indices, and plot such indices temporally, spatially, and versus load position, load level, frequency, etc. to facilitate effective interpretation. Once the data has been effectively reduced and interpreted, the preliminary model is then calibrated in Step 5 to minimize its discrepancies with the experiment. A calibrated model as a product of St-Id can help bridge engineers reduce modeling errors, uncertainties and unreasonable assumptions in the condition evaluation of existing foundations. The general goal of this process is to reconcile the experiment and model to identify and explain the root causes of the observed data/responses. The calibrated FE model can also be used in the Step 6 through scenario analysis, parametric studies, or what-if simulations, to assist risk analysis and bridge management. While St-Id may provide necessary information to the decision-making process, it is not sufficient to provide directly decisions. Further, it is important to recognize that St-Id remains an art and its value depends greatly on the talent, heuristics and insight of those that oversee and direct the application.

These steps require diverse expertise related to civil, mechanical, and computer and electrical engineering in the following aspects: 1) analytical, numerical, and computational modeling; 2) observation and measurement of constructed systems; 3) optimization for

parameter identification; 4) analytical model evaluation and calibration; and 5) asset management (Catbas and Kijewski-Correa 2013). Model calibration and parameter identification proves to be the most challenging stage of St-Id.

2.3.2 The Development of Structural Identification for Bridge Assessment

System identification techniques were first developed and applied in the aerospace and automobile industry to verify and improve analytical models subsequently used in the simulation and design studies of the products. This concept was first introduced as structural identification and applied to civil structures in 1978 (Liu and Yao 1978). After that, the definition and terminology of structural identification was explained by Aktan and Farhey 1996, and available tools and technologies for a successful structural identification of a constructed system were also discussed (Aktan et al. 1996; Lee et al. 1997). With the development of modal parameter extraction methods and model updating algorithms, structural identification has also been used for damage detection and identification.

Mathematical models such as finite element models have been widely used in the process of St-Id to present the properties of structures and to predict its performance for different scenarios. However, such models are created with idealization and assumptions related to the real structure. As a result, significant discrepancies may exist between the model and the actual structure. The uncertainties in such models include measurement errors, modeling errors, and statistical parameter uncertainties. Challenges remain in accurately capturing structure properties to match the model responses with the actual responses. The responses can be presented in different domains, such as time, frequency, modal, and time-frequency domains.

Finite element model updating has emerged in the 1990s as an important subject to the design, construction and maintenance of civil engineering structures (Friswell and Mottershead 1995). Calibrating or updating the preliminary model with experimental results is a critical step in the structural identification process, and the use of the experimental data to verify and validate a model removes some uncertainties regarding the model and the structure (Mottershead and Friswell 1993).

The model updating methods can be generally grouped into two categories: direct updating, and iterative methods. Direct updating consists of correcting the individual terms of the global mass and stiffness matrices and exactly representing the measured behaviors (Friswell, Inman, and Pilkey 1998). The main disadvantage of direct methods is that directly changing mass and stiffness matrices can lead to the loss of the original coordinate connectivity. Because of this shortcoming, the use of direct methods has largely died out. Conversely, iterative methods manually or automatically update model parameters in an iterative manner until the model responses match the measured data to a sufficient degree of accuracy. To determine which parts of the initial models are thought to have been modeled incorrectly, certain parameters associated with significant uncertainty (such as material properties, boundary conditions, connectivity, etc.) should be analyzed and then selected for updating. Sensitivity studies, where the model dependence on such parameters is evaluated, help selecting the most relevant parameters to update. Following that, an objective function should be properly formulated with the relevant parameters to accurately represent the distance between the measured data and the finite element model predicted data. In the final step, an optimization method is leveraged to identify parameters that minimize the objective function. In most cases, a gradient-based optimization strategy will

be used. Both Linear and nonlinear optimization algorithms, such as trust-region-reflective algorithm and genetic algorithm, have been implemented to automatically update the parameters by minimizing the objective function (Bakir, Reynders, and De Roeck 2007; Levin and Lieven 1998; Minshui and Hongping 2008). For nonlinear analysis, more specific methods like response surface modeling, particle swarm optimization, Monte Carlo optimization, and genetic algorithms can be used. Recently, finite element model updating has been conducted using Bayesian statistics which gives a probabilistic interpretation of model updating.

The modal analysis is a useful method for condition monitoring of bridges, and natural frequencies and mode shapes obtained from vibration testing can be used as a diagnostic parameter in structural assessment procedures. Over the past decades, modal analysis has gained global research interests for various types of structures (e.g., single or multiple degree of freedom systems), especially for civil infrastructures which are exposed to dynamic loads and serve an important role in people's daily life (Gentile and Saisi 2007; Hearn and Testa 1991; Ren, Zhao, and Harik 2004; Salawu 1997).

Mottershead and Friswell conducted a comprehensive literature survey of finite element model updating in 1993 (Mottershead and Friswell 1993), which has been used extensively for structural identification. Following that, more technical literature reviews on structural damage identification methods and model updating methods used for the detection, localization and quantification of structural damage were provided by other researchers (Doebling et al. 1996, 1998; Farrar, Doebling, and Nix 2001; Sohn et al. 2004).

A Hierarchical Bayesian model updating approach was proposed by Behmanesh and Moaveni to estimate the inherent variability of structural parameters and implement

probabilistic damage identification of structural systems (Behmanesh et al. 2015). Zhang demonstrated the use of dynamic macro strain measurement from long-gauge fiber optic strain sensors for structural identification on a steel stringer bridge model (Zhang et al. 2015). In 2017, Noël provided a broader perspective to nonlinear system identification by discussing the central role played by experimental models in the design cycle of engineering structures based on a ten-year survey in structural identification (Noël and Kerschen 2017).

Despite these attempts, few studies have used St-Id approaches to estimate the conditions of bridge considering also the conditions of the substructure (such as piers) which are essential characteristics for condition evaluation. In this thesis, structural identification approach is applied to the superstructure and substructure of highway bridges for characterization and condition assessment.

2.4 Technology Integration Strategy

The first challenge in this research consists in designing a rational technology integration strategy incorporating and utilizing possible advanced technology tools in at least four technology domains. The four domains are experimental arts (i.e., civil engineering domain knowledge, structural performance observation and identification, experiments design and execution, sensing and imaging technologies), information and computing technology (i.e., computer vision, machine learning, data mining and information retrieval technologies), simulation and scenario analysis (i.e., FE modeling, structural analysis, uncertainty analysis, and modeling and simulation of complex systems), and asset management (i.e., operational and preservation decision-making, risk analysis, lifecycle benefit/cost analysis,

emergency response system). Some of the technologies that have been used for bridge evaluation are shown in Figure 5.



Figure 5. Current technologies for bridge evaluation

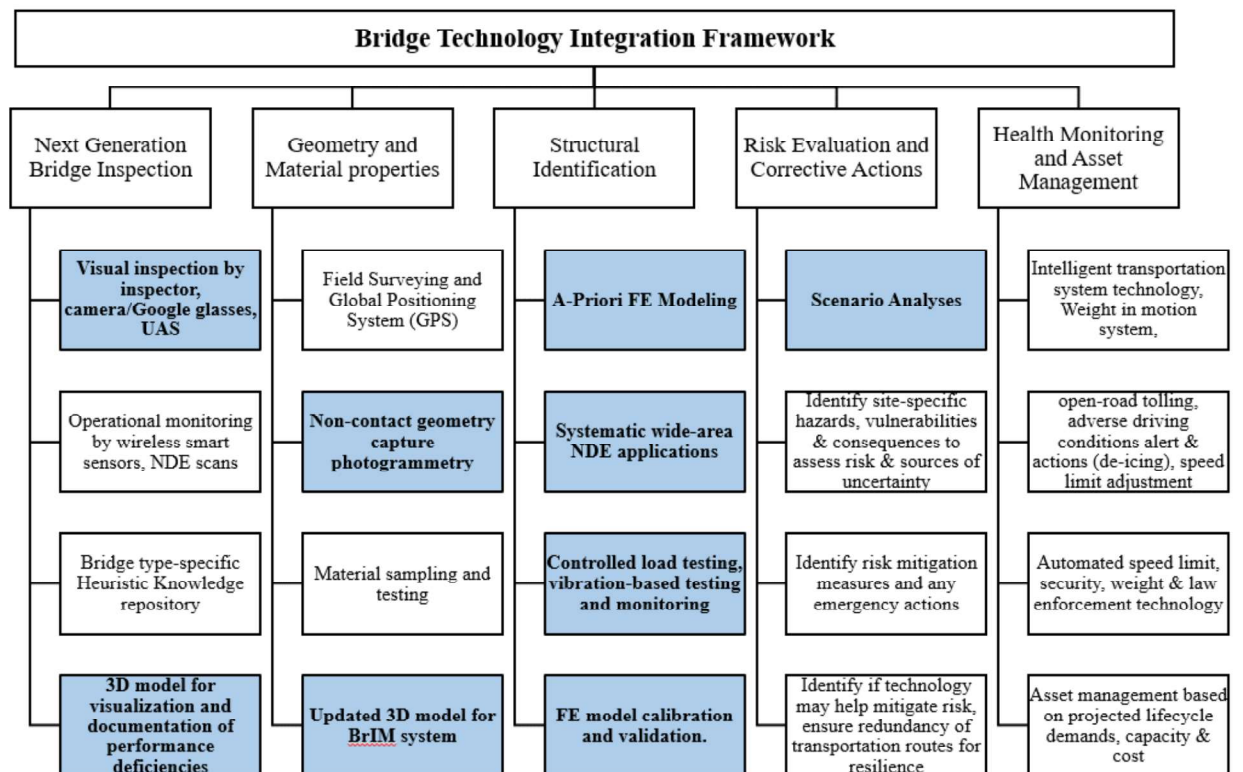


Figure 6. Technology Integration Framework for Bridge Management

Leveraging technologies in the above domains, a tentative framework presented in Figure 6 is proposed to integrate technologies for next generation visual inspection, field measurement, structure characterization, prognosis and risk evaluation, and asset management. The foundation of the strategy is the Structural-Identification principle.

Technologies summarized in Figure 6 are intended for application from top to bottom and left to right for each column. Every step would not be necessary unless a major long-span bridge is being evaluated. To illustrate the proposed integration strategy, a case study is provided and described in the following for a common bridge type. The case study demonstrates the challenges in the integration of data and information available from different technology tools and different domains. Further, the complexity of bridge behavior and performance in mechanistic terms becomes obvious. Without combining “sound” observation-based heuristic knowledge with the mechanistic understanding that is revealed by technology it may not be possible to understand and evaluate health and performance of bridges, especially when they are large and deteriorated.

Chapter 3: Observation and Conceptualization

This chapter and the following chapters present the adoption of St-Id following the six steps to assess the condition of a multi-girder highway bridge leveraging most of the available technologies. A study, named “The International Bridge Study,” took place in 2012-2013 with the participation of experienced bridge engineers and bridge research experts from Japan, Korea, EU (GB, Austria, Switzerland) and the US. The study was funded by the USDOT-FHWA and NJDOT as part of the FHWA’s Long-Term Bridge Performance Study. The International Bridge Study was coordinated by Prof. Aktan and colleagues at Drexel University with participation from Rutgers and Princeton University. The goal was to explore worldwide “best practices” for technology application that were considered ready for deployment and explore integrating and leveraging these technologies for bridge condition and performance evaluation and maintenance.

The candidate bridge was evaluated in terms of feasibility, relation to the overall bridge population and potential return on investment. The structure and site are analyzed considering access, testing and modeling and a set of critical questions regarding the structure are developed.

3.1 Bridge Selection

A bridge that is in service with a variety of performance concerns, the root causes of some of which cannot be identified just by heuristics, was sought as a case study for a demonstration of technology integration. The selected bridge (see Figure 7) was selected as case study by the New Jersey Department of Transportation (NJDOT) bridge engineers based on five aspects: the commonality of the bridge type, the availability of

documentation, the ease of access, the significance of inspection and maintenance challenges, and a variety of performance concerns.

The structure, a multi-girder steel stringer bridge carrying a major route (US202/NJ23 through Wayne, New Jersey) with over 90,000 annual average daily crossings with 4-5% trucks, was built between 1983 and 1984 and was 30 Years old at the time of the study. The bridge exhibited many performance concerns some of which were included in a recent inspection report by a professional engineering consultant. Inspectors had assigned a Condition Rating of Fair (5) to the superstructure (in reference to fatigue cracks in the webs of various steel girders, and settlements and drifting of the approach slabs due to fill erosion), and Satisfactory (7) for the substructures. Several additional critical performance concerns were observed that were not noted in the inspection report. The test bridge served as an excellent test specimen for exploring answers to the research objective questions as well as the broader concerns and questions in the introduction.



(a)



(b)

Figure 7. US202/NJ23 four-span highway bridge. (a)Field view of the bridge; (b) Bridge location in google maps (marked with red star).

3.2 Bridge Description

The bridge consists of two parallel structures (southbound and northbound), four spans per structure. Each span is about 62 feet wide simply-supported by 8 steel girders spaced 8 feet apart. The girders rest upon two concrete piers, except for the edge spans (Span 2 and Span 4 in Figure 8) that rest on a pier on one side and on reinforced concrete abutment on the other side. The total maximum length of the bridge is 450 feet.

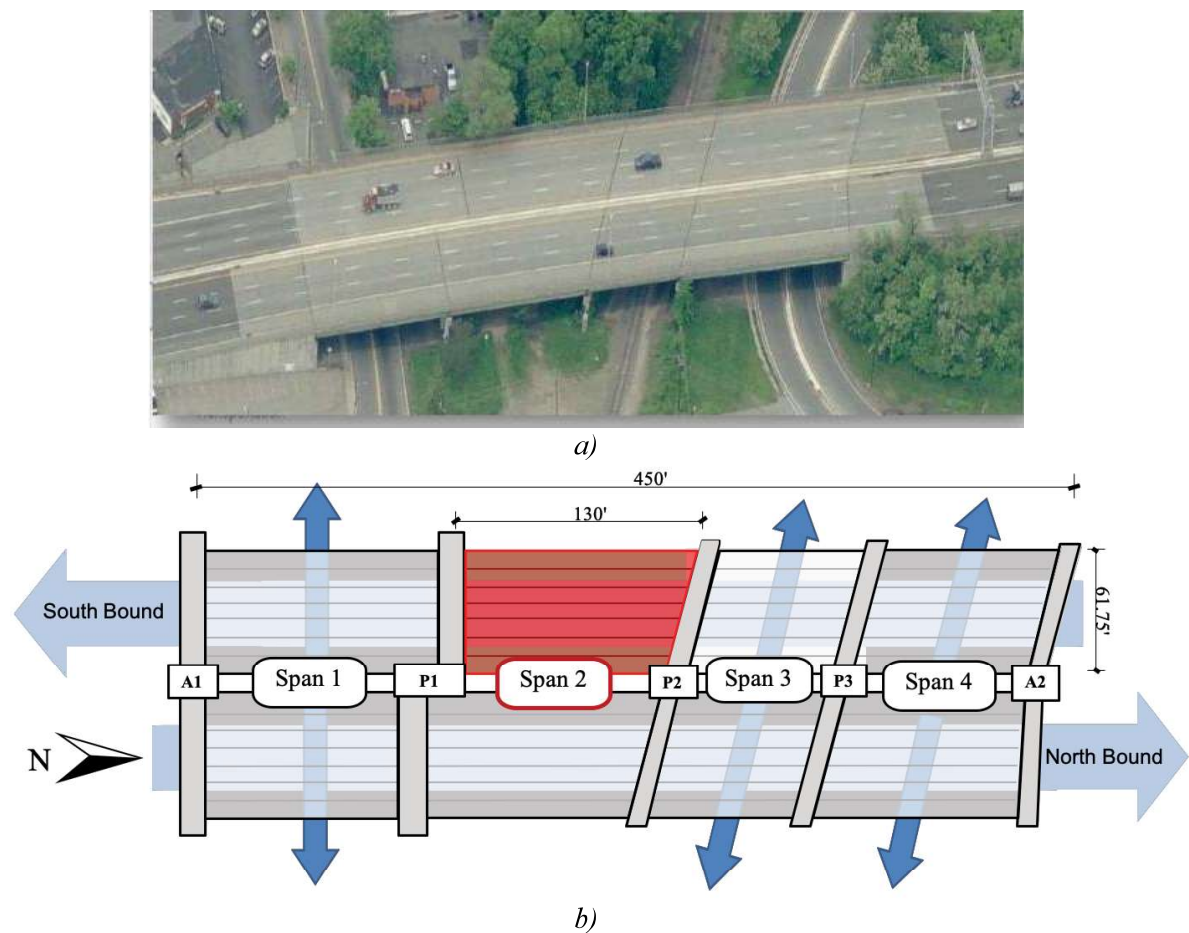


Figure 8. The selected bridge: a) view from Google Maps; b) site layout with Span 2 Southbound Highlighted

The bridge is a very heavily used bridge at all times during the day and night and serve a considerable number of trucks. The southbound direction has a total of four traffic lanes

and a sidewalk, and the details of the support structure at Pier 1W (which is P1 of the Span 2 southbound) is shown in Figure 9. Nominal simple support conditions for the spans are intended to be achieved by complex steel bearings. The spans are mechanically separated but rest on the same pier crossbeam.

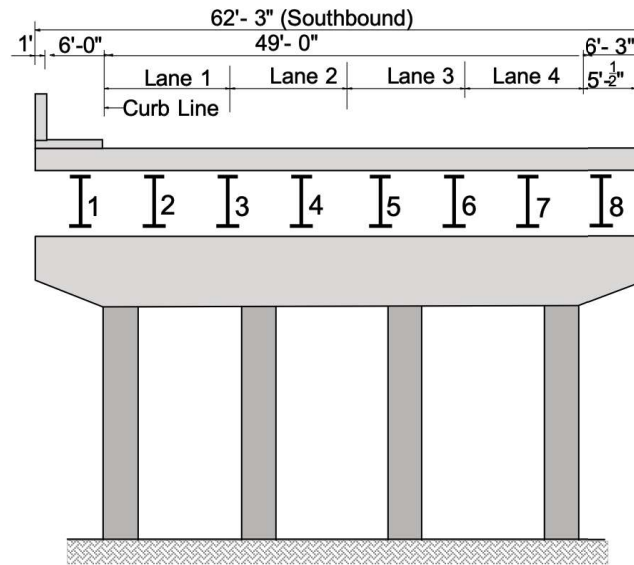


Figure 9. Pier 1W (View from South to North)

Span 2 Southbound (SB) (see Figure 8) was tested by most of the IBS groups due to its skew shape, high vibrations and because it was exhibiting every one of the performance concerns. Structural Assessment and Health Monitoring technologies applied in this case study included ambient vibration testing, forced dynamic excitation testing, controlled static load testing. Different sensing systems were deployed to capture static as well as dynamic deformation including laser tracking devices. While most of the testing was performed over short periods of time (1-2 days maximum), fiber optic sensing allowing long-term monitoring were also installed.

3.3 Performance Concerns

Fatigue cracks in the webs of the main beams adjacent to the gusset plates connecting the lateral “wind” bracing were observed by bridge inspectors starting in 2004, and this issue was addressed by drilling holes and installing bolts to arrest the cracks. According to the 2008 inspection report, the previously arrested cracks were investigated by dye penetrant testing and found that they had not progressed past the drilled hole. However, many new cracks were identified. 2 to 7-inch settlements of the approach slabs due to erosion of the abutment fill were reported. Additionally, the report noted bearing and joint deterioration and mentioned heavy vibration of the bridge under traffic loads.

The performance deficiencies that were noted by the inspectors were the settling and drifting of the approach slabs which caused a significant bump affecting the traffic entering and leaving the bridge, and, the progression of the fatigue cracks that formed at the webs of the outermost steel girders to which wind braces were connected as shown in Figure 10. The causes for these performance deficiencies were stipulated – the bridge was not designed properly for drainage, and rainwater seeping through the failed joints gradually washed out and eroded the fill under the approach slabs and abutments. Consequently, the approach slabs settled and drifted away from the bridge as shown in Figure 10(e).

The fatigue cracks were attributed to the localized lateral distortions at the girder web caused by the wind brace elements that were directly welded to the web. Due to significant lateral vibrations of the superstructure (discussed further in the following) the fatigue cracks continued to form and propagate. During earlier inspection cycles, the inspectors recommended drilling holes and inserting bolts at the ends of these cracks to try to stop their propagation. However, this did not stop new cracks forming.

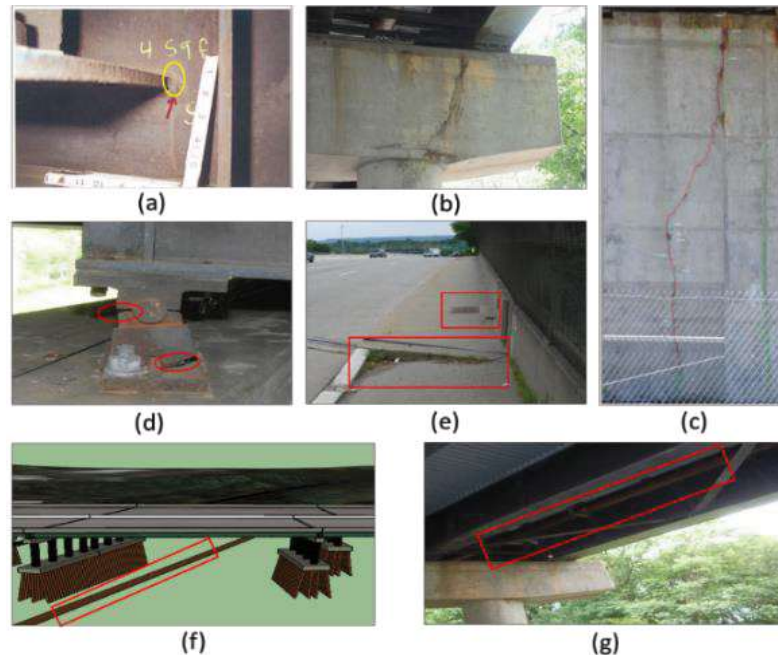


Figure 10. Examples of performance concerns: (a) fatigue cracking at girder web, (b) pier 1 cap cracking, (c) cracks on the abutment, (d) damaged bearing, (e) insufficient drainage damage, (f) water main crossing the bridge, (g) gas pipe.

There were additional performance concerns that were observed but were not referenced in the inspection report: (1) significant vertical vibrations exceeded 20%g under truck traffic; (2) the deck exhibited full width cracks along the span; (3) there was a wide shear crack at the cantilever extension of the pier cap, under the South end of girder one, as shown in Figure 10(b). Of the 4 pier-cap extensions at each end of the span being studied, as well as at any of the other spans, only one pier-cap exhibited such a crack; (4) joints between the simple spans had failed and rain-water draining through these joints severely corroded the bearings. In addition, the plates guiding the rocker bearings are damaged as the bearings were trying to move diagonally due to the asymmetric geometry; and, (5) a natural gas pipe ran under the superstructure while a water trunk line crossed the subgrade

within the pier foundations. It should be noted that the gas pipe was being affected by the vibrations of the bridge.

Whether the FAIR (5) condition rating of a 30-Year old bridge on a major artery serving over 100,000 vehicles per day - a substantial part of which was truck traffic - and with a multitude of performance deficiencies is acceptable should deserve further discussion. It is noted that the bridge conditions may have been better characterized with a lesser rating such as (4) indicating the bridge as structurally deficient (mainly due to pier-cap shear crack) and including it in a retrofit program. On the other hand, the need for retrofit of a bridge that is only 30 Years old, due to design, construction and possibly maintenance errors, would reflect poorly on any agency.

While the likely causes of some of the performance deficiencies could be identified by experienced bridge engineers based on heuristics, the causes for the unusual level of vibrations, deck cracking and especially the single pier-cap shear crack were difficult to explain. A structural identification study was carried out to explore if simulations can help explain the causes of distresses.

Although these performance concerns were observed during visual inspection, the root causes of some issues (such as bearing failures and vibrations) remained unknown. Identifying root causes of certain performance concerns using solely visual inspection requires extensive heuristic knowledge that only rare experienced bridge engineers possess. IBS researchers concluded that the fatigue issue was induced by vibration of the lateral bracing (bridge vertical and lateral vibrations were found to be highly coupled) and due to the differential deflections of girders. Although the fatigue cracks appeared to be the main

concern for bridge inspectors, several additional concerns were identified which were not recorded in the bridge inspection reports (Figure 10).

The next step of an assessment requires identifying potential risks based on the observed performance concerns. Relative risk of disutility of a structure should be analyzed under four lifecycle limit states (Chase et al. 2016): utility and functionality; serviceability and durability; life-safety and reparability; and resilience (Table 2).

Table 2. Performance Concerns Under Performance Limit States

Limit States	Performance concerns
Operational and functionality	-Insufficient Drainage
	-Bump at approaches
	-Approach slab movement and settlement due to fill erosion
	-Excessive vibrations
Serviceability and durability	-Joint failures
	-Bearing corrosion
	-Cracking of abutment and piers
	-Utility pipe (gas, water)
Safety and Failure Mode	-Fractured and damaged bearings
	-Pier cap cracking
	-Fatigue cracks on girder webs
	-Major link to GWB to NY city and NE
Resilience	-Major consequences to large number of users and to regional GDP if closed

These are universal limit-states for any constructed system and are not yet adopted by AASHTO documents which consider Strength, Serviceability and Fatigue as the critical

Limit-States when evaluating bridges. Table 2 shows how the performance concerns were classified under four performance limit-states. Scenario analyses for designing measures to correct performance concerns should be executed accounting for these performance limit states.

3.4 Bridge Information Modeling

Building Information Modeling (BIM) is a popular concept that has been developed and adopted in architecture, engineering, and construction industries for decades, and the National BIM Standards provides consensus-based standards through referencing existing standards, documenting information exchanges and delivering best business practices for the entire built environment. The Bridge Information Modeling (BrIM) Standardization has been provided by FHWA in 2016, and information models of two case study bridges were developed using several schemas: Industry Foundation Classes (IFC), LandXML, and OpenBrIM (Chipman et al. 2016). Although the Bridge Information Modeling (BrIM) has gained increased attention and the BrIM Standardization has identified and evaluated candidate open standards for BrIM, there is no common way to integrate information from different sources and benefit the inspection, maintenance, and operational phases associated with its asset management.

Based on the technology integration strategy proposed in Chapter 2, a BrIM model is developed to efficiently visualize the bridge information with advanced computer-aided modeling and analysis tools and techniques for highway bridge management.

A 3D geometric model is first created in Sketchup, and then imported to Cl3ver which is a web-based application delivering dynamic interactive 3D presentation to users. Menus and

events are created for efficiently view and interact with the model. Results of visual inspection, experimental tests, and simulations are organized and interpreted into the model, so researchers, engineers and managers can be familiar with the features and issues of the bridge in a short time through interaction with the model.

Screenshots of the user interface of this model are show in Figure 11.

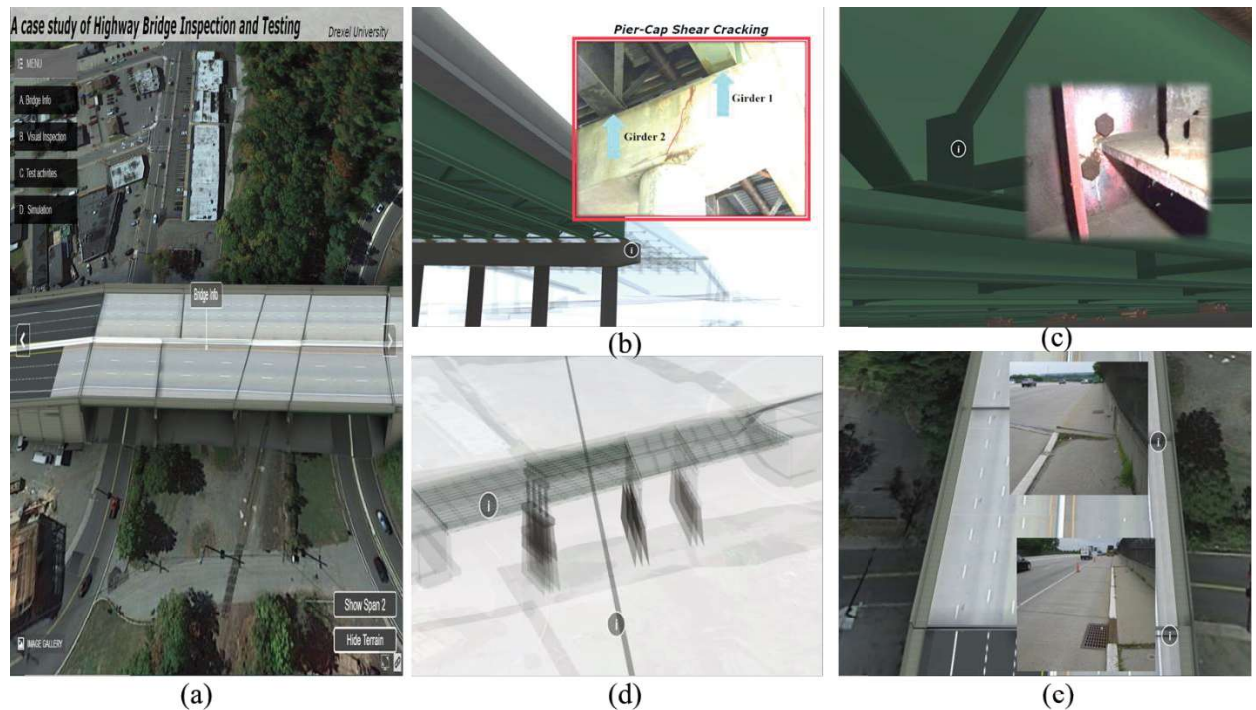


Figure 11. BrIM model of IBS bridge in Cl3ver Software

In Figure 11(a) the Home page of the application is presented with menus and buttons giving access to an image gallery of photos collected in the field from different views, highlighting the test area (Span 2 SB); the model of the structure can be seen also by hiding the background obtained directly from Google Earth. As discussed, the 3D visualization interface can be used to rapidly access images of critical elements such as the pier-cap shown in Figure 11(b); the images are provided together with the 3D model that is oriented in views that are consistent with the photo of interest. Similarly, Figure 11 (c) shows how

cl3ver provides a photo and location of the fatigue cracking at the juncture between wind bracing and girder web.

An X-ray view of the model allows the user to highlight other major concerns such as utilities carried by the bridge (a deteriorated gas pipeline) and crossing the structure such as an underground water main shown in Figure 11(d). Figure 11(e) provides two photos of insufficient drainage added to the corresponding location.

Virtual Reality (VR) and Augmented Reality (AR) technologies have rapidly advanced in the past few years, and several commercial applications have been developed and used in the field of Architecture, Engineering and Construction (AEC). The concept of VR refers to an interactive computer-generated experience in which users are surrounded by a simulated 3D representation and can perform operations in the virtual world.

From the perspective of the BrIM system, VR or AR can be viewed as means to improve the visualization and interaction of the model. After a quick overview of all the available VR tools, two tools, Modelo and Kubity, are selected and tested for the VR representation of the 3D SketchUp Model. The 3D SketchUp model is first imported into Modelo and Kubity, and then the model can be visualized on Modelo or Kubity mobile app with Cardboard or VR headsets. The Screenshot of bridge model in VR view on Modelo mobile app is shown in Figure 12.



Figure 12. Screenshot of bridge model in VR view on Modelo mobile app

Chapter 4: A-Priori Modeling

This chapter presents the details of the development and application of an a-priori model of the bridge, including the purpose of a-priori modeling, selection of software, model geometry, material properties definition, and investigations of modeling techniques.

4.1 Purpose of A-prior modeling

The use of a-prior models is of significant importance at initial steps to provide an understanding of bridge behavior and an estimate of bridge response quantities, and assist in identifying structural parameters and critical members, to guide the experimental sensor locations, and interpreting experimental data.

Many uncertain parameters that will affect the output of field experiments should be considered before conducting experimental tests, and these parameters include material properties, boundary conditions, composite actions and continuity conditions. To identify these parameters, an a-prior model is very critical in the St-Id process considering the complexity of the bridge.

For vibration-based experiments, the a-prior model will be able to provide a preliminary estimate of modal parameters and then help determining the bandwidth and sensor layout for the design of the experimental program.

For controlled load test, a-prior modeling can assist in the selection of loading locations and displacement and strain gauge installation locations although the final decision highly relies on the real condition of bridge, budget constraints, and traffic control. Most importantly if the model is properly created and analyzed, it can at certain point ensure the safety of the bridge under different load levels.

4.2 The development of an a-prior mode

An a-prior finite element model is established first based on the design drawings, and then refined and adjusted according to the real condition of the bridge. The selection of model resolution should be decided at the beginning in order to obtain reliable results and can be further calibrated and utilized throughout the whole process.

Obviously, a high-resolution model would be desirable. However, there is a trade-off between the model resolution and the time spent on the development and analysis. In most cases, at the first stage, time constraints do not permit the development of a very high-resolution model. Thus, the a-prior model may be a simplified and crude model at the beginning, and then be refined following the next steps of St-Id.

For the selected bridge, the a-priori model only includes the test span (Span 2 southbound), and it consists of superstructure and substructure with geometric simplifications. Although substructure/foundation is included in the initial model, the preliminary analysis is only based on the superstructure. The boundary conditions for the superstructure are assumed ideally simply supported with pin and roller supports at each end.

ABAQUS, which provides powerful solutions routines for sophisticated engineering problems such as dynamic vibrations, was selected for the development of the model. The software can also seamlessly interact with computational software packages such as MATLAB and support a wide range of user subroutines (written in Fortran, C, or C++). It also includes a built-in python API that offers pre-processing and running simulations, and post-processing and extracting results from Abaqus output database.

Benchmark Study for Element Type and Mesh Size Selection

To better determine the element type and mesh size for the deck and girders, a simply supported composite beam (see Figure 13) was studied using different element types.

4.2.1

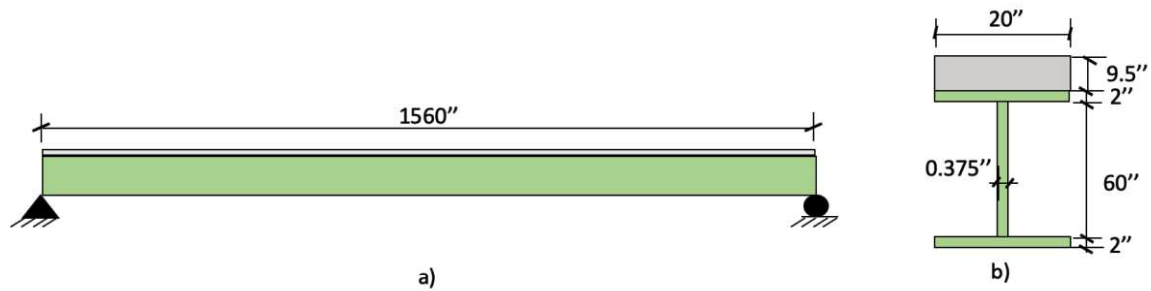


Figure 13. Simply supported composite beam a) side view of the beam; b) beam cross section

The length of the beam is 130 feet, and the dimension of girder is the same as one of the girders of Span 2. It is simply supported by pin and roller supports. The Young's modulus of the concrete deck is 3,000 ksi, and the Young's modulus of the steel girder is 29,000 ksi. The thickness of the deck is 9.5 inches which is the same as that of the Span 2 deck. The width the deck is the same as the width of the top flange which is 20 inches. The composite action between the girder and deck is assumed as fully composite. To compare the finite element model results with hand calculation results, a distributed surface load of 0.01 lb/in^2 was applied to the surface of the deck for the analysis of displacements and stresses under uniform load.

Three finite element models were created for the beam: 1) Model 1 with solid elements for deck and girder; 2) Model 2 with shell elements for deck and girder; 3) Model 3 with shell element for deck and beam element for the girder. Mesh density analysis was performed

on the solid element model, and the max displacements and stresses under uniform load obtained from 9 models with different mesh sizes are shown in Figure 14.

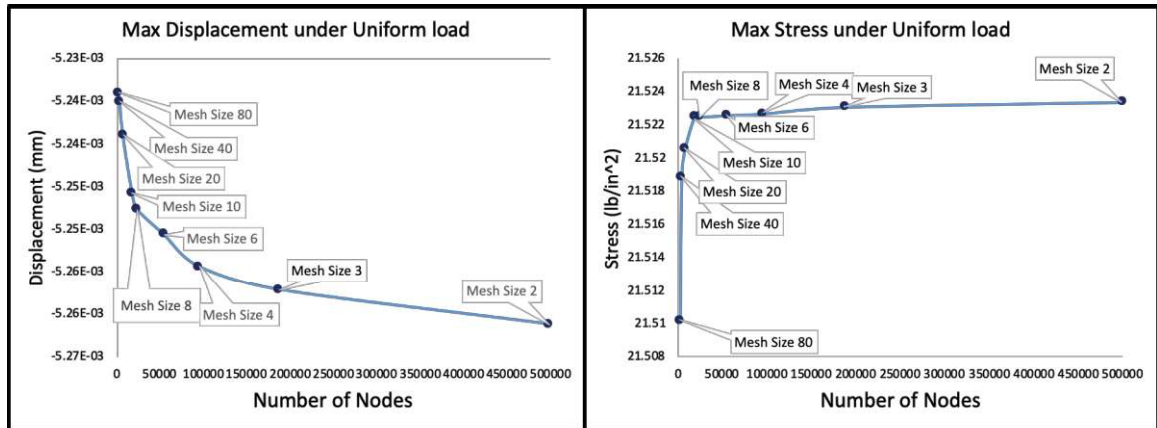
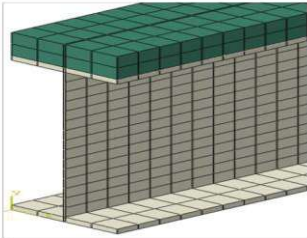
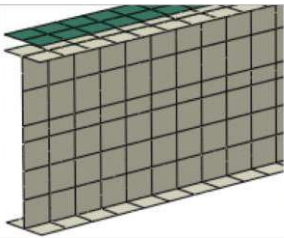
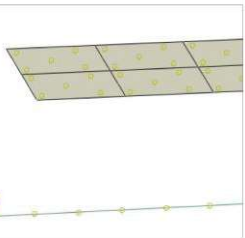


Figure 14. Mesh density analysis of solid element model

Based on the mesh density analysis, 4 inch was selected as a satisfactory mesh size, and the details of each model is summarized in Table 3.

Table 3. Finite Element Models of Composite Beam

FE model Info	Model 1 - Solid	Model 2 - Shell	Model 3 - Shell and Beam
			
Deck	Solid element	Shell element	Shell element
Girder	Solid element	Shell element	Beam element
Number of Nodes	94943	40238	8598
Number of Elements	13650	12870	2732
Element size	4inch * 4inch	4inch * 4inch	4inch * 4inch

The hand calculation for the displacements and stresses was based on Euler-Bernoulli beam theory and Timoshenko beam theory. Unlike Euler-Bernoulli beam theory, the latter also

accounts for shear deformation and rotational bending effects resulting in a larger deflection under a static load.

The max displacement of a simply supported beam under uniform load is located at mid-span, and Eq. 1 and Eq. 2 are equations to calculate the max deflection.

Euler-Bernoulli beam theory:

$$\delta_{max} = \frac{5wl^4}{384EI}$$

Eq. 1

Timoshenko beam theory:

$$\delta_{max} = \frac{5wl^4}{384EI} + \frac{wl^2}{8GA_s}$$

Eq. 2

where δ_{max} is the max displacement of the beam, w is the distributed uniform load, l is the length of the beam, E is Young's modulus of the beam, I is the moment of inertia, G is the shear modulus, and A_s is shear area.

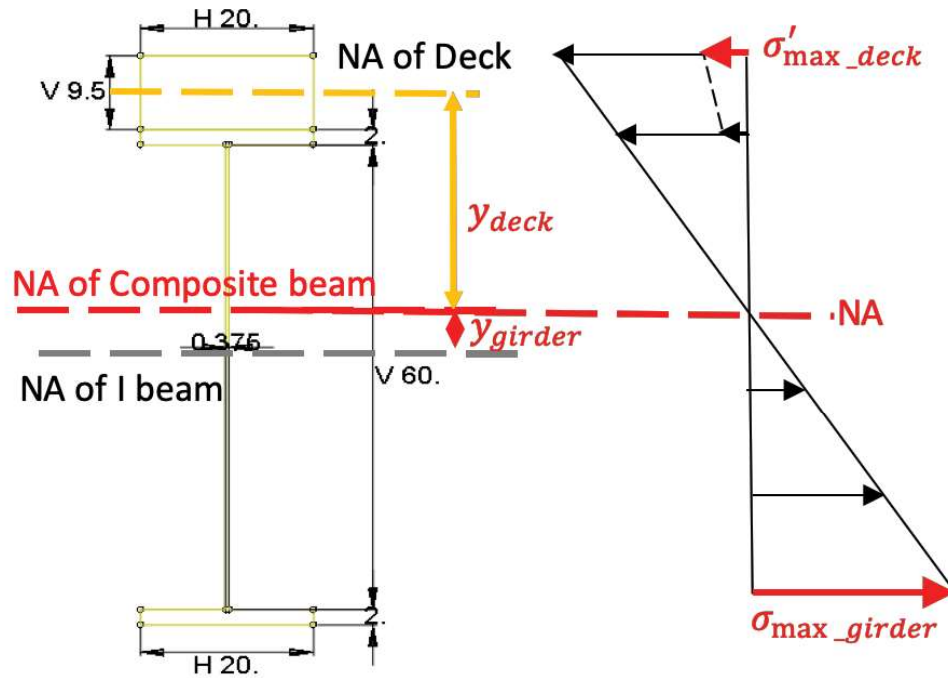


Figure 15. Stress analysis of the composite beam

The equations used to calculate the max stress are the same for both theories, and the equations including the calculation of the neutral axis (NA) for the composite beam are listed as follows.

$$\sigma = \frac{M_{max}y}{I} \quad \text{Eq. 3}$$

$$M_{max} = \frac{wl^2}{8} \quad \text{Eq. 4}$$

$$\sigma_{max_girder} = \frac{M_{max}y_{girder}}{I} \quad \text{Eq. 5}$$

$$\sigma'_{max_deck} = \frac{M_{max}y_{deck}}{nI} \quad \text{Eq. 6}$$

$$n = \frac{E_{steel}}{E_{concrete}} \quad \text{Eq. 7}$$

Where σ is the normal stress at location y , y is the distance to the neutral axis of the composite beam shown in Figure 15, M_{max} is the maximum moment of the beam, σ_{max_girder} , σ'_{max_deck} are the max normal stresses of steel girder and deck, y_{girder} , y_{deck} are the distance between neutral axis of girder, deck to the composite beam. σ_{max_girder} , σ'_{max_deck} , y_{girder} , y_{deck} are shown in Figure 15.

The deflection shapes under the distributed load are shown in Figure 16, and the comparison of maximum displacements and stresses for the hand calculation and finite element models are summarized in Table 4. It is notable that the maximum displacements obtained from Model 2 and Model 3 is very close to the result of Timoshenko beam theory, and the differences in stress are in a reasonable range (the maximum difference is at girder top flange with 1.63 psi difference).

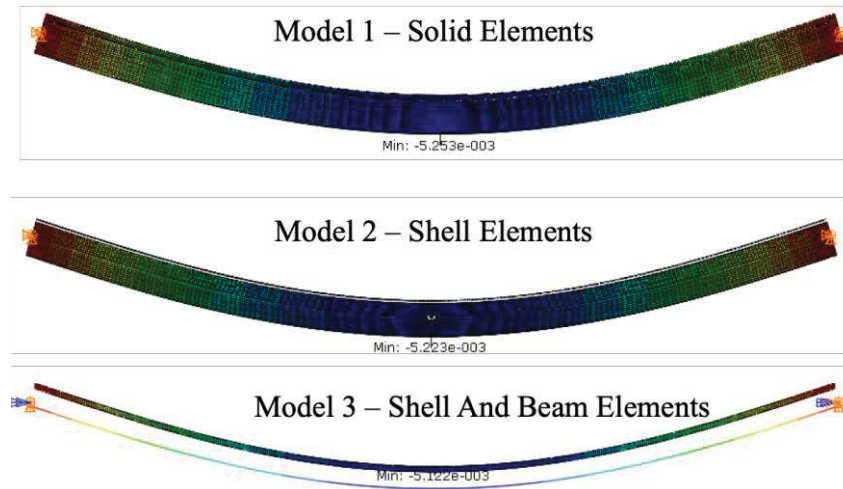


Figure 16. Deflection shapes of the finite element models

Table 4. Results comparison for hand calculation and finite element models

Methods	Max Displacement (inch)	Max Deck Stress (psi)		Max Girder Stress (psi)	
		Top	Bottom	Top	Bottom
<i>Theory-EB</i>	5.01E-03	-2.11	-1.55	-16.54	21.74
<i>Theory-TM</i>	5.22E-03	-2.11	-1.55	-16.54	21.74
<i>Model 1</i>	5.25E-03	-2.14	-1.53	-15.00	21.78
<i>Mode 2</i>	5.22E-03	-2.12	-1.52	-14.91	21.60
<i>Model 3</i>	5.12E-03	-2.11	-1.55	-14.97	21.75

Based on the Table 4, the element type of Model 2 which used shell elements for both deck and girders was selected for the modeling of the selected bridge. To save up computing time, the mesh size of most parts was set to 10 inches, and the mesh size of critical members and areas was set to 4 inches to 6 inches according to the dimension of the elements.

4.2.2

Parameter Selection and Model Information

A 3D full-scale model of Span 2 southbound was created in ABAQUS/standard version 6.14 (see Figure 17), and different types of elements were utilized to build the model of the steel multi-girder highway bridge. The reinforced concrete deck is located on the eight steel girders connecting by shear connectors, and girders are supported by two capped concrete piers and foundations. These components were modeled in ABAQUS separately, and then assembled together. Deck, girders, and stiffeners were modeled with S8R shell elements, cross frames and shear connectors were modeled with B32 beam elements, and cap, piers, foundation were modeled using C3D15 continuum solid elements. The span is simply

supported at the ends of the girders on fixed bearing and rocker bearings. One side of the bearings was modeled as pin restraints that restrain all the three translational degrees of freedom, while free the three rotational degrees of freedom. The other end of the bearings was modeled as roller restraints that restrain the vertical and transverse translational degrees of freedom.

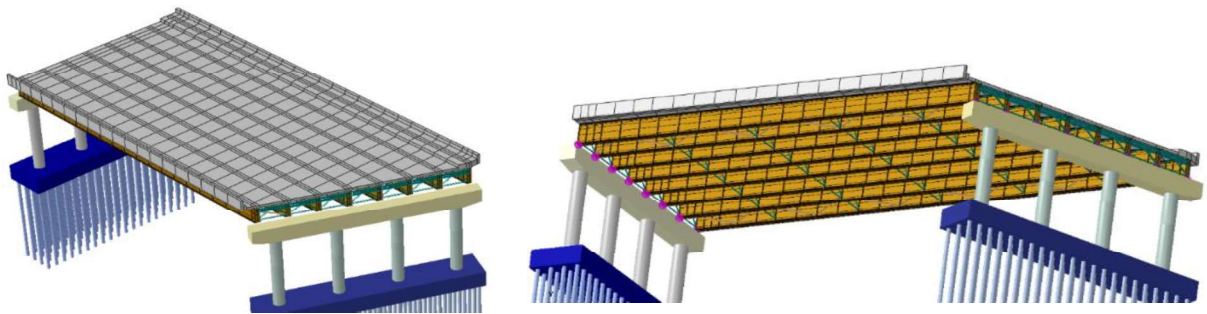


Figure 17. Two views of the a-prior model in ABAQUS

The model information of critical superstructure elements (such as deck, girder, cross frame, and wind-bracing) is shown in Figure 18. The length of the deck of Span 2 Southbound is 130 feet along the longer edge and 103.5 feet along the shorter edge. The parapet, barrier and curb are connected with deck according to the design drawings, and these parts are modeled as shell elements. The deck thickness is 9.5 inches, the curb is 6 feet wide with 7 to 9 inch thickness, the parapet is 1 foot wide with 2 feet and 3 inches height, and the barrier is 6 feet wide with 2 feet and 8 inches height. The model information for girders, bracing, and cross frame is shown in Figure 18.

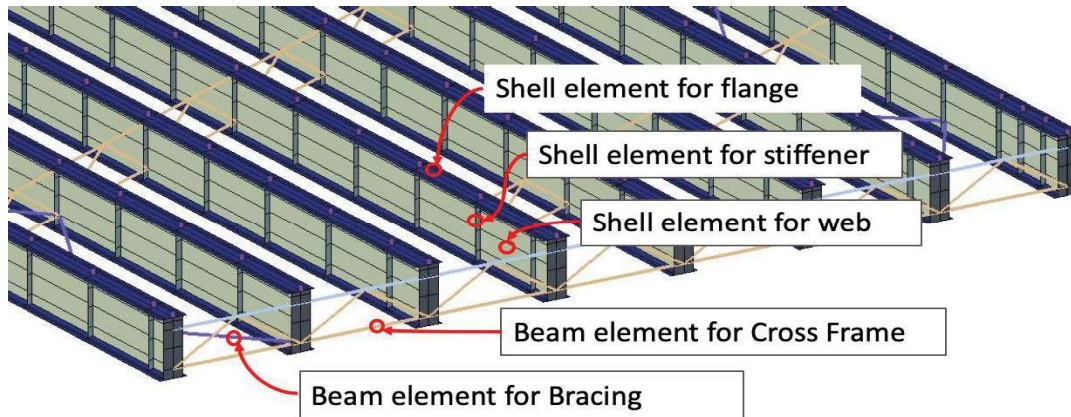


Figure 18. Finite Element Modeling of Girders and Bracing/Cross Frame

According to the engineering drawings of the bridge, the ASTM A36 steel was used as the structural steel, and concrete in structures has an ultimate compressive strength of 3 ksi. The material properties used in the FE model are listed in the Table 5. The composite action between girder and deck is assumed fully composite.

Table 5. Material Properties used in the A-Priori model

Parameters	Steel	Concrete
Density (lbf s ² /in)	7.35E-04	2.25E-04
Young's Modulus (psi)	2.90E+07	3.32E+06
Poisson's ratio	0.26	0.2

It is necessary to do model error screening to check for common human errors associated with model construction before using the model for analysis, such as member connections and material properties definition. The error screening can be conducted by running simple static or dynamic analysis to verify the output obtained from the model by comparing with the theory output. The static analysis allows for the verification of

reaction equilibrium, and the examination of load distribution and load path to detect duplicated members or disconnected elements. The deflection shapes under static loads and the mode shapes from the modal analysis also provide insights into the continuity and support conditions to reveal disconnected and unsupported members.

4.3 Preliminary analysis and results

The natural frequencies and mode shapes of Span 2 Southbound were obtained using the a-prior model (Figure 19).

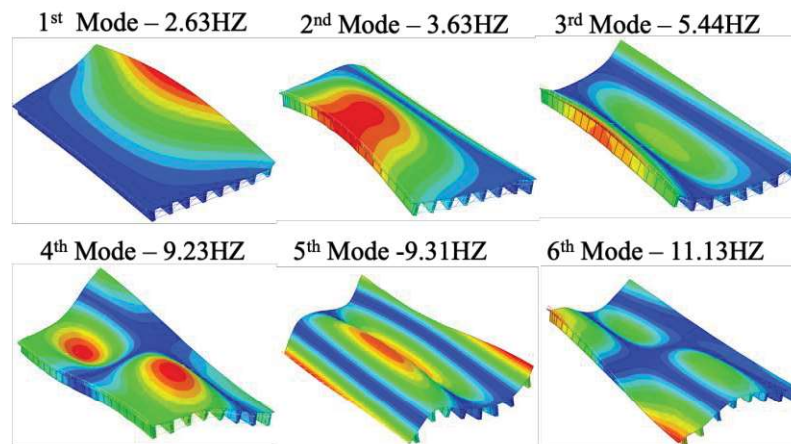


Figure 19. Frequencies and Mode shapes from the a-prior model

Since the experiments will primarily focus on vertical responses of the bridge which have a significant contribution to modal flexibility, the first 6 modes are represented in Figure 19 after filtering local modes and modes associated with transverse responses. The first 6 modes are within the range of 0-20 HZ. The primary mode shapes provide good guides for the design of the instrumentation plan and impact excitation input points.

Chapter 5: Controlled Experimentation and Data Processing

The access to the bridge and traffic control were provided by NJDOT. The experimental program that was carried out by various participants on the Southbound Span 2 is outlined in Table 6. Although some teams focused on the Northbound spans, the South-bound Span 2 (Figure 8) of the bridge offered greater challenges due to its asymmetric skew geometry, high vibrations observed and the pier-cap support showing a shear crack.

Table 6. Summary of Tests Conducted by Different Groups

Test Type	Time	Team	Location	Sensors (Equipment)
Ambient Vibration Test	April 2010	Drexel University	Span 1-4	Accelerometer (31 PCB 393C)
	Sep. 2010	Austria (VCE)	Span 1-4	BRIMOS Sensor
	July 2010	University of Sheffield	Span 1,2,3	Wireless sensors (outer 41 nodes=123 channels) and wired accelerometers (inner)
	June 2011	Utah State University	span 1-4	20 sensors. Sensor: Sercel L4C 1.0Hz. Seismometer
	2010	KEC & Sejong University, Korea	Span 2	15 Accelerometer (Model 393B12 (PCB))
Forced Excitation Test	June 2011	Drexel University	Span 2	Accelerometer, Impulse Hammer, Load Cell, NI cRIO (Hammer test)
	July 2010	University of Sheffield	Span 1,2,3	Wireless sensors (outer 41 nodes=123 channels) and wired accelerometers (inner)
Controlled Load Test	Sep. 2010	Drexel University	Span 1 & 2	Strain gages, displacement gages
NDE Deck Scanning	June 2011	Rutgers University	Span 1-4	IE, ER, HCP, USW, GPR
Long-term Monitoring	2011-2016	Princeton University	Span 2	Fiber Bragg Grating (FBG) Sensors

The ambient vibration testing measured selected displacements, strains and accelerations under traffic load and ambient vibrations. The forced excitation testing measured accelerations under controlled dynamic input induced by an instrumented impact hammer or shakers. Controlled load testing measured changes in displacements and strains of the

structure under a controlled static load induced by placing loaded trucks at various configurations. Tests were performed primarily using contact sensors (accelerometers, displacement gages, strain gages) with the exception of an operational vibration test where University of Western Michigan demonstrated the use of laser tracking to measure displacements due to moving traffic.

A fiber optic based long-term monitoring system was deployed by Princeton University to record strains and temperatures under traffic loads during the period 2011-2016. Finally, wide-area non-destructive testing (NDT) scans were conducted by Rutgers University as well as KEC to evaluate the condition of the bridge deck and the cracked pier cap respectively, identifying surface and subsurface defects and assessing delamination, concrete modulus and rebar corrosion activity.

5.1 Vibration Testing

Ambient and Forced Vibration methods have been widely used to extract the natural frequencies and mode shapes of bridges. Ambient vibration refers to the vibration of structures excited by environmental or vehicular inputs. Ambient vibration testing become especially valuable when long-span bridges or other massive structures cannot be excited with conventional excitation techniques such as shakers or controlled impacts. When budgetary constraints preclude the cost of access and traffic control, ambient vibration testing can provide a rapid and relatively in-expensive and non-obtrusive method for identifying the modal properties of a structure, in addition to characterizing the response, due to the operational inputs. The key is in the bandwidth and duration of acceleration measurements and signal processing.

Five teams conducted ambient vibration tests on Span 2 Southbound, and different devices and sensors had been used to collect bridge responses under its operating conditions.

The natural frequencies were extracted using operational modal analysis (OMA) methods, and the frequencies (within a 15Hz band) obtained by each team are listed in Table 7. The frequencies obtained by different parties indicated some variations as well as missed or spurious modes. The discrepancies were likely due to different vibration environments, imperfect sensor synchronization, sensor density/modal grid and/or signal processing settings and curve fitting algorithms when conducted by different parties with different hardware and software and at different times. Further, constructed systems may be considerably non-stationary due to how temperature and humidity may influence boundary and continuity (bearing) conditions.

Table 7. Comparison of Frequencies Obtained from Ambient Vibration Tests

Mode	Ambient Vibration Testing				
	Drexel University	Austria (VCE)	KEC & Sejong University	Utah State University	University of Sheffield
1	2.89	-	2.72	2.86	-
2	-	-	-	3.10	-
3	3.79	3.75	3.52	3.70	3.75
4	-	4.47	-	4.50	4.3
5	5.23	-	5.14	-	5.27
6	-	-	7.75	-	5.96
8	9.47	9.18	8.92	9.38	9.50
9	11.61	11.79	11.14	-	11.70
10	12.25	-	-	12.30	12.40
11	14.80	14.81	-	14.94	14.90

Forced excitation tests were executed by impact by Drexel researchers and by multiple shakers by Sheffield researchers. The natural frequencies obtained from the two research teams are listed in Table 8, indicating that the Multiple Input Multiple Output (MIMO) test by Drexel using a drop-hammer (Figure 20.a) revealed 7 modes while the multiple shaker

(Figure 20.b) harmonic testing by Sheffield revealed 6 of these modes (within a 15 Hz band). These discrepancies provide a measure of the uncertainty in the results of modal analysis on full scale constructed systems in the field by different experts, sensors and excitation. In addition to the variations due to the test design, constructed systems are non-stationary, as they are affected by weather and seasons.

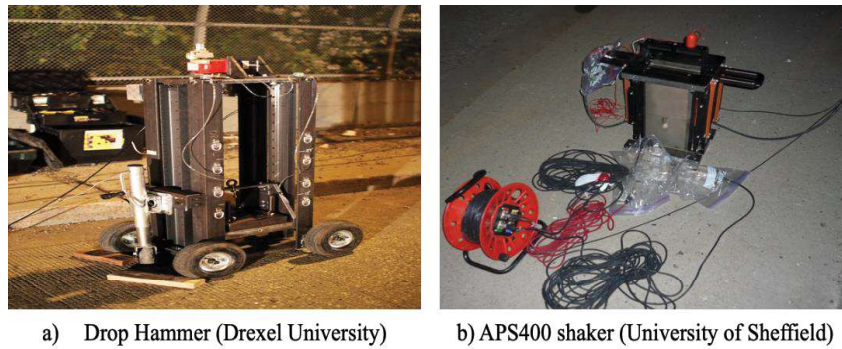


Figure 20. Devices used in Forced Vibration Tests

Table 8. Natural Frequencies Comparison Obtained from Forced Vibration Testing

Mode	Forced Vibration Testing	
	Drexel University	University of Sheffield
1	2.98	-
2	3.83	3.69
3	5.21	5.22
4	9.23	9.49
5	11.74	11.70
6	12.25	12.20
7	14.80	15.00

Based on Table 7 and Table 8, the results obtained from ambient vibration testing and forced vibration testing by Drexel University were selected for further analysis. The details of the two experiments, such as instrumentation design and mode shapes, will be described in detail.

For the design of the instrumentation layout, a series of sensor locations were selected shown in Figure 21(a) using the modes estimated by the a-priori model. The PCB 393A03 seismic accelerometer shown in Figure 21(b) was used to capture the response of the bridge. 31 accelerometers were installed along Girders 1, 3, 6 and 8, and 12 accelerometers were installed on the bottom flange of girders 6 and 8 while the remainder of the sensors were installed on the top of the deck. The blue markers in Figure 21 indicate locations where impact excitation was to be applied by drop hammer and sledgehammer on the deck.

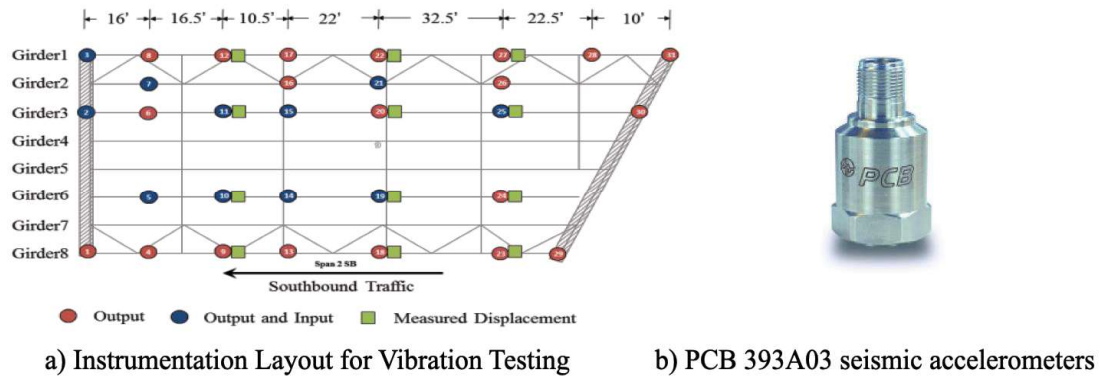


Figure 21. Instrumentation Layout and Accelerometers

The mode shapes of the seven modes extracted via forced vibration testing by Drexel University are shown in Figure 22. It is noteworthy that the straight-skew plan geometry of the span, as well as its mass and stiffness characteristics, led to an unusual “flapping” shape for the first two modes shown in Figure 22.

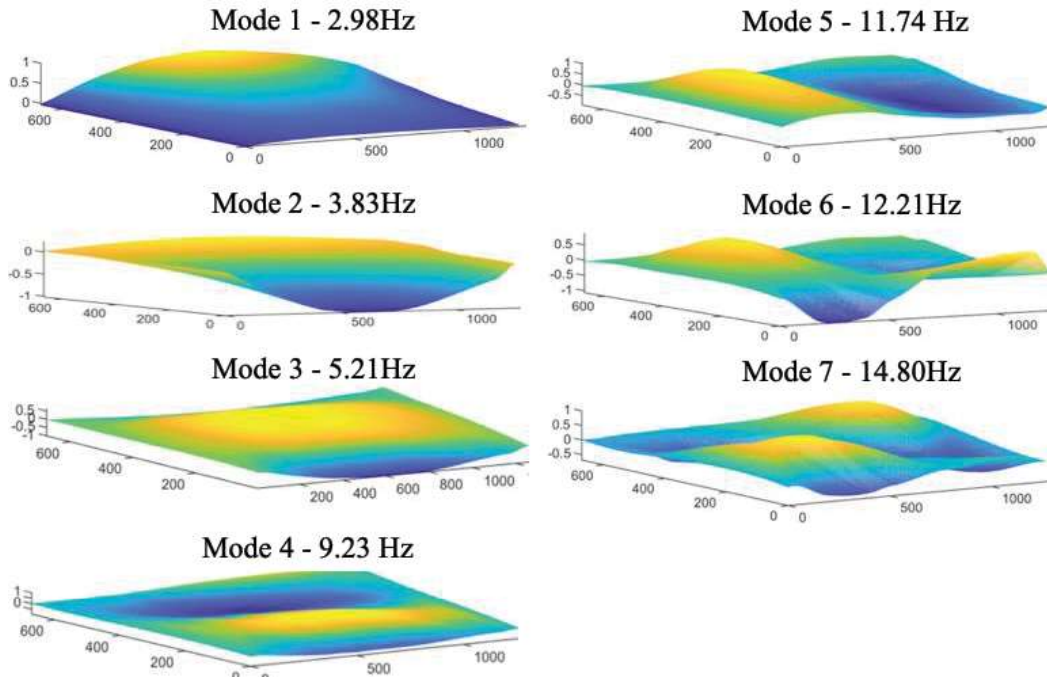


Figure 22. Mode Shapes from Forced Vibration Testing by Drexel Researchers

Moreover, significant vibrations with amplitudes of 20%g under ambient traffic conditions were observed. For instance, the acceleration records along Girder 3 are shown in Figure 23(a).

A broad spectrum of ambient conditions and traffic input of Span 2SB was extracted from datasets collected during various times of a day (30 minutes in total), and the averaged Power Spectral densities at mid-span are shown in Figure 23b. As observed from the figure, the input from ambient excitation provided significant energy in the 2-15 Hz Band. This vibration was hypothesized as the cause of deck cracking.

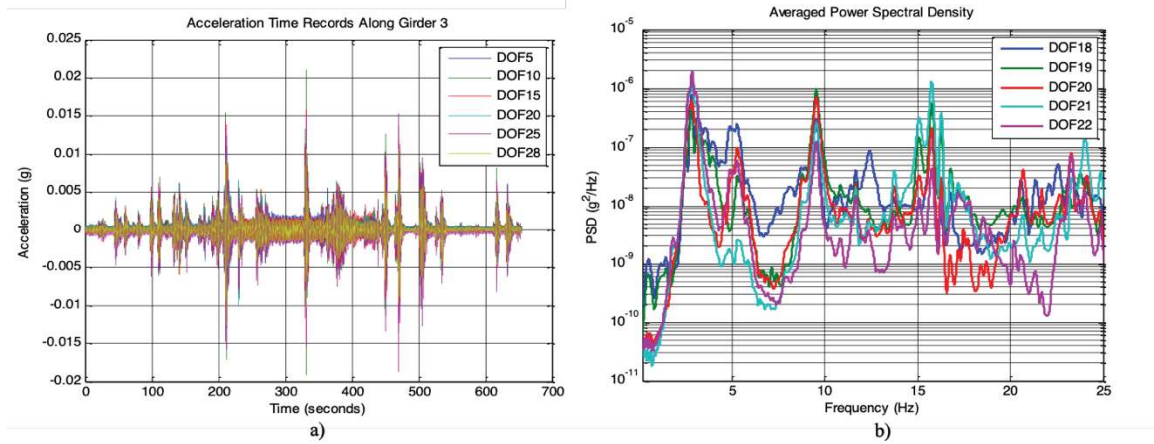


Figure 23. Results of Ambient Vibration Monitoring of Span 2 SB: a) Vertical acceleration time records of Girder #3; b) Averaged Power Spectral Densities at midspan

5.2 Controlled Load Testing

Load testing of a bridge for a reliable understanding of bridge stress levels and flexibility is costly and disruptive, and its value often depends on the experience and resources that can be dedicated: (a) constraints regarding traffic control; (b) the number and configuration of the trucks used in the loading, the loading program, as well as the maximum load to be positioned on the span; (c) instrumentation design; (d) real-time feedback of bridge responses for safety as different levels of load positioned on the bridge. Depending on (a)-(d) it is possible to perform high-speed, crawl or static testing by loaded trucks. In the research program, Dr. Jeff Weidner under Dr. Franklin Moon's mentorship designed, prepared and supervised the load test.

Strain and displacement sensors were installed on Span 2 along Girders 1, 3, 6, and 8 (see Figure 24). The primary sensors were clustered into a grid of twelve locations. At each location a vertical displacement response was measured, as well as two strain responses (strain gages mounted on the topside of the bottom flange and on the web as shown in

Figure 24b) to capture the strain profile and assess the composite action. In a few locations, a third strain gage was added to confirm the linearity of the strain profile.

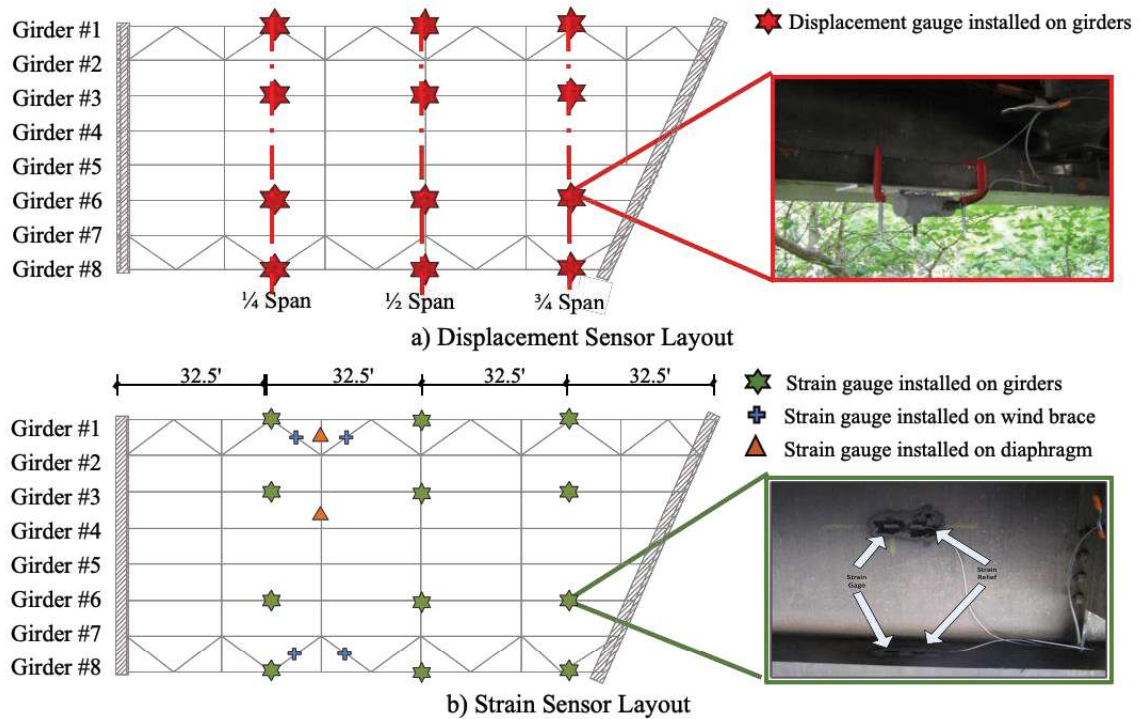


Figure 24. Instrumentation Layout and Sensor Installation Info of Controlled Load Test

For the controlled load testing, two of the three lanes were closed to traffic, with complete closure of all lanes when required by the load case. Loads were applied at the mid-span of the closure area with three load stage levels: 3 empty trucks (87 Kips); 3 fully loaded trucks (230 Kips) and 6 fully loaded trucks (460 Kips). For the 6 fully loaded trucks, the trucks positioned side-by-side and back to back occupied three lanes and the shoulder, and truck locations are shown in Figure 25.

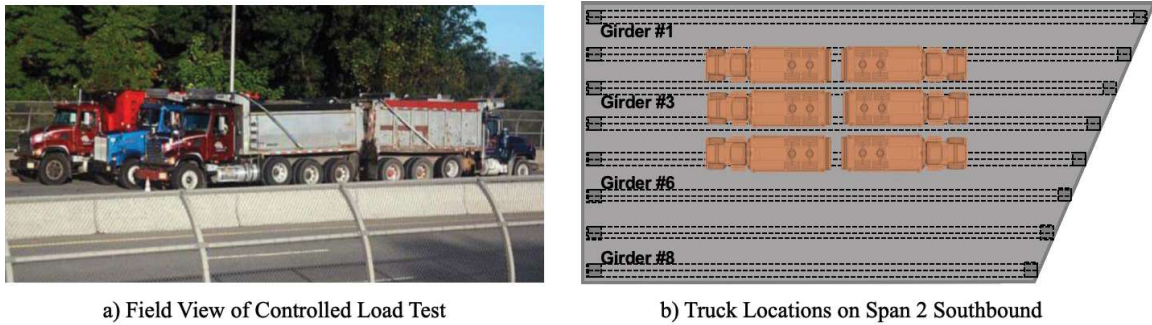


Figure 25. Truck Locations for the Controlled Load Test

A review of the displacement profiles (Figure 26a) of girders #1, #3, #6 and #8 obtained for the full load level indicates that at the mid-span girder #3 deflects the most. This is expected given the static load distribution. A maximum displacement slightly larger than 0.8 in was measured at the mid-span of Girder #3 corresponding to a drift of about $L/2000$ and implying that the span was 2.5 times stiffer than anticipated by the code ($L/800$). The load-displacement relations (Figure 26b) also confirm this. However, we also note that at full load, the left end gage of Girder #1 measured a displacement as large as that of Girder #3. This was attributed to the cracked pier-cap which allowed an additional vertical deformation of Girder 1 at its bearing. The pier-cap crack-width change was measured during the static test and the crack-width was observed to grow proportionally to the load. The strain profile (Figure 27) at midspan of girder #3 indicated linear response (proportionality of strain vs load) with ~5.40 ksi incremental steel stress under full load. However, Girders 6 and 8 reduced their loads at higher levels – indicating some mechanism causing nonlinearity as the load was increased.

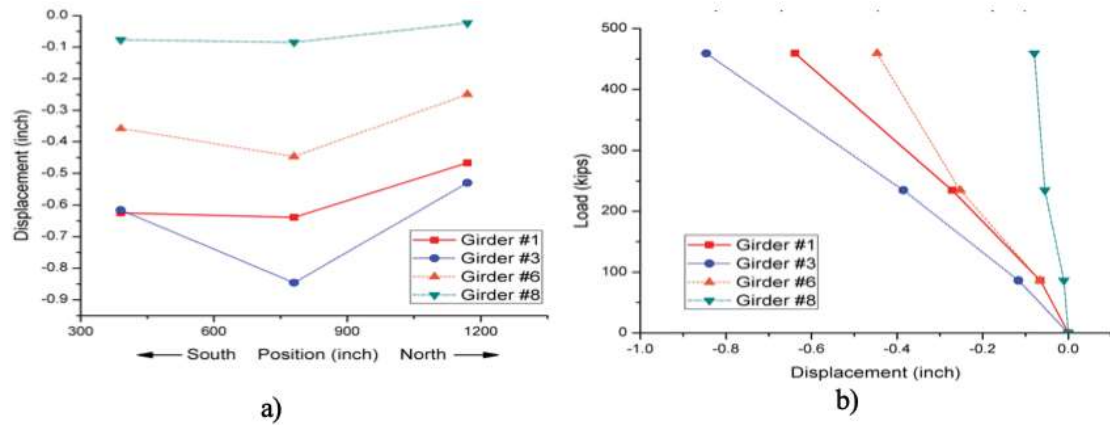


Figure 26. Controlled Static Load Testing results: a) Girder Displacement Profiles under 6 Full trucks; b) Midspan Load-Displacement Relations under Three Loading Scenarios at Center (Weidner, 2012)

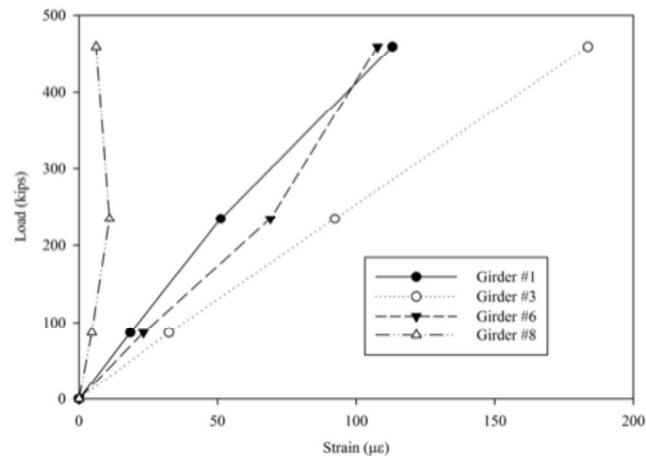


Figure 27. Mid-span Strains from the strain gages at bottom flange for the Three Load Scenarios (Weidner, 2012)

The controlled load testing proved to be the most expensive and disruptive experiment, lasting for six hours while restricting traffic to only one lane during the whole process. The test had to be conducted after midnight. However, the wealth of information and conceptual understanding from the displacements and strains made this the most valuable experiment.

In fact, in addition to understanding the incremental stress levels under proof level load, it was possible to measure the actual flexibility and nonlinear behaviour which was caused by the pier-cap crack. Although many load test applications rely only on strain measurements, the value of displacement measurements in a load test was observed to be greater, as discussed in the following in relation to parameter identification. Further, displacements and strains are easier to conceptualize and directly relate to any anomalies in structural system behaviour.

5.3 Non-destructive Testing

The non-destructive testing (NDT) of the deck was performed by Rutgers University. A Korean team of researchers also applied NDT to check the rebar details within the pier-cap at the crack location. The Rutgers team focused on assessing the bridge deck deterioration using six NDT methods, while the Korean team explored the material properties, dimensions, and explored the presence of internal defects, in the vicinity of the crack at the pier-cap.

Concrete bridge decks go through different stages of deterioration. In many cases, salting agents can penetrate the concrete and cause rebar corrosion, which results in micro and macro cracking (delamination and vertical cracks), and ultimately produces spalling of concrete. Therefore, the multi-faceted NDT survey of the bridge deck by Rutgers University concentrated on the detection and characterization of three deterioration types: corrosion, concrete degradation, and delamination.

The NDE survey consisting of six separate probes (see Figure 28) was conducted by Dr. Gucunski's team on June, 2011. Impact Echo (IE) to detect and characterize delamination,

Electrical Resistivity (ER) to describe corrosive environment and the related expected corrosion rate, Half-Cell Potential (HCP) to assess probability of active corrosion, Ultrasonic Surface Waves (USW) method to estimate concrete modulus, Ground Penetrating Radar (GPR) to quantify concrete cover and provide a qualitative deterioration assessment, and microwave technology MoistScan to detect areas with higher moisture content.

The survey was conducted by discretizing the deck by a 0.61 m (2 ft) by 0.61 m (2 ft) grid shown in Figure 29. The origin of the coordinate system was the intercept of joints bounding spans 1 and 2, and the curb. The first survey line was one foot away from the curb, and the scanned area covered the first two lanes of Span 1SB and Span 2SB. All the different scan technologies took measurements at all grid points. Each of the technologies excel in detecting and characterizing one common deterioration mechanism. Some of the NDT results of Span 2SB, the area of which is 6.0 m (20ft) by 40.0 m (130ft), are shown in Figure 30, and the results of the survey corresponding to delamination and corrosion are discussed further in the following.

ER and HCP results shown in Figure 30a and Figure 30b indicated low corrosion activity of the deck. The impact echo test results shown Figure 30c point to significant delamination in the deck. This was somewhat surprising, considering the low corrosion activity measured by Half-Cell Potential and fair corrosive environment obtained from Electrical Resistivity.



Figure 28. Field View of NDE Survey conducted on Span 2 Southbound



Figure 29. Field view of NDE survey grid

Given that the extent of delamination was not caused by corrosion of reinforcement, the NDT scans further pointed to large superstructure vibrations as a possible reason for the widespread delamination. USW results shown in Figure 30(e) point to a low strength concrete, considering that the measured modulus was mostly in a 13.8 to 27.5 GPa (2,000-4,000 ksi) range. This was later confirmed through the review of design plans, which specified a “low modulus” concrete for the deck. It was further noticed that the lower concrete modulus was primarily measured in the slow lane.

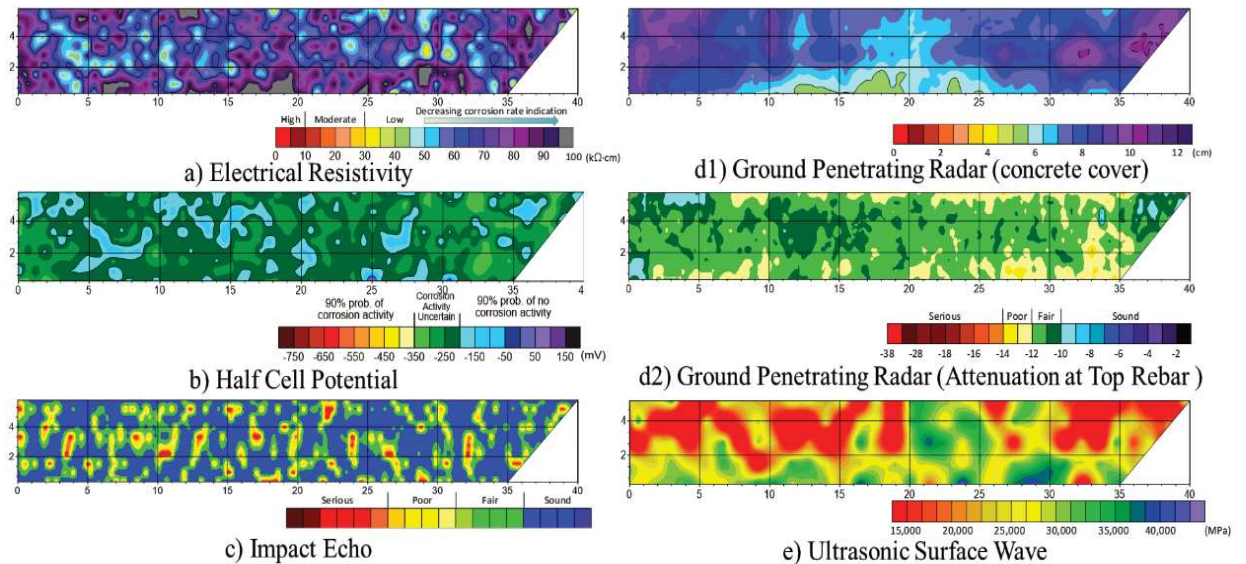


Figure 30. NDE results of span 2 southbound

The NDTs applied by Korean team included the measurement of concrete strength of abutments and piers by Schmidt Hammer test, the measurement of crack depth using concrete ultrasonic tester, the detection of rebar at the abutment and pier structures by Reinforced Concrete (RC) radar (see Figure 31a), the measurement of paint thickness of steel girders using a digital coating thickness gauge, the measurement of the thickness of steel members and the detection of internal defects in welded areas with a steel ultrasonic

tester. One noteworthy finding was the poor arrangement of rebars in the pier-cap crack location. In the cracked area (see Figure 31b), the measured spacing of horizontal rebars (= 43 cm) is larger than the recommended design spacing (= 30 cm). In addition, in the cracked pier cap (see Figure 10b), there was no vertical rebar (see Figure 31b) within a distance of 1 meter around the detected vertical crack.

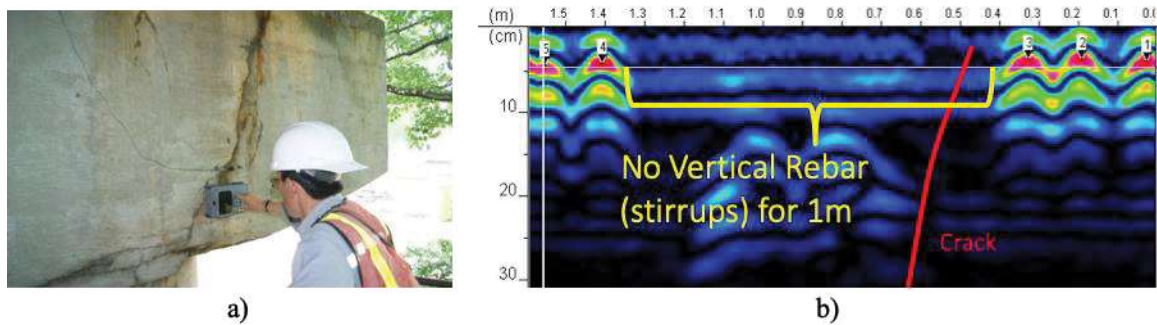


Figure 31. Application of RC Radar: a) field test on pier cap; b) corresponding radar results in P1 pier cap

5.4 Long-Term Monitoring by Fiber-Optic Sensors

A long-term SHM system based on fiber-optic sensors was installed by Princeton University researchers. Six cross sections (marked on instrumentation grid in Figure 32) were equipped with long-gauge Fiber Bragg grating (FBG) sensors in parallel topology (strain and temperature sensors). As shown in the figure, the six cross sections are located along Girders #2 and #5 of Span 2 SB, and sensors installed along top and bottom flanges of each section.



Figure 32. Sensor Instrumentation Layout for Long-term Monitoring with Fiber-Optic sensors

Dynamic strain data from large events were used to evaluate the structural behavior by estimating the location of the neutral axis (NA) through interpolation of the strain measurements at different cross sections.

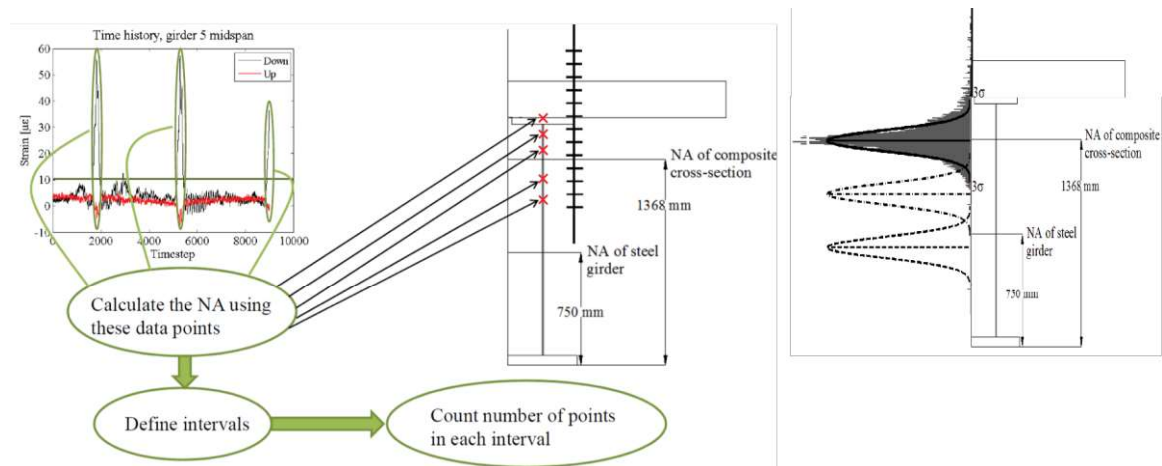


Figure 33. Neutral Axis Analysis based on Dynamic Strain Data from Large Events

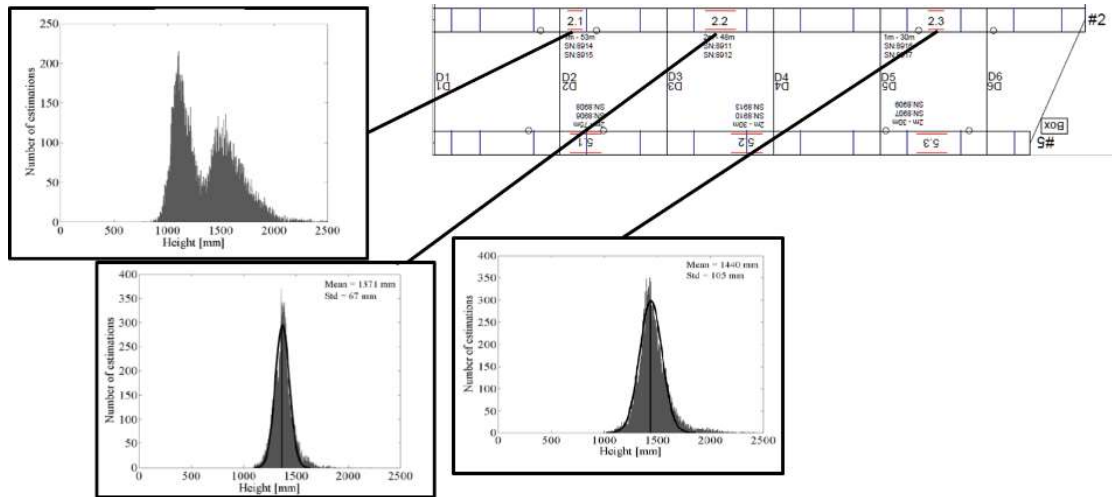


Figure 34. Neural Axis analysis results of Girder 2 obtained by Princeton University in probabilistic approach with one-year data.

Analysis of data after 1-Year of monitoring (Figure 34) revealed that the neutral axis locations along the length of the girders remained stable except at the left end of Girder 2. The neutral axis locations shifted in the course of the year implying a progression of delamination of the deck in the vicinity of the area close to the cracked pier cap.

Chapter 6: Model Calibration and Parameter Identification

The calibration of the A-Priori model is needed for representing the current condition of the bridge, and the experimental data obtained from vibration-based tests and static load tests will be processed and interpreted for model updating. The NDE test results can also be used to define the bounds for material properties.

6.1 Parameters Assumption and Selection

Two finite element models were developed with Abaqus for the test bridge. The a-priori model was adjusted to account for the actual condition of the critical parts observed during the visual inspection. The close-up details of the model, showing how the girder, deck, pier and the bearings are represented, are illustrated in Figure 35 and Figure 36. The bridge deck, as well as webs, flanges and stiffeners of the steel girders, were modeled using 8-node 3D shell elements. Wind-bracings and cross frames, which connect the girders, were modeled using 3-node quadratic 3D beam elements (Timoshenko beams). The parapet and barrier were modeled as beam elements connected to the deck using rigid links. The steel girders were connected to the deck by shear connectors modeled using beam elements with high value of the elastic modulus for the base-line modeling representing fully composite action. Bridge piers were modeled with 3D solid elements shown in Figure 35a. A mesh size of 6 inch was chosen for all the parts of the model after a mesh size convergence analysis, and the meshed model is shown in Figure 35b.

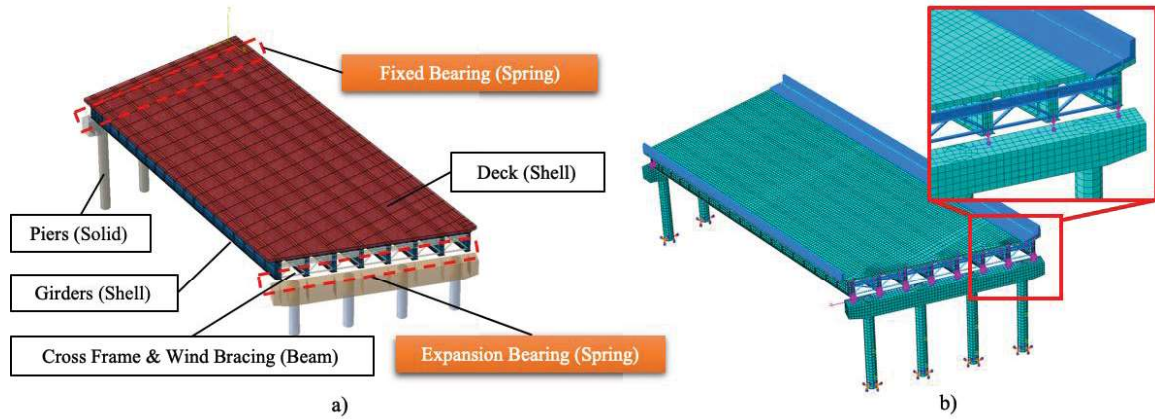


Figure 35. Finite Element Model (with Piers) in Abaqus software: a) modeling information; b) view of the model with defined meshes

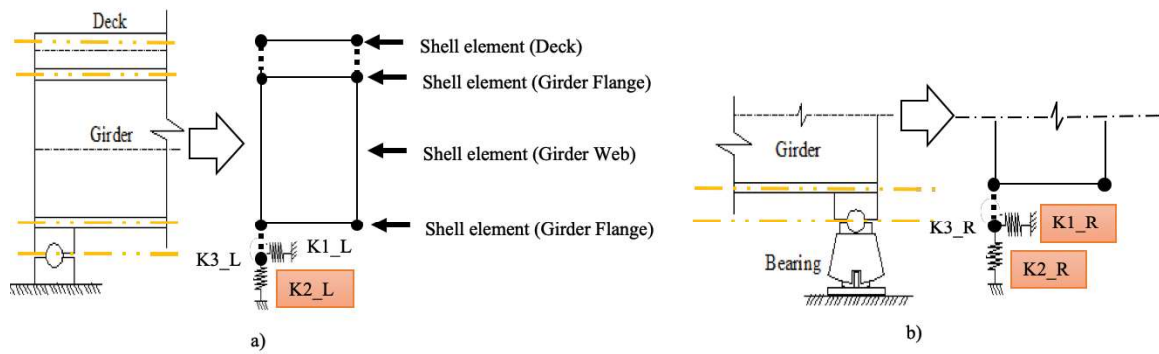


Figure 36. Details of bridge bearings: a) fixed bearing; b) expansion bearing; L and R stand for Left (South) and Right (North)

The supports at the southbound of span 2 SB are fixed bearings (see Figure 35a), and those at the northbound are expansion (rotating movable) bearings. The boundary conditions at each bearing were represented by spring elements acting in 3 directions (K1 for stiffness along longitudinal direction, K2 for vertical direction, and K3 for lateral direction perpendicular to the page) shown in Figure 36.

The material properties of steel for girders, cross frames and bracings complied with the specifications of ASTM A36 according to the design drawings. The NDE test results were used to define the bounds for material properties in the FE model. The initial values of the parameters listed in Table 9 were used as one of the starting points for the optimization. The density of deck was not updated in the optimization for vibration testing data.

The adjusted model was both manually and automatically calibrated by considering the experimental data. Manual calibration consisted of adjusting parameter values based on their expected influence on model characteristics and responses. The goal of this approach was to identify a set of parameter values which adequately represented the experimental behavior. Although labour intensive, this process allows the user to explore the parameter space with more freedom and helps the development of heuristics and intuition about the bridge's characteristics.

Table 9. Initial Values of Parameters to be Calibrated in the FE Model

Parameters	Description	Initial Value
D_Deck	Density of Deck	0.086 lb/in ³
E_Deck	Young's Modulus of Deck	3453 ksi
E_Parapet	Young's Modulus of Parapet	3453 ksi
K2_L, K2_R	Vertical bearing stiffness at Left and Right side	500 k/in
K2_L1	Vertical pin bearing stiffness above pier-cap (along South Side)	500 k/in
K3_R	Lateral Rocker Bearing stiffness (along North Side)	500 k/in
E_shear_connector	Young's Modulus of shear connectors	3e4 ksi

The Abaqus Scripting Interface, a customized extension of Python, was used to modify parameters in the Abaqus models and to obtain static and dynamic responses from the models. The automated calibration utilized the Matlab optimization function `fminsearch` (Lagarias et al. 1998), (which is based on the Nelder-Mead simplex algorithm) to minimize the objective function of interest. Parameter boundaries were included in Python scripts to bound the search region of the `fminsearch` function which is an unconstrained multivariable function. To mitigate the influence of local minima, multiple iterations of the automated calibration were performed using different sets of initial parameters.

In previous studies, FE models of Span 2 SB were developed in Strand7 and SAP2000 by two research groups, complemented with the computational software package MATLAB for automatic optimization. Four FE models were calibrated using different experimental data, and the FE natural frequencies obtained from the models are compared in Table 10.

Table 10. Comparison of Integrated Experimental Result with Finite Element Model Results

Experimental results	Drexel- Strand7 (Calibrated with Drop Hammer test)	Drexel- Strand7 (Calibrated with Ambient monitoring)	Drexel-Strand7 (Calibrated with Static load test)	KEC & Sejong University -SAP2000 (Calibrated with Ambient monitoring)
2.81	3.05(8.48%)	2.85(1.37%)	2.6(-7.52%)	2.72(-3.25%)
3.72	3.94(6%)	3.71(-0.19%)	3.8(2.23%)	3.57(-3.96%)
4.42	4.21(-4.82%)			
5.22	5.92(13.32%)	5.54(6.05%)	5.21(-0.27%)	5.18(-0.84%)
7.75			8.69(12.13%)	7.93(2.32%)
9.30	9.7(4.27%)	8.99(-3.36%)	9.78(5.13%)	8.09(-13.04%)
11.60	10.65(-8.22%)	10.61(-8.56%)	11.58(-0.2%)	11(-5.2%)
12.28	12.81(4.32%)	13.13(6.92%)	13.06(6.35%)	

14.89	14.76(-0.87%)		
15.43	15.44(0.09%)	14.75(-4.38%)	
16.51			16.98(2.85%)
20.43	20.84(2.01%)	18.13(-11.26%)	

6.2 Parameter Identification based on Vibration Testing

To simulate the dynamic properties of the bridge such as frequencies and mode shapes, the entire FE model was analyzed as the inertia properties of the substructures do significantly impact the frequencies of the system. In simulating the static properties of the system, only a free-body-diagram of the super-structure was analyzed.

Parameter identification was performed using six of the modes derived from ambient and forced vibration testing conducted by Drexel University researchers and shown in Table 7 and Table 8. The 6th experimental frequency of 12.25 Hz and the corresponding mode shape was not available from the eigen-analysis of the a-priori model, therefore this was assumed spurious and excluded from the experimental findings. Modes derived from analytical models may include local modes of members, therefore, finding the corresponding modes for the 6 modes extracted experimentally is a critical step in the automated updating process. In this study, the Modal Assurance Criteria (MAC) of the mode shapes, a statistical indicator that is sensitive to the largest difference between comparative values and insensitive to small changes or small magnitudes, was used in conjunction with a frequency comparison to pair experimentally and numerically extracted modes. The MAC value is bounded between 0 and 1, with 1 indicating fully consistent

mode shapes and 0 indicating that the modes are not consistent. The Modal Assurance Criterion (MAC) is defined as:

$$MAC_{ij} = \frac{|\phi_{a_i}^T \phi_{e_j}|^2}{\phi_{a_i}^T \phi_{a_i} \phi_{e_j}^T \phi_{e_j}}$$

Eq. 1

where ϕ_{a_i} is the i th mode shapes of analytical model; ϕ_{e_j} is the j th mode shapes of test bridge; $\phi_{a_i}^T, \phi_{e_j}^T$ are the transpose of mode shapes, MAC_{ij} is the MAC value for the ij -th mode pair.

Consistent analytical mode shapes of a sought mode can be identified by finding the max MAC value for the modes within an interval (i.e. ± 5 Hz frequency range around the mode frequency). Local modes and modes with predominant in plane motion can also provide large MAC values and thus, it will be helpful to filter out such modes before the comparison with the experimental mode shapes. For instance, a simple filtering method was proposed to remove lateral modes, by limiting the maximum horizontal displacement to 0.3 times the maximum vertical displacement and the maximum lateral displacement to less than half of the maximum vertical displacement.

When both natural frequencies and mode shapes were leveraged, the objective function implemented for model updating was defined as:

$$f = \frac{1}{n} w_{f_i} \sqrt{\sum_{i=1}^n (f_{e_i} - f_{a_i})^2} + \frac{1}{n} \sum_{i=1}^n w_{m_i} \left(\frac{1 - \sqrt{MAC_{ii}}}{\sqrt{MAC_{ii}}} \right)$$

Eq. 8

where w_{f_i} , w_{m_i} are weighting factors (assumed $w_{f_i}=10$, $w_{m_i}=1.0$), f_{e_i} is the i -th modal frequency of test bridge, f_{a_i} is the i -th modal frequency of FE Model, MAC_{ii} is MAC value for the i -th mode pair, n is the number of modes.

A series of analyses were performed automatically with Matlab, Python and Abaqus to optimize the parameters until the discrepancies between the experimental data-sets and the simulated model properties and responses were minimized. Table 11 presents the parameter values corresponding to the updated models (calibrated with ambient and forced vibration data), while the frequencies and mode shapes are shown in Figure 37.

It is noteworthy that the updated value of K2_L1, the vertical stiffness of the spring representing the South Support Stiffness under Girder 1 (i.e. stiffness provided by the cracked pier-cap), is significantly decreased. All other parameters remain fairly uniform irrespective of the experimental dataset used for calibration.

Table 11. Values of Critical Parameters Updating using Vibration Testing Datasets

Parameter	Units	Initial Model	Bounds	Calibrated with Ambient Vibration data	Calibrated with Forced Vibration data
D_Deck	lb/in ³	0.086	[0.07,0.1]	0.085	0.085
E_Deck	ksi	3453	[3000,4500]	3733	3555
E_Parapet	ksi	3453	[3000,4500]	3555	3733
K2_L, K2_R	k/in	500	[0,1000]	350	350
K2_L1	k/in	500	[0,1000]	100	100
K3_R	k/in	500	[0,1000]	485	485
E_shear_connector	ksi	3.0E04	[2.9E4-1E10]	3.0E05	3.0E05

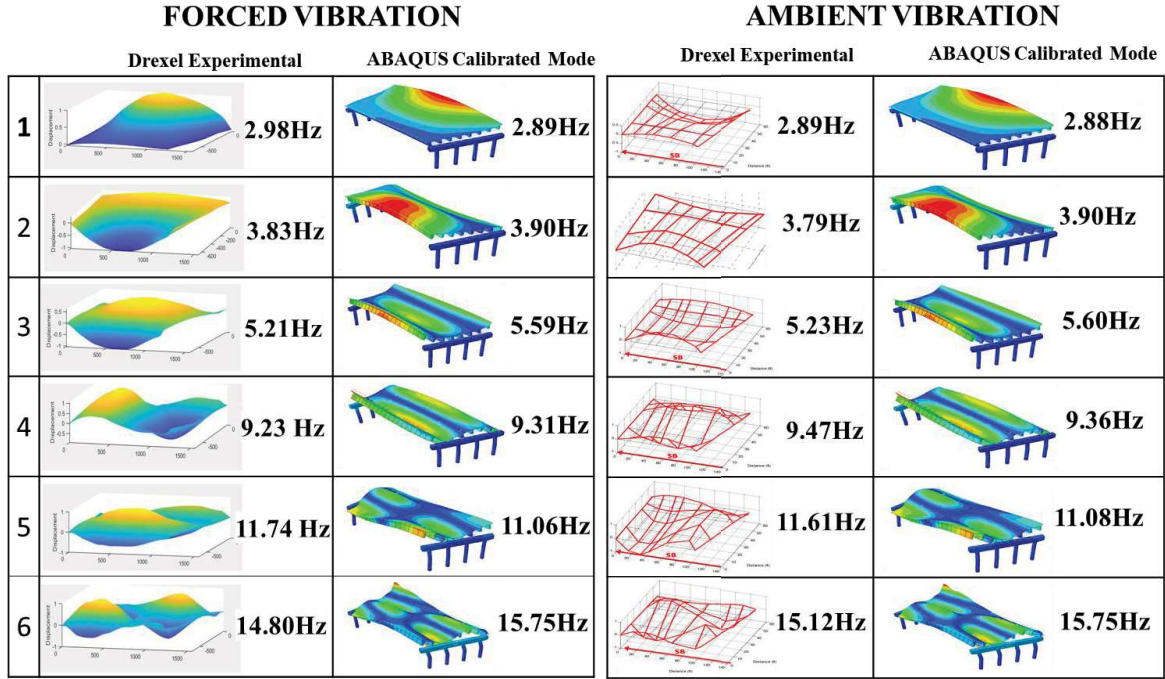


Figure 37. Comparison of Experimental and Analytical Frequencies and Modes

6.3 Parameter Identification based on Load Testing

The displacements and strains obtained from 12 locations (at 1/4, 1/2, 3/4 of Girder #1, #3, #6, and #8 shown in Figure 24) for a 6 full truck load were used for model updating. The automated calibration was executed using both measurand types, as well as by considering each response modality independently. The objective functions implemented were defined for the three scenarios (assuming limited measurements of either displacement or strain were available and the case where all measurements were collected):

Displacement:

$$f = \frac{1}{n} w_d \sqrt{\sum_{i=1}^n (Disp_{e_i} - Disp_{a_i})^2}$$

Eq. 9

Strain:

$$f = \frac{1}{n} w_s \sqrt{\sum_{i=1}^n (Strain_{e_i} - Strain_{a_i})^2}$$

Eq. 10

Displacement and Strain:

$$f = \frac{1}{n} w_d \sqrt{\sum_{i=1}^n (Disp_{e_i} - Disp_{a_i})^2} + \frac{1}{n} w_s \sqrt{\sum_{i=1}^n (Strain_{e_i} - Strain_{a_i})^2}$$

Eq. 11

where w_d , w_s are weighting factors ($w_d = \frac{1.0}{(Disp_{max} - Disp_{min})}$), $w_s = \frac{1.0}{10^3 * (Strain_{max} - Strain_{min})}$) for displacement and strain, $Disp_{e_i}$, $Strain_{e_i}$ are the displacement and strain at i -th node, $Disp_{a_i}$, $Strain_{a_i}$ are the corresponding displacement and strain from the Abaqus model for the i -th node.

Table 12 presents the experimental results and calibrated analytical results using displacement and strain measurements for model optimization. First, only the displacements were considered in calibration (Eq. 3). Then only the strains were considered (Eq. 4); finally, Objective Function in Eq. 5 that incorporates both displacements and strains.

Calibration using only displacement data and both displacement and strain data resulted in the same parameters for the final calibrated model. Calibration using only strain data did not produce the same calibrated model, likely due to the fact that the strain responses were highly localized and did not affect the selected parameters as much as displacements.

Table 12 Values of Manual Parameters Updating using controlled load testing datasets

Parameter	Units	Initial Model	Bounds	Calibrated with Displacement	Calibrated with Strain	Calibrated with Displacement and Strain
E_Deck	ksi	3453	[2000,4500]	3733	3733	3733
E_Parapet	ksi	3453	[2000,4500]	3750	3555	3750
K2_L, K2_R	k/in	500	[0,1E04]	920	829	920
K2_L1	k/in	500	[0,1E04]	200	350	200
K3_R	k/in	500	[0,1E04]	500	485	500
E_shear_connector	ksi	3.0E04	[0,1E07]	3.0E06	3.0E04	3.0E06

The vertical displacements of girders 1, 3, 6, and 8 obtained from the manually calibrated model with displacement data is compared with the displacements measured during controlled load testing (Figure 38). A discrepancy in the vertical displacement at $\frac{1}{4}$ span (the node located at 390 inches from the south support) of Girder #1 remained even after calibration. This suggests that the linear model is unable to accurately simulate the cracked pier-cap's lack of stiffness. The actual impacts of the pier-cap crack onto the serviceability, durability and safety of the bridge is paramount. Due to the structural damage of the pier-cap, the superstructure ends up transferring the loads to other bearings that are properly supported by the undamaged middle region of the pier. The continued degradation of the deck in the vicinity of the cracked pier which was indicated by the long-term monitoring by Princeton researchers corroborates this observation. To address the discrepancy, an additional parameter **E_shear_connector_L1** (Young's modulus of shear connectors of $\frac{1}{3}$ span of Girder #1 and #2), was added for automated calibration. The initial value of the new set of parameters is shown in Table 13.

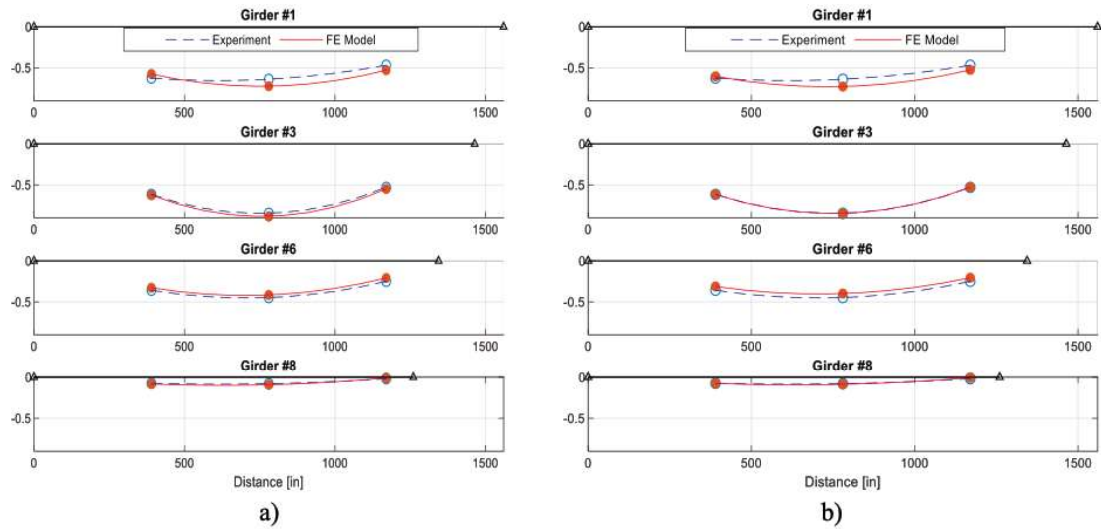


Figure 38. Vertical displacements comparison: a) results obtained from manually calibrated model with initial parameters; b) results obtained from automatically calibrated model with new start point

Table 13 summarizes the parameter optimization results obtained by leveraging both the displacements and strains measured during the truck load test under full load. The simulated displacement profiles of the instrumented girders correlate well with the experimental measurements as shown in Figure 38(b).

Table 13 Values of Automated Parameters Updating using controlled load testing datasets

Parameter	Units	Initial Model (new point)	starting Bounds	Calibrated with Displacement	Calibrated with Strain	Calibrated with Displacement and Strain
E_Deck	ksi	3453	[2000,4500]	4500	4500	4500
E_Parapet	ksi	3453	[2000,4500]	4500	4500	4500
K2_L, K2_R	k/in	500	[0,1E04]	1275.33	9685.12	1303.93
K2_L1	k/in	0.1	[0,1E04]	0.0	0.0	0.0
K3_R	k/in	500	[0,1E04]	92.95	575.78	106.82

E_shear_connector	ksi	3.0E06	[0,1E07]	6.77E06	9.84E06	4.25E06
E_shear_connector_L1	ksi	0.1	[0,1E07]	0.12	0.0	0.10

The numerical values of measured versus simulated displacements and strains are correlated in Table 14.

Table 14 Summary of model updating leveraging Static Testing

Location	Measured Disp. (in)	Simulated Model Disp. (in)	Diff (%)	Measured Strain	Simulated Model Strain	Diff (%)
Girder 1 – 1/4	-0.625	-0.603	3.47	8.60E-05	8.60E-05	0.32
Girder 3 – 1/4	-0.616	-0.617	-0.22	1.12E-04	1.35E-04	-20.66
Girder 6 – 1/4	-0.358	-0.312	12.86	7.70E-05	7.70E-05	1.09
Girder 8 – 1/4	-0.075	-0.075	0.00	1.60E-05	3.60E-05	-131.51
Girder 1 – 2/4	-0.639	-0.728	-13.98	1.13E-04	1.22E-04	-7.86
Girder 3 – 2/4	-0.846	-0.847	-0.07	1.84E-04	2.36E-04	-28.55
Girder 6 – 2/4	-0.447	-0.398	10.92	1.08E-04	1.19E-04	-10.05
Girder 8 – 1/4	-0.079	-0.086	-8.30	6.00E-06	3.00E-05	-383.60
Girder 1 – 3/4	-0.467	-0.525	-12.37	8.40E-05	1.03E-04	-22.93
Girder 3 – 3/4	-0.53	-0.528	0.33	1.18E-04	1.24E-04	-4.75
Girder 6 – 3/4	-0.249	-0.205	17.65	7.00E-05	6.90E-05	1.58
Girder 8 – 3/4	-0.019	-0.006	70.22	5.00E-06	1.90E-05	-273.20

As the measured displacement or strain become small, the percentage error between measured and simulated responses increase given the nature of the objective function which prioritizes larger measurement values. In general, displacement discrepancies of 15% and strain discrepancies of 25% are obtained if we ignore the extremely low responses close to the measurement systems' sensitivity threshold.

In summary, in spite of the nonlinearity (due to deck cracking and delamination and shear crack in one pier-cap), it was possible to calibrate a finite-element model with errors within

5% for frequencies, 15% for girder displacements and 25% for girder strains for those responses that exceed sensor sensitivity.

While the finite-element model does point to a damage at a location corresponding to the pier-cap crack, it does not directly indicate the severity of the damage given its resolution. To increase such resolution, individual shear studs representing composite action could be considered as independent variables to update. However, this would have resulted in too many parameters to update causing other uncertainties in the optimization process. A digital twin (high resolution FE model) of the structure could also incorporate the NDE scan results to account for the local distribution of delamination as well as estimated concrete stiffnesses.

Chapter 7: Utilization of Model for Pier-Cap Stress Analysis

As previously mentioned, the pier-cap at the south end of Girder 1 was the only cracked pier-cap for the entire bridge. This could be a consequence of design or construction shortcomings as also indicated by the radar test results in the vicinity of the crack (Figure 31b). However, it is not known if other piers had similar design and construction flaws. The calibrated model was used for scenarios simulations to understand what is the dynamic amplification factor (DAF) of the shear stress at the cracked pier-cap under moving vehicle loads, and how the skew shape affects the amplification factor.

In the past few decades, a large number of studies have investigated and explored the dynamic behavior of bridge-vehicle coupled systems subjected to moving loads on the bridge-vehicle coupled vibration systems (Brady, OBrien, and Znidaric 2006; Deng et al. 2014; Frýba and Ladislav 1973; KIM 2005; Kou and DeWolf 1997; Law and Zhu 2004; Meng, Lui, and LIU 2001; Paultre, Chaallal, and Proulx 1992), and the influences of some parameters (such as structure natural frequencies and damping properties, boundary conditions, vehicle weights and speed, axle spacing and locations, bridge-vehicle interaction, road surface conditions, deck aspect ratios, and skew angles) were examined in these studies. In this study, the effects of various parameters of bridge, such as structure natural frequencies, boundary conditions, axle spacing and locations, skew angles, were considered and studied.

A benchmark study was first conducted on two simply supported plates, one with rectangle shape and the other with skew shape, to investigate the effects of plate skewness axle spacing and locations, boundary conditions, and skewness on DAF of structure responses (such as displacement and reaction force) subjected to a moving load. Then, the dynamic

amplification factor of shear stress under three moving truck loads was analyzed based on the calibrated model.

7.1 Benchmark Study of Dynamic Amplification Factor under Moving Loads

Two plates, plate 1 for rectangular shape and plate 2 for skew shape (shown in Figure 39), were created in Abaqus with a mesh size of 5 inch. The area of plate 2 is the same as that of Span 2 Southbound: the length of the longer edge is 1560 inches and 1242 inches for the shorter edge, the width is 767 inches. The two plates have the same area and are both supported by 8 pin supports (L1-8) and 8 roller supports (R1-8) at each side. The support locations of plate 2 are the same as that of the Span 2 Southbound bearings.

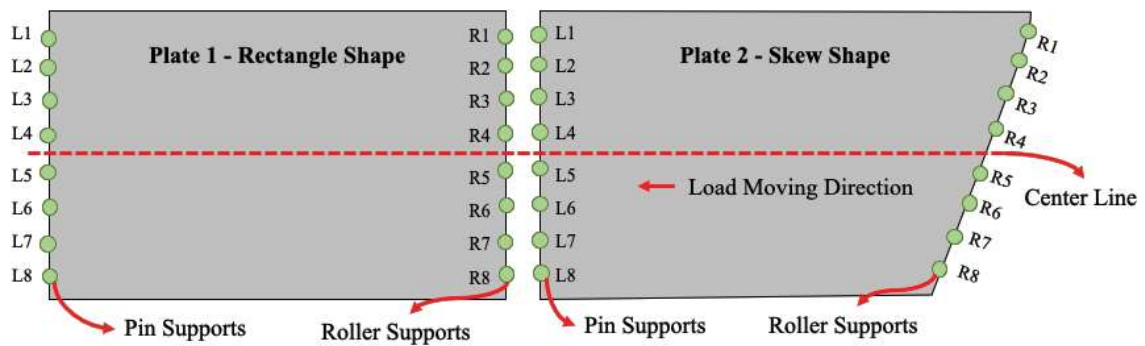


Figure 39. Model Information of Finite Element Models of the Two Plates

A moving load, representing a moving vehicle load, was applied along the center line of each plate with 1,000 inch/second (56 mph) speed. The length of the center line was 1,410 inches. The thickness of the plate was 9.5 inches. The loading area was 20-inch width by 10-in length, and the value of total load was 72kip which is equal to the load of a HS-20 truck. The material properties of concrete deck calibrated in Chapter 6 were used in the model: 3,733 Ksi Young's modulus and 0.086 lb/in³ density.

The first two modes of the two plates were obtained from the finite element modes and are shown in Figure 40. The natural frequencies (0.29-0.3HZ) of the first mode of the two plates are about 10 times smaller than that of Span 2 SB (around 2.9HZ) as expected given the missing stiffness of the girders. As discussed in several studies (Deng et al. 2014; Law and Zhu 2004; Paultre et al. 1992), the difference in natural frequencies will have an impact on the DAF.

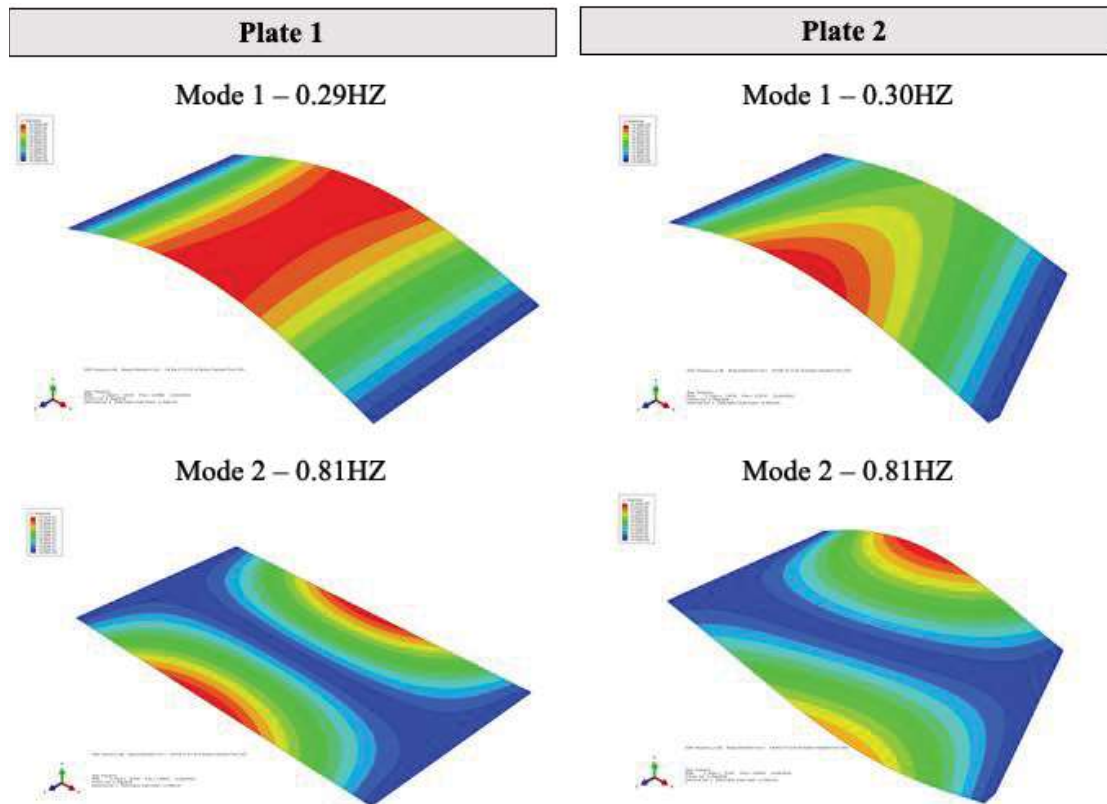


Figure 40. First Two Modes (Frequency and Mode shape) of FE Models of Plate 1 (left) and Plate 2 (right)

Fortran subroutine DLOAD, a user subroutine to specify nonuniform distributed loads, was used to simulate the moving load for static and dynamic analysis. For static analysis, the time step is 0.05 second with a total time of 1.5 second considering that it took 1.41 seconds

to pass each plate. For dynamic analysis, the time step is 0.001 second with a total time of 4.5 seconds. The Fortran subroutine scripts used in the simulations were added in the Appendices section.

The displacements and stresses of the center point (middle point along the center line) obtained from static and dynamic analysis are shown in Figure 41 and Figure 42.

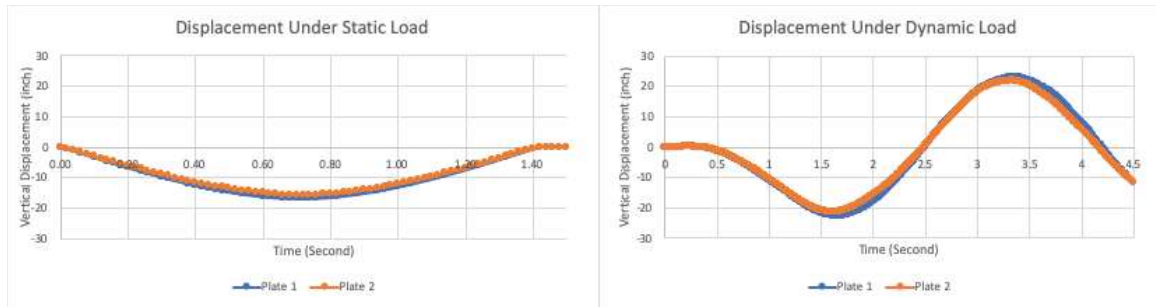


Figure 41. Displacements at Center Point under Static and Dynamic Load of Plates 1 and 2

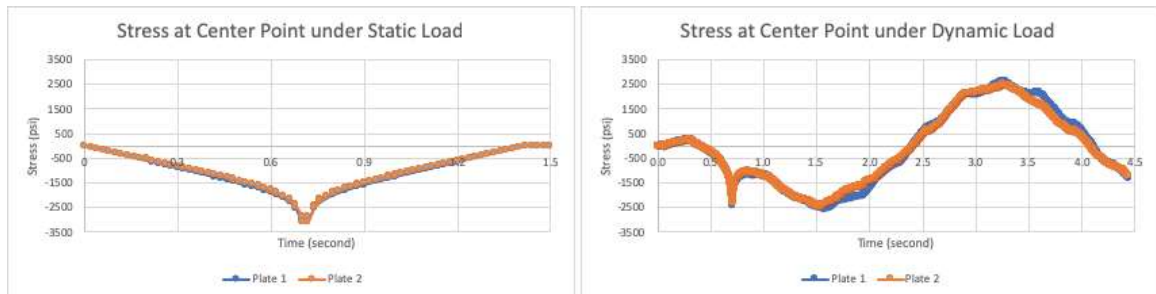


Figure 42. Stresses at Center Point under Static and Dynamic Loads of Plates 1 and 2

The DAFs of maximum displacement and stress for plates 1 and 2 were calculated and summarized in Table 15. As shown in the table, the dynamic amplification factors of maximum stress at the center point were less than 1, and the dynamic amplification factor of the maximum displacement for Plate 2 was slightly larger than that for Plate 1.

The max reaction forces of each pin and roller support under static and dynamic load were extracted and compared in Figure 43.

Table 15. Dynamic Amplification Factor for Maximum Displacement and Stress of Plates 1 and 2

Model	Max Displacement (inch)			Max Stress (psi)		
	Dynamic	Static	DAF	Dynamic	Static	DAF
Plate 1	-22.96	-16.83	1.36	-2582.16	-3046.60	0.85
Plate 2	-21.93	-15.84	1.38	-2491.34	-3104.80	0.80

It is worth noting that the maximum reaction forces at supports L4-5, R4-5 (supports near the center line) of Plates 1 and 2 were larger than all the other supports under static load due to the load being applied along the center line; however, under dynamic load, the maximum reaction forces for Plate 2 were at L1 and R8 exceeding reaction forces of all the other supports. This indicates that the dynamic amplification factor for edge supports (such as L1, L8, R1 and R8) can be significantly affected by the shape of the plate.

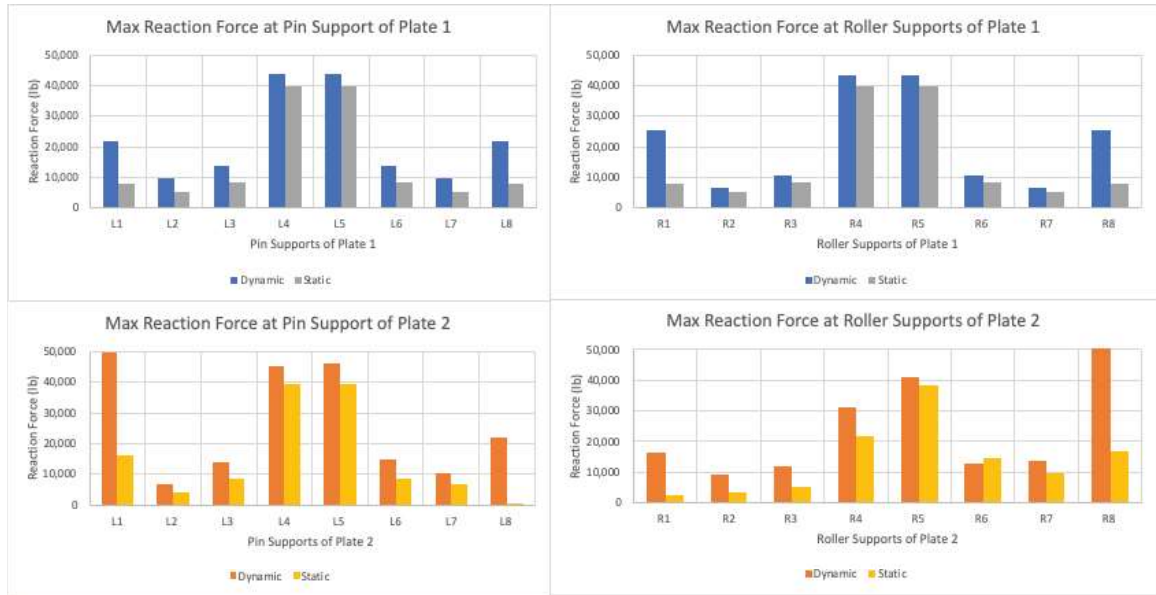


Figure 43. Max Reaction Forces at Supports under Static and Dynamic Load

The dynamic amplification factors for the maximum total reaction force were calculated and compared in Table 16, and the values were close to 3 which indicated a large dynamic amplification effect on reaction forces for the two models. The DAF of the skewed plate (Plate 2) is slightly larger than that of the rectangular plate (Plate 1).

Table 16. Dynamic Amplification Factor of Total Reaction Force of Plates 1 and 2

Model	Max Total Reaction Forces		
	Dynamic	Static	DAF
Plate 1	202.97 kip	72 kip	2.82
Plate 2	215.38 kip	72 kip	2.99

The boundary conditions of the two plates were modeled with pin and roller supports assuming infinity stiffnesses of bearings. However, the real boundary condition of bridge deck and girders should be modeled as springs and dashpots accounting for bearing stiffness and damping respectively. The effect of damping on the dynamic amplification is

not explored in this thesis, and the boundary conditions were modeled as springs with 500 k/in stiffness to explore how the boundary condition would affect the dynamic amplification. The total reaction force was calculated by:

$$F = \sum_{i=1}^8 k_i * U_i$$

Eq. 12

where F is the total reaction force, k_i is the i th spring stiffness, and U_i is the i th vertical displacement of spring.

The DAF of the total reaction force under truck moving along mid-span was calculated and summarized in Table 17 for the plates supported by springs. Compared to the results obtained from the model with pin and roller supports, the DAFs were increased for both plates.

Table 17. Dynamic Amplification Factor of Total Reaction Force (Model with Springs)

Model	Max Total Reaction Forces		
	Dynamic	Static	DAF
Plate 1	265.00 kip	72 kip	3.68
Plate 2	254.60 kip	72 kip	3.54

The loading location and the loading area are two factors that may affect the dynamic amplification of structure responses. Therefore, different loading locations and loading areas were considered in the simulations. The new loading locations were modeled according to the real truck moving paths along Span 2 SB Lane 1 and Lane 2 shown in Figure 47. The details of truck moving path and load area are described in Section 7.2. The results shown in Table 18 were obtained from the new simulations. The DAFs were decreased compared to Table 16 and Table 17. For Plate 1 DAF=2.3 for truck load along

Lane 1 and DAF=2.24 for truck load along Lane 2 compared to 2.82 for mid-span dynamic load with pin and roller supports and 3.68 for mid-span dynamic load with spring supports.

*Table 18. Dynamic Amplification of Total Reaction Force
under Moving Truck Loads at Different Location*

Model (6 Tires)	Maximum Total Reaction Force (kip)					
	Truck Moving along Lane 1			Truck Moving along Lane 2		
	Dynamic	Static	DAF	Dynamic	Static	DAF
Plate 1	165.84	72.00	2.30	161.36	72.00	2.24
Plate 2	206.17	72.00	2.86	192.00	72.00	2.67

7.2 Pier-Cap Stress Analysis

As mentioned in previous chapters, large shear cracks, (highlighted in red in Figure 44) were noticed in the pier-cap of Pier 1W. To find the root cause of the observed crack, the pier-cap stress analysis was performed for both static and dynamic cases. The cracked pier-cap location is underneath bearing #1 (the bearing supporting girder #1) and in the proximity of Lane 1, and it is mainly subjected to its self-weight and loads V (shear force applied on pier-cap which is equal to the reaction force at bearing #1 as shown in Figure 45). The area of the cross section (Figure 46) is 48-inch wide by 60-inch height, and the maximum shear stress at Neutral Axis can be calculated by:

$$\tau_{max} = \frac{VQ_{max}}{I_c b} = \frac{3V}{2A}$$

Eq. 13

$$I_c = \int_{y_1=0}^{\frac{h}{2}} y^2 dA = \frac{bh^3}{12}$$

Eq. 14

$$Q_{max} = \int_{y_1=0}^{\frac{h}{2}} y dA = \frac{bh^2}{8}$$

Eq. 15

where τ_{max} is the maximum shear stress occurring at the neutral axis, V is total shear force applied on the pier cap, Q_{max} is the maximum first moment of area of the pier cap cross section, I_c is the centroidal moment of inertia of the entire cross section, A is the area of the cross section, y is the coordinate of element dA with respect to the axis of interest (neutral axis for this section), b is the width of the cross section, h is the height of the cross section.

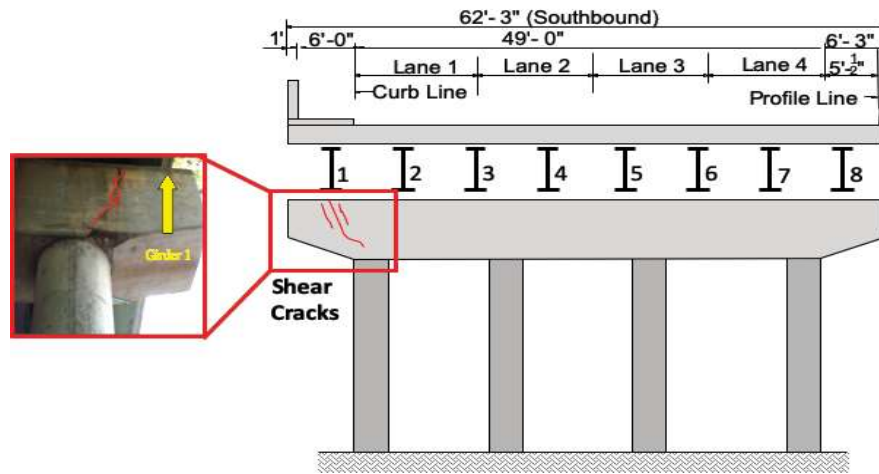


Figure 44. Pier-Cap Cracking Location of Span 2 SB Pier 1W

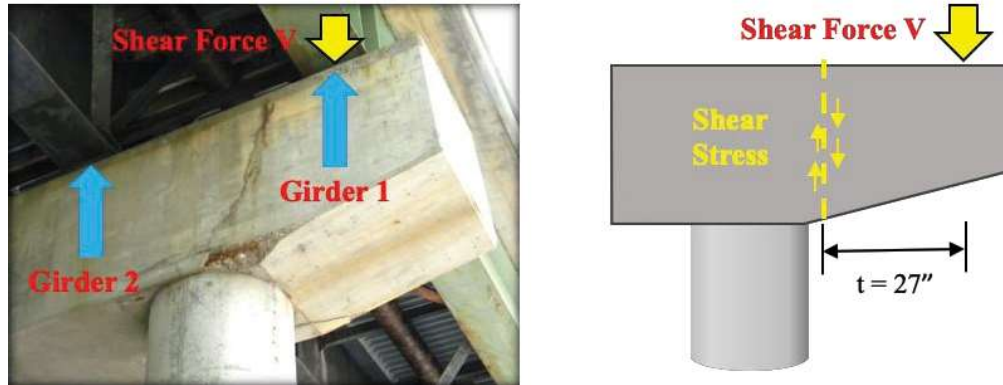


Figure 45. Field View of Cracked Pier-cap (left) and Shear Stress of the Pier-cap (right)

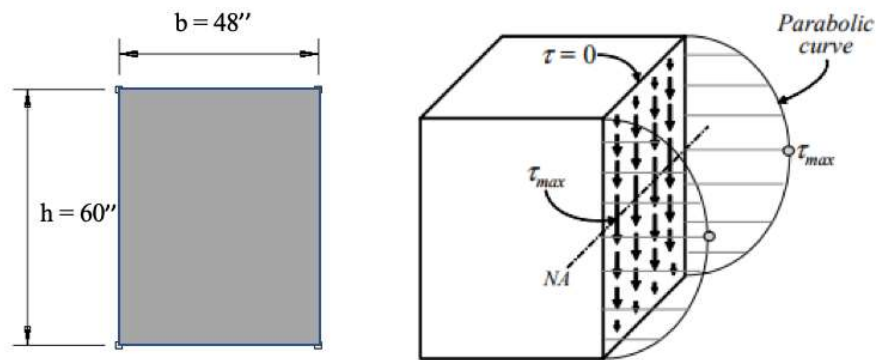


Figure 46. Cross Section (left) of Cracked Pier-cap and Shear Stress Distribution (right)

Given there were no shear stirrups (see Figure 31b) within a distance of 1 meter around the shear cracks based on the RC radar results, the shear strength of the cross section is primarily provided by the concrete. According to building code requirements for structural concrete (ACI 318), the nominal shear strength provided by concrete is computed as:

$$V_c = 2\sqrt{f'_c}b_wd$$

Eq. 16

where V_c is the shear strength provided by concrete, f'_c is compressive strength of concrete, b_w is the width of the section, d is the height of the section.

According to the bridge drawings, the ultimate compressive strength of pier concrete is 3,000 psi which indicates that shear cracks could be caused by shear stresses exceeding 110 psi ($2\sqrt{f'_c}$). Static and dynamic analysis were conducted to obtain the shear stresses of cracked cross section under dynamic and static loads, and the dynamic amplification of moving trucks was studied by comparing dynamic and static structural responses.

Static Analysis for Pier-cap Stress

7.2.1

The cracked pier-cap carries its self-weight and the loads transferred from Bearing 1S and Bearing 1N shown in Figure 47. The reaction forces at the bearings under dead load were extracted from the Abaqus Model, and the reaction force distribution (see Figure 48) showed that the maximum reaction force was at Bearings 1S and 1N for Span 1 SB and Span 2 SB respectively under dead loads (bridge self-weight) in accordance with the extra loads transferred from the bridge parapet which is above Bearing 1S and 1N. The shear stresses under deal load were calculated and list in Table 19.

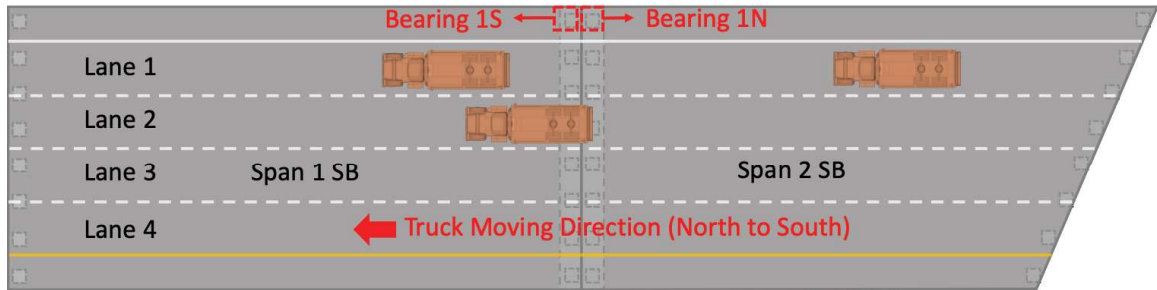


Figure 47. Example of loading scenario generating large bearing reaction: two Moving Trucks on Lane 1 and one Moving Truck on Lane 2

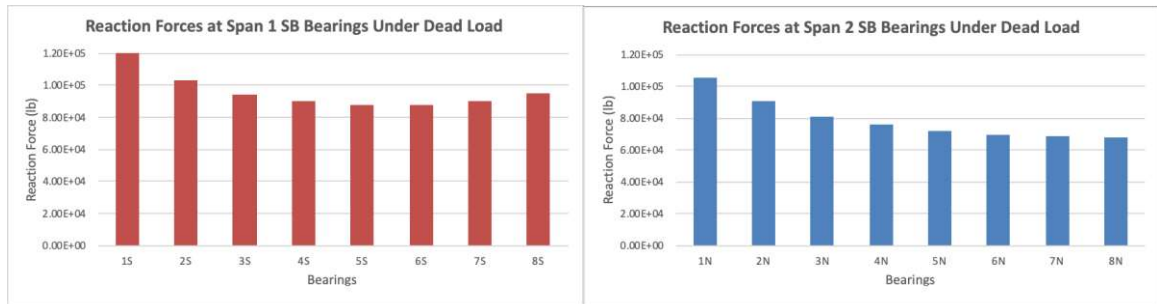


Figure 48. Reaction Force Distribution of Span 1 SB (left) and Span 2SB (right) under Dead Load

Table 19. Shear Stresses of Pier-cap under Dead Load

Dead Load	Load (lb)	Shear Stress (psi)
Pier-cap Self Weight	1.26E+04	6.54
Bearing 1S	9.86E+04	51.33
Bearing 1N	1.08E+05	56.16
Total Shear Force (V)	2.19E+05	114.03

Although the total shear stress, 114 psi, is already larger than the ultimate shear stress of concrete 110 psi, simulations with 3 moving trucks were conducted to understand the dynamic impacts of truck loads.

Dynamic Analysis for Pier-cap Stress

The trucks simulated are moving from the right side of Span 2 to the left side of Span 1 shown in Figure 47. Each span has four lanes, and the slow lane is Lane 1 where most trucks pass travel at rush hour. So, the truck load was designed to be applied on Lane 1 and 2 with a speed of 56 mph. The three-axle truck, HS-20 truck, was selected and used as the reference for truck loading. The total load of a HS-20 truck was 72 kips, 8 kips for front axles and both 32 kips for two rear axles shown in Figure 49. The contacting area of each tire was assumed to be 20-inch width by 10-inch length. The distance between two axles was 168 inches, and the distance between the two parallel tires was 72 inches.

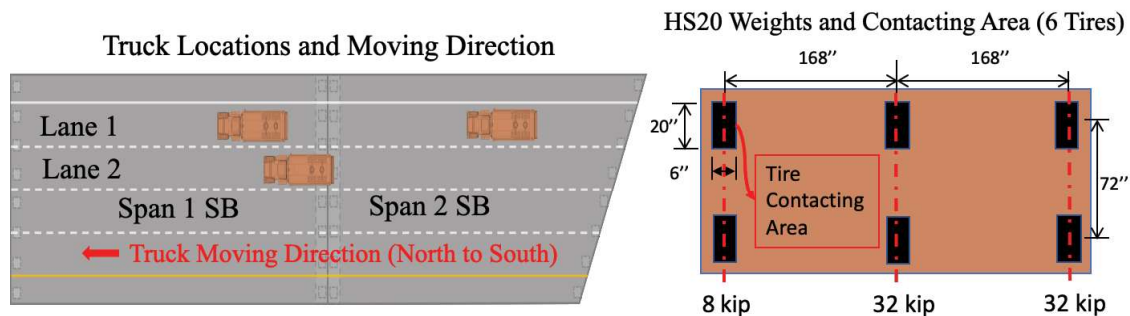


Figure 49. Truck Weights and Dimensions of HS 20 Truck

The model calibrated with displacement measurements was used for several simulations with moving vehicles, and assuming fully composite action and idealized supports (fixed bearing and expansion bearing). The time step for the simulation was 0.001 second with mesh size of 6-inch. In one simulation, one HS20 truck was moving along Lane 1. In another simulation the same truck was assumed moving along Lane 2 separately at the

same speed of 56 mph. The surface of the deck was assumed in perfect condition. This does not account for profile irregularities that can significantly increase the dynamic forces. The displacements at mid-span points of Span 1 SB and Span 2SB were extracted, and the displacement-time graphs of moving truck on Lane 1 and Lane 2 were shown in Figure 50. The DAFs of maximum displacement (Table 20), maximum total reaction force (Table 21), and maximum shear force at Bearings 1S and 1N (Table 22) were also calculated based on the dynamic simulations.

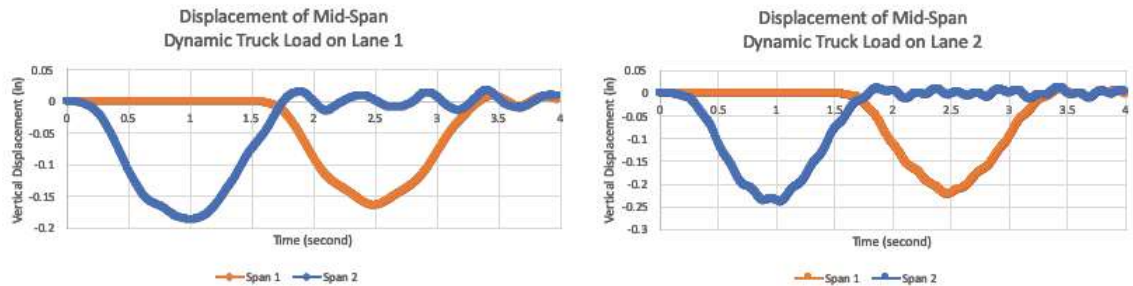


Figure 50. Mid-span Displacements under Truck Load moving along Lane 1 and Lane 2

Table 20. DAF for Maximum Displacement under Moving Truck Loads

Model	Maximum Vertical Displacement (inch)					
	Truck Moving along Lane 1			Truck Moving along Lane 2		
	Dynamic	Static	DAF	Dynamic	Static	DAF
Span 1 SB	-0.164	-0.158	1.04	-0.224	-0.215	1.04
Span 2 SB	-0.187	-0.183	1.02	-0.240	-0.235	1.02

Table 21. DAF for Maximum Total Reaction Force under Moving Truck Loads

Model	Maximum Total Reaction Force (kip)					
	Truck Moving along Lane 1			Truck Moving along Lane 2		
	Dynamic	Static	DAF	Dynamic	Static	DAF
Span 1 SB	81.98	72.00	1.14	88.28	72.00	1.23
Span 2 SB	87.16	72.00	1.21	82.76	72.00	1.15

Table 22. DAF of Maximum Shear Force for Bearings 1S and 1N

Model	Maximum Shear Force (kip)					
	Truck Moving along Lane 1			Truck Moving along Lane 2		
	Dynamic	Static	DAF	Dynamic	Static	DAF
Bearing 1S	17.08	15.24	1.12	18.28	15.80	1.16
Bearing 1N	17.75	16.27	1.09	17.72	15.51	1.14

Given the small acceleration obtained from the Abaqus model compared to the measured accelerations obtained from field tests shown in Figure 51, the real DAF on displacements subjected to moving truck loads should be significantly larger than 1.02 -1.04 obtained from the model.

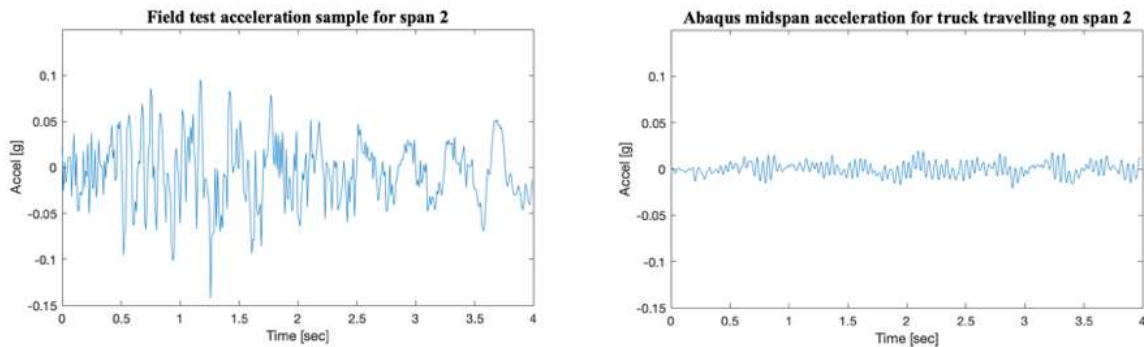


Figure 51. Vertical acceleration at Mid-span due to Moving Truck Load Obtained from Field Test (left) and Abaqus Model (right)

Although Table 16 and Table 18 indicated larger DAF on total reaction force for the skewed plate under truck loads moving along Lane 1 and Lane 2, a larger DAF was only obtained from Span 2 SB (skewed span) when the truck was moving on Lane 1 shown in Table 21. For the simulation of the truck moving on Lane 2, a smaller DAF 1.15 was

obtained for Span 2 SB while 1.23 was obtained for Span 1 SB which indicated the influence of truck locations on DAF for skewed span.

In order to find the most severe load combination due to the three trucks with two trucks moving along Lane 1 and one truck moving along Lane 2, the analysis of correlation between the two series of shear forces of Bearing 1S and Bearing 1N was performed for loads on Lane 1 and Lane 2. Given the minimum distance (50 ft) between two trucks on the same lane, a linear combination of three trucks was obtained with the correlation analysis for both dynamic and static analysis. The simulation results shown in Figure 52 represented a load scenario maximizing shear stress at the cross section of the cracked pier-cap.

Numerical values of the maximum shear stresses in the pier cap were summarized in Table 23, and the DAF value of 1.28 was calculated by comparing dynamic and static shear stresses. The maximum shear stress under dead load and dynamic truck loads is 135 psi, and it is obviously exceeding the capacity of concrete at the pier-cap. Such stresses, in absence of shear reinforcement (see Figure 31b), are likely responsible for the shear crack of the corbel. Consequently, the South end of Girder 1 virtually lost its support while the loads had to be redistributed to other bearings.

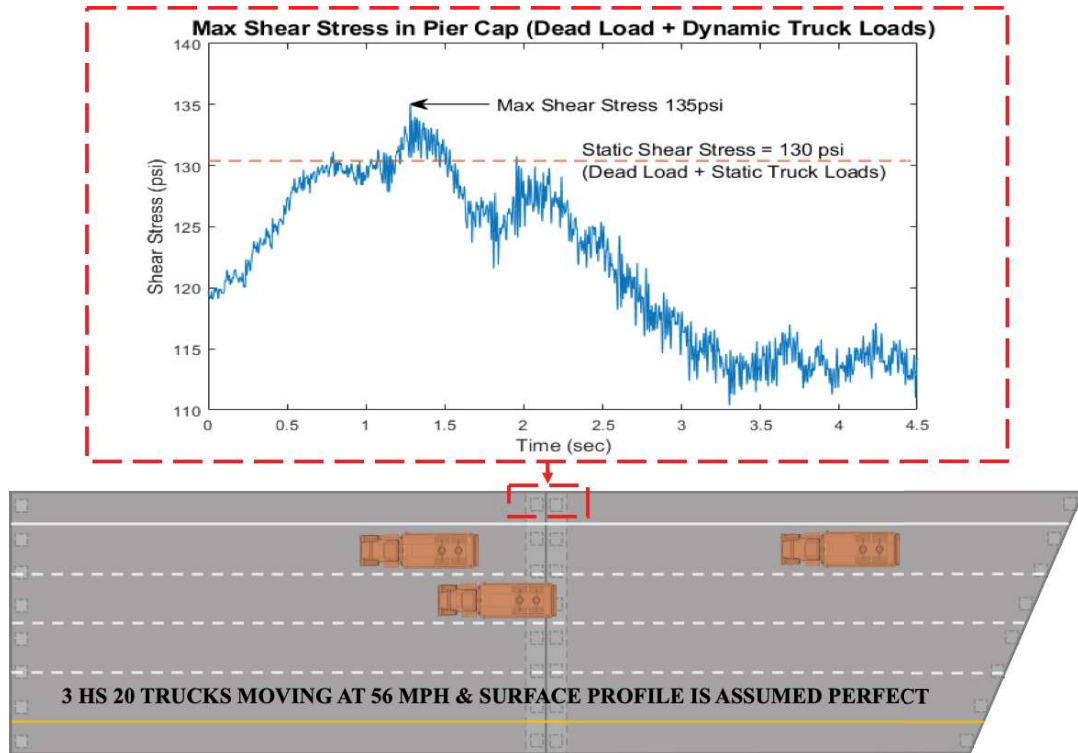


Figure 52. Simulation Results of Three Moving Trucks

Table 23 Maximum shear stresses obtained from simulation of three moving trucks

Actions	Max Shear Stress and DAF
Dead Load	114.0 psi
Static Truck Load	16.36 psi
Dynamic Truck Load	21.00 psi
DAF	1.28

The American Associations of States Highway and Transportation (AASHTO) Load and Resistance Factor Design (LRFD) specification (AASHTO 2010) specified the dynamic amplification factor as 1.33 for bridges. The DAF 1.28 obtained from finite element model simulations is very close to the DAF 1.33 defined in the design code. However, the influence of surface roughness, which had been proven to be an important factor for DAF (Kalyankar and Uddin 2016; KIM 2005; Law and Zhu 2004), was not taken into account

for the simulation. To obtain a more reliable dynamic amplification factor under moving truck loads, further analysis should be conducted in the future by taking other related parameters, such as surface roughness, vehicle speed, structure damping properties, vehicle mass, stiffness and damping of suspensions and tires, into account.

7.3 Summary and Correlation of Test Results

Recommendations for the rehabilitation of the tested bridge were provided based on the analysis of the experimental data, and model simulations: 1) to deal with approach slab settlements, rapid and complete drainage of surface water should be guaranteed; 2) the gas pipe poses a major risk and should be replaced and possibly routed underground; 3) fatigue cracks occurred primarily due to distortion of the wind braces (which were directly welded to the girder webs and appeared to be redundant for lateral loading), so removal of wind bracing elements should be considered; 4) deteriorated or damaged bearings should be replaced with multi-directional elastomeric bearings since FE model simulations indicated ideal bearing movements were biaxial and not uniaxial along the longitudinal direction of the span; 5) the pier-cap with shear cracking should be post-tensioned by coring through the concrete cap in conjunction with epoxy injection; 6) mitigation of excessive vibrations should be considered to improve durability and performance.

The study showed a tentative exploration of effectively integrating and leveraging NDE and SHM technologies for objective bridge condition and performance evaluation and asset-management. To improve asset management strategies, the integration of SHM and NDE data in the visual inspection practice should be considered. This could be achieved by leveraging technology before and during the inspection, by sharing images in real-time

and remotely consulting senior engineers; by installing sensors and capturing data to quantify operational strains, tilts, displacements and accelerations; and by leveraging properly captured and archived heuristic data. Moreover, inspection results should include documenting performance concerns for all performance limit states. Finally, technology leveraging requires strategy and integration. Constructing an intelligent monitoring system for a bridge (or a type of bridge) equipped with advanced sensing and imaging devices requires the integration of heuristic knowledge with quantitative data. This represents a potential strategy for a mechanistic understanding of the bridge global performance and to discover the root causes of performance concerns, and it can also be utilized for developing efficient maintenance and asset management systems.

Chapter 8: Conclusions, Recommendations, and Future Work

8.1 Summary of Conclusions and Recommendations

The “International Bridge Study” revealed design, construction and maintenance shortcomings that have led to multiple bridge performance concerns. It was possible to pinpoint the root causes of some deteriorations and damage by heuristics. For example, the settlements of the approach slabs were obviously caused by fill erosion as bridge drainage was not properly designed. The connections of the wind-brace elements to the girder webs created lateral distortions at these points that were aggravated by vibrations and led to fatigue cracking. These braces were observed to cause web fatigue cracking at several other bridges and their direct welding on to the web were understood to be fatigue-critical details. The stiffness provided by these braces could be better provided using diaphragms. The failures of many rocker bearings were due to the tendency of these supports to rock along directions which were different from the natural tendency of the bridge to deform under live loads and with temperature effects. However, it was also proven that heuristics is not sufficient in diagnosing all of the root causes of performance deficiencies of the test bridge. The study demonstrated the value of an integrated and scientific approach to field testing leveraging the structural-identification concept. By designing and interpreting the field experiments supported by proper analytical prediction using the A-Priori model, a greater value was achieved from the field experiments. It was possible to design real-time controlled load testing by monitoring critical bridge responses; integration of a sufficient number of sensors such as accelerometers, strain and displacement transducers to obtain necessary information for a mechanistic understanding and robust analytical modelling.

Based on the analysis of the field experiments and model updating, the following conclusions were formulated:

- 1) Ambient vibration testing, when properly performed and when data was processed properly, revealed the first several modes of the structure. These were shown as sufficient for parameter identification of an analytical model of the bridge; the forced vibration test, which can be more time consuming and costly, did not offer a clear advantage against ambient vibration except that the uncertainty in the test results would be less.
- 2) Controlled static load testing was especially useful in demonstrating the location and effects of damage (even when damage is not visible) and for parameter identification for a digital-twin. However, this kind of test should only be reserved for the most critical cases due to the high cost and disruptions; the considerable expertise required in test planning and execution; and the risks associated with proper loading and measuring critical bridge responses. Especially, both displacement and strain measurements were found to be much more essential than just strain measurements. Unfortunately, most load tests are currently executed with only strain gages. Parameter identification proved the relative value of displacements to strains. It is recommended when possible to use both types of measurements!
- 3) NDT applications were useful in revealing the variation in material properties and the extent of concrete deck delamination. NDT also indicated that the delamination for the tested bridge was not due to the corrosion of the deck reinforcement. This leaves vibration as the probable cause discussed in the following. It is also

important to note that NDT applications without vibration or load testing of the system are not very valuable as they are not sufficient for identifying damage or deterioration due to overlapping of multiple causes, and cannot help determine the capacity and possible failure modes of the system; Other experimental approaches, such as long-term monitoring, provided highly useful complementary insights;

- 4) Operational vibrations that are in the 20% g range are often detrimental to the serviceability and durability of a bridge, and the design of bridges should incorporate the effects of geometry on their vibration characteristics. Dynamic amplifications of stresses were shown to further aggravate stresses in cracked members even though conservative estimates were obtained since trucks were assumed to move over a perfect deck profile. The amplifications caused by vibration were attributed also to the unusual straight-skew geometry and the corresponding mode shapes. Dynamics obviously played a significant role in the deterioration of the deck as well as fatigue cracking, although proper design would have mitigated the latter.

A careful visual inspection by a professional bridge engineer who is equipped with excellent heuristics resulting from decades of practice, could have observed and recorded all the damage and deterioration including the pier-cap crack. However, we have little heuristics in bridge dynamics, as bridges are designed, inspected, maintained and managed by assuming static behaviour. In design and rating, load effects are increased but not to the level of amplification that was measured for the tested span.

Perhaps the most important recommendation regards the necessity of measurements during bridge inspections. Accelerations, strains, tilts and displacements can now be measured by

wireless sensors that may be quickly deployed, and operational monitoring of a bridge would reveal a wealth of information regarding the root causes of distresses and deteriorations. Since we are rapidly losing the truly experienced bridge engineers with heuristic knowledge, we should be making a transformation to objective metrics that will quantify the conditions and performance of a bridge. Given the cost of typical overpass and ramp bridges often easily exceed \$Tens of Millions, we cannot justify not demanding a new era of rational bridge engineering.

8.2 Further Work

To extend the work of this thesis to general type of bridges, the following areas of future work should be considered:

- 1) Advanced technologies in other domains should be utilized and implemented in the process of St-Id, such as:
 - a. Unmanned aerial systems, such as drones, can be used to assist in the observation and conceptualization step especially for the areas with limited access and associated personal high safety risk, and the high-resolution imagery obtained from the system could also be used for automated damage identification using computer vision technologies;
 - b. Machine Learning and Deep Learning technologies could be used to analyze long-term monitoring data, such as classifying extreme events caused by truck loads, identifying outliers of the measurements, and predicting the responses of bridges under specific scenarios;
- 2) Additional tools and technologies need to be explored for non-destructive evaluation and proper positioning of sensors for different types of experiments:

- a. The NDE testing conducted on the bridge deck requires traffic control, and the deck condition and environment factors would affect the accuracy of the results.
Thus, it is necessary to explore and implement more advanced non-destructive applications and technologies; High speed scanning of bridge decks providing RGB and IR imaging already provide full mapping of bridge decks with detection of cracks and subsurface delamination;
 - b. Wireless sensors and additional technologies are increasingly available and should be implemented in St-Id;
- 3) For finite element model calibration, different parameters and spatial distribution of these parameters should be considered. The piers and foundations of the structure should also be carefully modeled and analyzed for more reliable risk assessment analysis when scour critical conditions are present and for dynamic analysis;
- 4) For analysis of dynamic amplification factors of bridge responses under moving truck load, several factors should be considered in future studies: bridge natural frequencies and damping properties, influence of geometry, vehicle frequencies and damping ratio, vehicle speed, and surface roughness;
- 5) Various types of bridges should be evaluated following the integration strategies to strengthen the conclusions reached in this study.

List of References

- AASHTO. 2010. *AASHTO LRFD Bridge Design Specifications*. Fourth edition with 2008 interim revisions. Washington, D.C. : American Association of State Highway and Transportation Officials, [2008] ©2007.
- Aktan, A. Emin, Daniel N. Farhey, David L. Brown, Vikram Dalal, Arthur J. Helmicki, Victor J. Hunt, and Stuart J. Shelley. 1996. “Condition Assessment for Bridge Management.” *Journal of Infrastructure Systems* 2(3):108–17.
- Aktan, Ahmet Emin, Franklin L. Moon, and Jeffrey Scott Weidner. 2016. “Leveraging Technology for Infrastructure Condition and Performance Assessment.” *Frontiers in Built Environment* 2:36.
- American Society of Civil Engineers. 2013. “Structural Identification of Constructed Systems - Approaches, Methods and Technologies for Effective Practice of St-Id” edited by F. N. Çatbaş, T. Kijewski-Correa, and A. E. Aktan. *American Society of Civil Engineers* 1–248.
- ARTRB. 2019. *2019 Bridge Report*.
- Bakir, Pelin Gundes, Edwin Reynders, and Guido De Roeck. 2007. “Sensitivity-Based Finite Element Model Updating Using Constrained Optimization with a Trust Region Algorithm.” *Journal of Sound and Vibration* 305(1–2):211–25.
- Behmanesh, Iman, Babak Moaveni, Geert Lombaert, and Costas Papadimitriou. 2015. “Hierarchical Bayesian Model Updating for Structural Identification.” *Mechanical Systems and Signal Processing* 64–65:360–76.
- Brady, Sean, Eugene OBrien, and Ales Znidaric. 2006. “Effect of Vehicle Velocity on the Dynamic Amplification of Two Vehicles Crossing a Simply Supported Bridge.” *Journal of Bridge Engineering - J BRIDGE ENG* 11.
- Catbas, F. Necati, and Tracy Kijewski-Correa. 2013. “Structural Identification of Constructed Systems: Collective Effort toward an Integrated Approach That Reduces Barriers to Adoption.” *Journal of Structural Engineering* 139(10):1648–52.
- Çatbaş, Necati, Ahmet Türer, Zongfen Zhang, and Emin Aktan. 1998. “Structural Identification: Analytical Aspects.”
- Chan, Tommy H. T., Demeke B. Ashebo, H. Y. Tam, Y. Yu, T. F. Chan, P. C. Lee, and

- Eduardo Perez Gracia. 2009. "Vertical Displacement Measurements for Bridges Using Optical Fiber Sensors and CCD Cameras — A Preliminary Study." *Structural Health Monitoring: An International Journal* 8(3):243–49.
- Chase, S. B., Y. Adu-Gyamfi, A. E. Aktan, and E. Minaie. 2016. *Synthesis of National and International Methodologies Used for Bridge Health Indices*.
- Chipman, Tim, Aaron Costin, Charles Eastman, Roger Grant, Thomas Liebich, Dana Smithh, and Donghoon Yang. 2016. *Bridge Information Modeling Standardization*.
- Cosser, Emily, Gethin W. Roberts, Xiaolin Meng, and Alan H. Dodson. 2003. "THE COMPARISON OF SINGLE FREQUENCY AND DUAL FREQUENCY GPS FOR BRIDGE DEFLECTION AND VIBRATION MONITORING."
- Deng, Lu, Yang Yu, Qiling Zou, and C. Cai. 2014. "State-of-the-Art Review of Dynamic Impact Factors of Highway Bridges." *Journal of Bridge Engineering* 20:4014080.
- Doebbling, S. W., C. R. Farrar, M. B. Prime, and D. W. Shevitz. 1996. *Damage Identification and Health Monitoring of Structural and Mechanical Systems from Changes in Their Vibration Characteristics: A Literature Review*. Los Alamos, NM.
- Doebbling, Scott W. SW, CR Charles R. Farrar, MB Michael B. Prime, Scott W. SW Doebbling, CR Charles R. Farrar, and MB Michael B. Prime. 1998. "A Summary Review of Vibration-Based Damage Identification Methods." *Shock and Vibration Digest* 30:1–34.
- Farrar, C. R., S. W. Doebbling, and D. A. Nix. 2001. "Vibration-Based Structural Damage Identification." *Philosophical Transactions of the Royal Society A: Mathematical, Physical and Engineering Sciences* 359(1778):131–49.
- Ferri, M., L. Belsito, F. Mancarella, L. Masini, A. Roncaglia, J. Yan, A. A. Seshia, J. Zalesky, and K. Soga. 2011. "Fabrication and Testing of a High Resolution Extensometer Based on Resonant MEMS Strain Sensors." Pp. 1056–59 in *2011 16th International Solid-State Sensors, Actuators and Microsystems Conference*. IEEE.
- FHWA. 1992. "Additional Guidance on 23 CFR 650 D." Retrieved June 8, 2018 (<https://www.fhwa.dot.gov/bridge/0650dsup.cfm>).
- FHWA. 2001. "Reliability of Visual Inspection for Highway Bridges - FHWA-RD-01-020." *Federal Highway Administration*. Retrieved May 27, 2018 (<https://www.fhwa.dot.gov/publications/research/nde/01020.cfm>).
- FHWA. 2006. "Bridge Load Ratings for the National Bridge Inventory - National Bridge Inspection Standards - Bridge Inspection - Safety - Bridges & Structures - Federal Highway Administration." Retrieved June 8, 2018 (<https://www.fhwa.dot.gov/bridge/nbis/103006.cfm>).

- FHWA. 2015. "Nondestructive Evaluation (NDE) Web Manual, Version 1.0." Retrieved (<https://fhwaapps.fhwa.dot.gov/ndep/Default.aspx>).
- FHWA. 2016. "National Highway Performance Program (NHPP) - NHPP - Federal-Aid Programs - Federal-Aid Programs and Special Funding - Federal Highway Administration." Retrieved June 8, 2018 (<https://www.fhwa.dot.gov/specialfunding/nhpp/160309.cfm>).
- FHWA. 2018. "Tables of Frequently Requested NBI Information - National Bridge Inventory - Bridge Inspection - Safety - Bridges & Structures - Federal Highway Administration." Retrieved June 8, 2018 (<https://www.fhwa.dot.gov/bridge/britab.cfm>).
- Freeby, Gregg A. 2013. *Bridge Inspection Manual*. Vol. 1.
- Friswell, M., and JE Mottershead. 1995. "Finite Element Model Updating in Structural Dynamics."
- Friswell, Michael I., D. J. Inman, and D. F. Pilkey. 1998. "Direct Updating of Damping and Stiffness Matrices." *AIAA Journal* 36(3):491–93.
- Frýba, and Ladislav. 1973. *Vibration of Solids and Structures under Moving Loads* /.
- Fuchs, P. A., G. A. Washer, S. B. Chase, and M. Moore. 2004. "Laser-Based Instrumentation for Bridge Load Testing." *Journal of Performance of Constructed Facilities* 18(4):213–19.
- Gentile, C., and A. Saisi. 2007. "Ambient Vibration Testing of Historic Masonry Towers for Structural Identification and Damage Assessment." *Construction and Building Materials* 21(6):1311–21.
- German, Stephanie, Ioannis Brilakis, and Reginald DesRoches. 2012. "Rapid Entropy-Based Detection and Properties Measurement of Concrete Spalling with Machine Vision for Post-Earthquake Safety Assessments." *Advanced Engineering Informatics* 26(4):846–58.
- Guan, Shanyue, Jennifer A. Rice, Changzhi Li, Yiran Li, and Guochao Wang. 2015. "Dynamic and Static Structural Displacement Measurement Using Backscattering DC Coupled Radar." *Smart Structures and Systems* 16(3):521–35.
- Gucunski, Nenad, Arezoo Imani, Francisco Romero, Soheil Nazarian, Deren Yuan, Herbert Wiggensauser, Parisa Shokouhi, Alexander Taffe, and Doria Kutrubes. 2012. *Nondestructive Testing to Identify Concrete Bridge Deck Deterioration*. Washington, D.C.: Transportation Research Board.
- Gucunski, Nenad, Seong-Hoon Kee, Hung La, Basily Basily, and Ali Maher. 2015.

- “Delamination and Concrete Quality Assessment of Concrete Bridge Decks Using a Fully Autonomous RABIT Platform.” *Structural Monitoring and Maintenance* 2(1):19–34.
- Gucunski, Nenad, Francisco Romero, Sabine Kruschwitz, Ruediger Feldmann, Ahmad Abu-Hawash, and Mark Dunn. 2010. “Multiple Complementary Nondestructive Evaluation Technologies for Condition Assessment of Concrete Bridge Decks.” *Transportation Research Record: Journal of the Transportation Research Board* 2201(1):34–44.
- Hearn, George, and Rene B. Testa. 1991. “Modal Analysis for Damage Detection in Structures.” *Journal of Structural Engineering* 117(10):3042–63.
- Huston, Dryver, Jianhong Cui, Dylan Burns, and David Hurley. 2011. “Concrete Bridge Deck Condition Assessment with Automated Multisensor Techniques.” *Structure and Infrastructure Engineering* 7(7–8):613–23.
- Kabir, Shahid. 2010. “Imaging-Based Detection of AAR Induced Map-Crack Damage in Concrete Structure.” *NDT & E International* 43(6):461–69.
- Kalyankar, Rahul, and Nasim Uddin. 2016. “Simulating the Effects of Surface Roughness on Reinforced Concrete T Beam Bridge under Single and Multiple Vehicles” edited by L. Nobile. *Advances in Acoustics and Vibration* 2016:3594148.
- KIM, C. 2005. “Three-Dimensional Dynamic Analysis for Bridge–Vehicle Interaction with Roadway Roughness.” *Computers & Structures* 83(19):1627–45.
- Ko, J. M. M., and Y. Q. Q. Ni. 2005. “Technology Developments in Structural Health Monitoring of Large-Scale Bridges.” *Engineering Structures* 27(12):1715–25.
- Kou, Jine-Wen, and John DeWolf. 1997. “Vibrational Behavior of Continuous Span Highway Bridge—Influencing Variables.” *Journal of Structural Engineering* 123:333–44.
- Lagarias, Jeffrey C., James A. Reeds, Margaret H. Wright, and Paul E. Wright. 1998. “Convergence Properties of the Nelder--Mead Simplex Method in Low Dimensions.” *SIAM Journal on Optimization* 9(1):112–47.
- Law, S. S., and X. Q. Zhu. 2004. “Dynamic Behavior of Damaged Concrete Bridge Structures under Moving Vehicular Loads.” *Engineering Structures* 26(9):1279–93.
- Lee, Kuo-Liang, Alper Levi, David L. Brown, A. Emin Aktan, Victor J. Hunt, Arthur J. Helmicki, Daniel N. Farhey, Arthur J. Helmicki, David L. Brown, Victor J. Hunt, Kuo-Liang Lee, and Alper Levi. 1997. “Structural Identification for Condition Assessment: Experimental Arts.” *Journal of Structural Engineering* 123(12):1674–84.

- Levin, R. I., and N. A. J. Lieven. 1998. "Dynamic Finite Element Model Updating Using Simulated Annealing and Genetic Algorithms." *Mechanical Systems and Signal Processing* 12(1):91–120.
- Li, Hong-Nan, Dong-Sheng Li, and Gang-Bing Song. 2004. "Recent Applications of Fiber Optic Sensors to Health Monitoring in Civil Engineering." *Engineering Structures* 26(11):1647–57.
- Liu, Shih-Chi, and James T. P. Yao. 1978. "Structural Identification Concept." *Journal of the Structural Division* 104(12):1845–58.
- Megaw, E. D. 1979. "Factors Affecting Visual Inspection Accuracy." *Applied Ergonomics* 10(1):27–32.
- Meng, J. Y., Eric Lui, and Y. LIU. 2001. "Dynamic Response of Skew Highway Bridges." *Journal of Earthquake Engineering - J EARTHQU ENG* 5:205–23.
- Minnesota Department of Transportation. 2006. "Mn/DOT Celebrates Interstate Highway System's 50th Anniversary." Retrieved (<https://web.archive.org/web/20071204072603/http://www.dot.state.mn.us/interstate50/50facts.html>).
- Minshui, Huang, and Zhu Hongping. 2008. "Finite Element Model Updating of Bridge Structures Based on Sensitivity Analysis and Optimization Algorithm." *Wuhan University Journal of Natural Sciences* 13(1):87–92.
- Mottershead, J. E., and M. I. Friswell. 1993. "Model Updating In Structural Dynamics: A Survey." *Journal of Sound and Vibration* 167(2):347–75.
- N. Gucunski, F. Romero, S. Kruschwitz, R. Feldmann, and H. Parvardeh. 2011. *Comprehensive Bridge Deck Deterioration Mapping of Nine Bridges by Non-Destructive Evaluation Technologies*.
- National Academies of Sciences, Engineering, and Medicine. 2014. *State Bridge Load Posting Processes and Practices*. edited by G. Hearn. Washington, DC: The National Academies Press.
- Noël, J. P., and G. Kerschen. 2017. "Nonlinear System Identification in Structural Dynamics: 10 More Years of Progress." *Mechanical Systems and Signal Processing* 83:2–35.
- NTSB. 2008. "NTSB Determines Inadequate Load Capacity Due to Design Errors of Gusset Plates Caused I-35W Bridge to Collapse." *National Transportation Safety Board Office of Public Affairs*. Retrieved May 30, 2018 (https://www.nts.gov/news/press-releases/Pages/NTSB_Determines_Inadequate_Load_Capacity_due_to_Design_Err

ors_of_Gusset_Plates_caused_I-35W_Bridge_to_Collapse.aspx).

- Paultre, Patrick, Omar Chaallal, and Jean Proulx. 1992. "Bridge Dynamics and Dynamic Amplification Factors — a Review of Analytical and Experimental Findings." *Canadian Journal of Civil Engineering* 19(2):260–78.
- Ren, Wei-Xin, Tong Zhao, and Issam E. Harik. 2004. "Experimental and Analytical Modal Analysis of Steel Arch Bridge." *Journal of Structural Engineering* 130(7):1022–31.
- Rossi, G., R. Marsili, V. Gusella, and M. Giofrè. 2002. "Comparison between Accelerometer and Laser Vibrometer to Measure Traffic Excited Vibrations on Bridges." *Shock and Vibration* 9(1–2):11–18.
- Ryan, Thomas W., J. Eric Mann, Zachary M. Chill, and Bryan T. Ott. 2012. *Bridge Inspector's Reference Manual*.
- Salawu, O. S. 1997. "Detection of Structural Damage through Changes in Frequency: A Review." *Engineering Structures* 19(9):718–23.
- Sohn, Hoon, C. R. Farrar, F. M. Hemez, D. D. Shunk, D. W. Stinemates, B. R. Nadler, and J. J. Czarnecki. 2004. *A Review of Structural Health Monitoring Literature : 1996 – 2001, Technical Report. Report Number LA-13976-MS*.
- Tata, Uday, S. Deshmukh, J. C. Chiao, Ronald Carter, and H. Huang. 2009. "Bio-Inspired Sensor Skins for Structural Health Monitoring." *Smart Materials and Structures* 18(10):104026.
- Te, H. I., W. A. Take, and M. D. B. Olton. 2003. "Soil Deformation Measurement Using Particle Image Velocimetry (PIV) and Photogrammetry." 53(7):619–31.
- U.S. Department of Transportation. 2014. "2010 Conditions and Performance - Policy | Federal Highway Administration." *Policy and Governmental Affairs* chapter 1. Retrieved June 8, 2018 (<https://www.fhwa.dot.gov/policy/2004cpr/chap15a.cfm>).
- Washer, Glenn, Richard Fenwick, and Naveen Bolleni. 2010. "Effects of Solar Loading on Infrared Imaging of Subsurface Features in Concrete." *Journal of Bridge Engineering* 15(4):384–90.
- Webb, G. T., P. J. Vardanega, and C. R. Middleton. 2015. "Categories of SHM Deployments: Technologies and Capabilities." *Journal of Bridge Engineering* 20(11):04014118.
- Zhang, Jian, S. L. Guo, Z. S. Wu, and Q. Q. Zhang. 2015. "Structural Identification and Damage Detection through Long-Gauge Strain Measurements." *Engineering Structures* 99:173–83.

Appendices

Supplementary information for:

1. DLOAD Fortran Subroutine used for applying dynamic and static load on Rectangle and Skew shape plates mentioned in section 7.1.

1) Moving load applied along mid-span over one loading area

```

SUBROUTINE DLOAD(F,KSTEP,KINC,TIME,NOEL,NPT,LAYER,KSPT,
1 COORDS,JLTYP,SNAME)
C
C   INCLUDE 'ABA_PARAM.INC'
C
C   DIMENSION TIME(2), COORDS (3)
C   CHARACTER*80 SNAME
C----- Parameters 50mph = 838 inch/second
C   SPEED=1000.
C----- Define Wheel loading F1 - Front, F2 - Middle, F3 - Rear
C   Area=200.
C   FORCE = 72000.
C   F1 = FORCE/Area
C   F=0.
C Define the frist truck moving path
C   StartPts=1410.
C   Location = TIME(1)*SPEED
C   ST1=StartPts-Location
C   contactLen = 10
C   ST1_2=ST1 + contactLen
C Mesh Size 5
C   meshsize = 5.
C   meshhalf = meshsize/2.
C Min two elements - Max three elements
C   extraD = ceiling(ST1/meshsize)*meshsize - ST1
C   IF(extraD .NE. 0)THEN ! three elements
C     F1_E1 = F1
C     F1_E2 = F1
C     F1_E3 = 0.
C     ST1_E1_Start = ST1
C     ST1_E3_End = ST1_2
C     F1_E1 = F1 * extraD / meshsize
C     F1_E3 = F1 * (meshsize - extraD) / meshsize
C     ST1_E1_Start = ST1 - 5 + extraD
C     ST1_E3_End = ST1_2 + extraD
C     ST1_E1_End = ST1_E1_Start + meshsize
C     ST1_E3_Start = ST1_E3_End - meshsize
C     IF(COORDS(1) .GE. ST1_E1_Start .AND. COORDS(1) .LE. ST1_E3_End)THEN
C       IF(COORDS(1) .LE. ST1_E1_End) THEN
C         F = F1_E1
C       ELSE IF(COORDS(1) .LE. ST1_E3_Start) THEN
C         F = F1_E2
C       ELSE
C

```

```

        F = F1_E3
    ENDIF
ELSE
    F=0.
ENDIF
ELSE !two elements
    IF(COORDS(1) .GE. ST1 .AND. COORDS(1) .LE. ST1_2)THEN
        F = F1
    ELSE
        F=0.
    ENDIF
ENDIF
RETURN
END

```

2) Moving load applied along Lane 1 (Iroad 1) or Lane 2 (Iroad 2) over six loading area

```

SUBROUTINE DLOAD(F,KSTEP,KINC,TIME,NOEL,NPT,LAYER,KSPT,
1 COORDS,JLTYP,SNAME)
C
    INCLUDE 'ABA_PARAM.INC'
C
    DIMENSION TIME(2), COORDS (3)
    CHARACTER*80 SNAME
    !----- Parameters 56mph = 1000 inch/second
    SPEED=1000.
    Trucklen_1=168.
    Trucklen_2=168.
    TireWidth=20.
    TruckWidth=72.+TireWidth
    TireContact_len=6.
    StartPts=1488. !1518.
    meshsize = 6.
    StartPts=1488.
    !----- Lanes Info
    !----- Define the lanes in abaqus Model according to Current z coordinate -- COORDS(3)
    !----- Rect: [767, 0] Lane 1: 683,527; Lane 2: 527,383; MidSpan: 393.5,373.5
    !----- Skew: [0,-767] Lane 1: -84,-240; Lane 2: -240,-384; MidSpan: -393.5,-373.5
    ! Lane 1
    ! Rect
    L1_L1=643.5
    L1_L2=L1_L1+TireWidth
    L1_R1=L1_L2-TruckWidth
    L1_R2=L1_R1+TireWidth
    ! Skew
    L21_L1=-123.5
    L21_L2=L21_L1+TireWidth
    L21_R1=L21_L2-TruckWidth
    L21_R2=L21_R1+TireWidth
    ! Lane 2
    ! Rect
    L2_L1=483.5
    L2_L2=L2_L1+TireWidth
    L2_R1=L2_L2-TruckWidth
    L2_R2=L2_R1+TireWidth

```

```

! Skew
L22_L1=-283.5
L22_L2=L22_L1+TireWidth
L22_R1=L22_L2-TruckWidth
L22_R2=L22_R1+TireWidth
! MidSpan
! Rect
L5_L1=383.5-10.
L5_L2=L5_L1+TireWidth
! Skew
L25_L1=-383.5-10.
L25_L2=L25_L1+TireWidth

IF((COORDS(3).GE.L1_L1.AND.COORDS(3).LE.L1_L2).OR.(COORDS(3).GE.L1_R1.AND.COORDS(
3).LE.L1_R2)) THEN
  Iroad=1
ELSE
IF((COORDS(3).GE.L2_L1.AND.COORDS(3).LE.L2_L2).OR.(COORDS(3).GE.L2_R1.AND.COORDS(
3).LE.L2_R2)) THEN
  Iroad=2
ELSE
IF((COORDS(3).GE.L21_L1.AND.COORDS(3).LE.L21_L2).OR.(COORDS(3).GE.L21_R1.AND.COOR
DS(3).LE.L21_R2)) THEN
  Iroad=1
ELSE
IF((COORDS(3).GE.L22_L1.AND.COORDS(3).LE.L22_L2).OR.(COORDS(3).GE.L22_R1.AND.COOR
DS(3).LE.L22_R2)) THEN
  Iroad=2
ELSE IF(COORDS(3).GE.L25_L1 .AND. COORDS(3).LE.L25_L2) THEN
  Iroad=5
ELSE IF(COORDS(3).GE.L5_L1 .AND. COORDS(3).LE.L5_L2) THEN
  Iroad=5
ELSE
  Iroad=0
ENDIF
! Define the frist truck moving path
Location = TIME(1)*SPEED
ST1=StartPts - Location
FT1=ST1+TireContact_len
! ---- Define pressure according to mesh size
! Mesh Size 6
len_extra = TireContact_len - meshsize
!----- Define Wheel loading F1 - Front, F2 - Middle, F3 - Rear
Area=2.*TireWidth*TireContact_len
F1=8000./Area
F2=32000./Area
F3=32000./Area
F=0.
! two elements
extraD = ceiling(ST1/meshsize)*meshsize - ST1
ST_start_extra = 0.
FT_end_extra = 0.
F_E1 = 1. ! first element factor
F_E2 = 1. ! second element factor
IF(Iroad.EQ.1)THEN
  IF(extraD .NE. 0.) THEN !two element

```

```

    F_E1 = extraD / meshsize
    ST_start_extra = -meshsize + extraD
    FT_end_extra = meshsize - TireContact_len + extraD
    F_E2 = (TireContact_len - extraD) / meshsize
ELSE ! one element
    F_E2 = 0.
ENDIF
ST1_start = ST1 + ST_start_extra
FT1_end = FT1 + FT_end_extra
ST2_start = ST1_start + Trucklen_1
FT2_end = FT1_end + Trucklen_1
ST3_start = ST2_start + Trucklen_2
FT3_end = FT2_end + Trucklen_2
! For Front wheels
IF(COORDS(1).GE.ST1_start.AND.COORDS(1).LE.FT1_end)THEN
    F_curr = F1
    ST_start = ST1_start
    FT_end = FT1_end
    IF(extraD.NE.0) THEN ! two element
        ST_E1_End = ST_start + meshsize
        IF(COORDS(1).LE.ST_E1_End) THEN
            F = F_curr * F_E1
        ELSE
            F = F_curr * F_E2
        ENDIF
    ELSE ! one elements
        F = F_curr
    ENDIF
! For Middle wheels
ELSE IF(COORDS(1).GE.ST2_start.AND.COORDS(1).LE.FT2_end)THEN
    F_curr = F2
    ST_start = ST2_start
    FT_end = FT2_end
    IF(extraD.NE.0) THEN ! two element
        ST_E1_End = ST_start + meshsize
        IF(COORDS(1).LE.ST_E1_End) THEN
            F = F_curr * F_E1
        ELSE
            F = F_curr * F_E2
        ENDIF
    ELSE ! one elements
        F = F_curr
    ENDIF
! For Rear wheels
ELSE IF(COORDS(1).GE.ST3_start.AND.COORDS(1).LE.FT3_end)THEN
    F_curr = F3
    ST_start = ST3_start
    FT_end = FT3_end
    IF(extraD.NE.0) THEN ! two element
        ST_E1_End = ST_start + meshsize
        IF(COORDS(1).LE.ST_E1_End) THEN
            F = F_curr * F_E1
        ELSE
            F = F_curr * F_E2
        ENDIF
    ELSE ! one elements

```

```

      F = F_curr
    ENDIF
  ELSE
    F=0.
  ENDIF
ELSE
  F=0.
ENDIF
RETURN
END

```

2. DLOAD Fortran Subroutine used for applying dynamic and static load on Span 1 SB and Span 2 SB mentioned in section 7.2.

1) Moving truck load applied along Lane 1 (Iroad 1) or Lane 2 (Iroad 2) over six loading area

```

      SUBROUTINE DLOAD(F,KSTEP,KINC,TIME,NOEL,NPT,LAYER,KSPT,
1 COORDS,JLTY,SNAME)
C
C   INCLUDE 'ABA_PARAM.INC'
C
C   DIMENSION TIME(2), COORDS (3)
C   CHARACTER*80 SNAME
C----- Parameters 56mph = 1000 inch/second
      SPEED=1000.
      Trucklen_1=168.
      Trucklen_2=168.
      TireWidth=20.
      TruckWidth=72.+TireWidth
      TireContact_len=6.
      StartPts=1488.
C----- define wheels (left and righth, front middle and rear)
C Lane 1: 84 -- 84+156; Lane 2: 240 -- 240+144; Lane 3: 384 -- 384+144; Lane 3: 528 -- 528+144;
C Lane width
      L1=156.
      L2=144.
      L3=144.
      L4=144.
      z_start = -37.5
      LaneTruckSpace = (L1-TruckWidth)/2.
C Lane 1 Tire
      L1_L1 = 66.
      L1_L2=L1_L1+TireWidth
      L1_R2=L1_L1+TruckWidth
      L1_R1=L1_R2-TireWidth
C Lane 2
      L2_L1 = 226.
      L2_L2=L2_L1+TireWidth
      L2_R2=L2_L1+TruckWidth
      L2_R1=L2_R2-TireWidth
C Lane 3
      L3_L1=384. + z_start+LaneTruckSpace
      L3_L2=L3_L1+TireWidth

```

```

L3_R2=L3_L1+TruckWidth
L3_R1=L3_R2-TireWidth
C Lane 4
L4_L1=528. + z_start + LaneTruckSpace
L4_L2=L4_L1+TireWidth
L4_R2=L4_L1+TruckWidth
L4_R1=L4_R2-TireWidth
C Define the lanes in abaqus Model according to Current z coordinate -- COORDS(3)

IF((COORDS(3).GE.L1_L1.AND.COORDS(3).LE.L1_L2).OR.(COORDS(3).GE.L1_R1.AND.COORDS(
3).LE.L1_R2)) THEN
    Iroad=1
ELSE
IF((COORDS(3).GE.L2_L1.AND.COORDS(3).LE.L2_L2).OR.(COORDS(3).GE.L2_R1.AND.COORDS(
3).LE.L2_R2)) THEN
    Iroad=2
ELSE
IF((COORDS(3).GE.L3_L1.AND.COORDS(3).LE.L3_L2).OR.(COORDS(3).GE.L3_R1.AND.COORDS(
3).LE.L3_R2)) THEN
    Iroad=3
ELSE
IF((COORDS(3).GE.L4_L1.AND.COORDS(3).LE.L4_L2).OR.(COORDS(3).GE.L4_R1.AND.COORDS(
3).LE.L4_R2)) THEN
    Iroad=4
ELSE
    Iroad=0
ENDIF
C Define the frist truck moving path
Location = TIME(1)*SPEED
ST1=StartPts - Location
FT1=ST1+TireContact_len
C ---- Define pressure according to mesh size
C Mesh Size 6
meshsize = 6.
len_extra = TireContact_len - meshsize
C----- Define Wheel loading F1 - Front, F2 - Middle, F3 - Rear
Area=2.*TireWidth*TireContact_len
F1=8000./Area
F2=32000./Area
F3=32000./Area
F=0.
C two elements
extraD = ceiling(ST1/meshsize)*meshsize - ST1
ST_start_extra = 0.
FT_end_extra = 0.
F_E1 = 1. ! first element factor
F_E2 = 1. ! second element factor
!F_E3 = 0. ! third element factor
IF(Iroad.EQ.1)THEN
    IF(extraD.NE. 0.) THEN !two element
        F_E1 = extraD / meshsize
        ST_start_extra = -meshsize + extraD
        FT_end_extra = meshsize - TireContact_len + extraD
        F_E2 = (TireContact_len -extraD)/meshsize
    ELSE ! one element
        F_E2 = 0.

```

```

ENDIF
ST1_start = ST1 + ST_start_extra
FT1_end = FT1 + FT_end_extra
ST2_start = ST1_start + Trucklen_1
FT2_end = FT1_end + Trucklen_1
ST3_start = ST2_start + Trucklen_2
FT3_end = FT2_end + Trucklen_2
C For Front wheels
IF(COORDS(1).GE.ST1_start.AND.COORDS(1).LE.FT1_end)THEN
  F_curr = F1
  ST_start = ST1_start
  FT_end = FT1_end
  IF(extraD.NE.0) THEN ! two element
    ST_E1_End = ST_start + meshsize
    IF(COORDS(1).LE.ST_E1_End) THEN
      F = F_curr*F_E1
    ELSE
      F = F_curr*F_E2
    ENDIF
  ELSE ! one elements
    F = F_curr
  ENDIF
C For Middle wheels
ELSE IF(COORDS(1).GE.ST2_start.AND.COORDS(1).LE.FT2_end)THEN
  F_curr = F2
  ST_start = ST2_start
  FT_end = FT2_end
  IF(extraD.NE.0) THEN ! two element
    ST_E1_End = ST_start + meshsize
    IF(COORDS(1).LE.ST_E1_End) THEN
      F = F_curr*F_E1
    ELSE
      F = F_curr*F_E2
    ENDIF
  ELSE ! one elements
    F = F_curr
  ENDIF
C For Rear wheels
ELSE IF(COORDS(1).GE.ST3_start.AND.COORDS(1).LE.FT3_end)THEN
  F_curr = F3
  ST_start = ST3_start
  FT_end = FT3_end
  IF(extraD.NE.0) THEN ! two element
    ST_E1_End = ST_start + meshsize
    IF(COORDS(1).LE.ST_E1_End) THEN
      F = F_curr*F_E1
    ELSE
      F = F_curr*F_E2
    ENDIF
  ELSE ! one elements
    F = F_curr
  ENDIF
ELSE
  F=0.
ENDIF
ELSE

```

```
F=0.  
ENDIF  
RETURN  
END
```

Vita

Shi Ye entered Hunan University in China as an undergraduate in September 2006. She received her Bachelor's Degree in Civil Engineering in June 2010. She entered Drexel University in September 2012 and received the Master's Degree of Civil Engineering in June 2014. She worked with Dr. Pradhan and Dr. Bartoli as a research assistant focusing on studies related to Computer Vision and Machine Learning in Civil Engineering domain from March 2013 to September 2014, and she continued working with Dr. Bartoli as a Ph.D. student focusing on projects related to information technology, computer vision, Non-destructive evaluation, structural health monitoring and finite element model updating from September 2014 to March 2020. She has worked as a Civil Engineering Senior Associate at Ankura in Washington DC starting in October 2018.